DOE/NASA/0015-1
NASA CR-182165

Improving the Fatigue Resistance of Adhesive Joints in Laminated Wood Structures

Theodore L. Laufenberg, Bryan H. River, Lidija L. Murmanis, and Alfred W. Christiansen
USDA Forest Service
Forest Products Laboratory

August 1988

Prepared for
NATIONAL AERONAUTICS AND SPACE ADMINISTRATION
Lewis Research Center
Under Contract C-80015-F

for
U.S. DEPARTMENT OF ENERGY
Conservation and Renewable Energy
Wind/Ocean Technology Division

DISCLAIMER

Printed in the United States of America

Available from
National Technical Information Service
U.S. Department of Commerce
5285 Port Royal Road
Springfield, VA 22161

NTIS price codes[1]
Printed copy: A05
Microfiche copy: A01

[1]Codes are used for pricing all publications. The code is determined by the number of pages in the publication. Information pertaining to the pricing codes can be found in the current issues of the following publications, which are generally available in most libraries: *Energy Research Abstracts (ERA); Government Reports Announcements* and Index (*GRA* and I); *Scientific and Technical Abstract Reports (STAR);* and publication, NTIS-PR-360 available from NTIS at the above address.

DOE/NASA/0015-1
NASA CR-182165

Improving the Fatigue Resistance of Adhesive Joints in Laminated Wood Structures

Theodore L. Laufenberg, Bryan H. River, Lidija L. Murmanis, and Alfred W. Christiansen
USDA Forest Service
Forest Products Laboratory
Madison, Wisconsin 53705-2398

August 1988

Prepared for
National Aeronautics and Space Administration
Lewis Research Center
Cleveland, Ohio 44135
Under Contract C-80015-F

for
U.S. DEPARTMENT OF ENERGY
Conservation and Renewable Energy
Wind/Ocean Technology Division
Washington, D.C. 20545
Under Interagency Agreement DE-AI01-76ET20320

IMPROVING THE FATIGUE RESISTANCE OF ADHESIVE JOINTS IN LAMINATED WOOD STRUCTURES

Theodore L. Laufenberg, Bryan H. River, Lidiga L. Murmanis,
and Alfred W. Christiansen
Forest Products Laboratory
USDA Forest Service
U.S. Department of Agriculture
Madison, Wisconsin

SUMMARY

The premature fatigue failure of a laminated wood/epoxy test beam containing a cross-section finger joint was the subject of a multi-disciplinary investigation at the Forest Products Laboratory. Primary objectives of this research were to identify the failure mechanisms which occurred during the finger joint test and to provide avenues for general improvements in the design and fabrication of adhesive joints in laminated-wood structures.

This investigation included the following five thrusts: (1) analysis of the data collected during fatigue testing, (2) microscopic examination of failed and unfailed surfaces and materials, (3) chemical characterization of the adhesive resin and its cure in the presence of wood and asbestos fibers, (4) testing of the filled adhesive on various adherend systems for its mechanical properties and its performance in prototype finger joints, and (5) analysis of the finger joint's load-carrying capabilities, including the effects of specific design modifications.

Four major problem areas were identified which appear to have contributed to the premature fatigue failure of the finger joint test beam. These are the excessive void content in the epoxy adhesive bond lines, both between laminates and between fingers in the joint; the wide finger tip geometry which caused excessive shear stresses; the limited adhesion of the epoxy to the wood surface; and the surface damage to the wood fingers caused during machining.

Solutions are recommended to the problems identified during this investigation which should improve the fatigue strength of this type of structural joint. Recommendations are given on ways to reduce the void content in the veneer-veneer and finger tip bond lines, to improve the configuration of the finger tips, to improve the penetration and bonding of the adhesive to the wood substrate, and to provide finger tips with cleanly machined, undamaged surfaces.

The approach used to investigate the failure of this specific bonded joint is recommended for application to all types of adhesively bonded joints.

INTRODUCTION

This investigation is part of a program of research on materials suitable for the rotor blades of large, horizontal-axis wind turbines. This program, which is managed by the NASA Lewis Research Center and sponsored by the U.S. Department of Energy, has led to the use of laminated Douglas fir/epoxy blades fabricated by Gougeon Brothers, Inc. (GBI) of Bay City, Michigan, with lengths up to approximately 70 feet. Because of transportation limits, blade sections significantly longer than this would require structural joints made at the installation site. The largest laminated-wood rotor designed thus far was that for the 400-ft diameter Mod-5A wind turbine generator (ref. 1). Although this turbine was never built, extensive research was done to obtain design data for the two wood-to-wood structural splices required to build a rotor of this immense size.

A finger joint splice was selected for the Mod-5A wind turbine rotor, because it offered the best combination of strength and manufacturability, both during shop fabrication of the blade segments and during final assembly at the turbine site. Fatigue was known to be a potential failure mode in wind turbine blades, so a subscale model of the blade finger joint was subjected to cyclic loading to verify fatigue life predictions (Ref. 2). This joint, which was contained in a 16-in square box beam tested as a cantilever, failed prematurely at stress levels which were not expected to produce fatigue damage.

The Forest Products Laboratory was asked to investigate the causes of this premature fatigue failure and to make recommendations for improving the fatigue strength of finger joint splices. The investigation which was undertaken included the following five thrusts: (1) Analysis of the data collected during the fatigue testing, (2) microscopic examination of failed and unfailed surfaces and materials, (3) chemical characterization of the adhesive resin and its cure in the presence of wood and asbestos (filler) fibers, (4) test of the filled adhesive on various adherends to determine its mechanical properties and its performance in prototype finger joints, and (5) analysis of the load-carrying capability of the finger joint, including the effects of specific design modifications.

This report documents the failure investigation and the development of methods for improving adhesive structural joints of this type and is organized as follows: First, the body of the report presents an analysis of the fatigue test beam and the data taken during the test, a summary of the results of the total investigation, and recommendations for improving joint fatigue strength. Four appendices then document the details of the interdisciplinary studies which were conducted.

Appendix A contains a report of the microscopic examination of the Douglas fir/epoxy laminate material and of significant areas in the finger joint. Chemical characterizations of the epoxy adhesive and the interface between the epoxy and the wood are presented in Appendix B. Appendix C gives the results of mechanical characterization of the adhesive/adherend combination. Finally, Appendix D describes the macro-mechanical analysis which was performed to determine the finger joint's load-carrying capability.

WOOD/EPOXY MATERIAL

The material used to fabricate the test component is a composite of Douglas-fir veneer and epoxy. Eighty percent of the composite, by weight, is made up of the veneer with the remainder epoxy. This material system was developed by GBI and subsequently chosen by NASA for wind turbine blades because of its good fatigue performance, low density, low processing costs, low material costs, high resistance to the elements, and its low electromagnetic interference.

Wood veneer is an anisotropic material with properties varying in the principal directions of a right circular cylinder (i.e., tangential, radial, and longitudinal) as shown in Figure 1. Tension and compression strengths in the longitudinal direction may be approximately ten times greater than tension and compression strengths in the tangential and radial directions. On the other hand, shear strength in the longitudinal direction is much lower than in the tangential and radial directions (across the grain). Douglas-fir is further characterized as a coarse-textured wood. "Coarse-textured" in this report means there are striking differences between the density of earlywood and latewood bands of the annual rings. Figure 2 illustrates these bands and growth rings.

The earlywood band is the portion of the annual ring that forms during the early part of the growing season. The latewood is the portion that forms after earlywood growth has ceased. One band of earlywood and one band of latewood form one year's increment of growth or one annual ring. The cells in the latewood of Douglas-fir are smaller in overall size and have thicker walls than the earlywood cells. As might be expected the latewood of Douglas-fir is much more dense and mechanically stronger and stiffer than the earlywood. With regard to the present problem, the latewood is also more difficult to bond than the earlywood.

The test material was fabricated by laminating 0.1-in thick Douglas-fir veneers. An epoxy resin adhesive developed by GBI was used for bonding the laminates in layers to obtain the required thickness of material. Characteristics of this adhesive are described in Appendix B of this report. The veneers used in the fatigue test beam and the veneers used in tests performed at the Forest Products Laboratory were all commercially cut, although from different sources. These veneers are produced by rotary cutting or "peeling" the veneer in a continuous layer from a log, in a manner analogous to pulling paper towel from a roll. As shown in Figure 3, a knife cuts or "peels" the veneer from the log as the log is turned against the knife. A pressure bar just above the knife helps to minimize cracking of the veneer as it is cut. In spite of the pressure bar, cracks do form on the knife side where the veneer flexs in tension as it is bent away from the log. These cracks are called "lathe checks" and are described further in Appendix A on microscopic studies. Although lathe checks are inherent in peeled Douglas-fir veneers, their severity can be controlled by processing variables such as the steaming preparation of the logs and the sharpness of the lathe knife. During bonding, a considerable amount of the epoxy adhesive flows into the lathe checks and strengthens the peeled veneers.

The laminated material is molded with the veneer fibers oriented parallel to each other and to the long dimension of the laminate. The laminate displays anisotropy, similar to that of the veneer, with longitudinal (grain) direction strength and stiffness substantially higher than strength and stiffness in the tangential and radial directions (Fig. 4). The maximum veneer length is typically 8 feet, so end-jointing of individual veneers in the laminate is commonly required. This may be done by simply butting the veneer ends together (butt-jointing) or by tapering the ends of the veneers and creating a steep-angled scarf-joint. Scarf joints have been found to have somewhat better structural qualities than butt joints, although they are more expensive to make. End joints between veneers must be offset to minimize the loss of net area at any cross-section through the laminate.

FATIGUE TEST BEAM

The test component shown in Figures 5 and 6 is a hollow cantilever beam 20 feet long built by GBI from the Douglas fir/epoxy laminated material (Ref. 2). The shapes of cross sections in this beam vary from nearly circular to rectangular. A transverse finger joint 65 inches from the root (built-in) end of the cantilever beam is the critical section of the test component. The loading was applied by an hydraulic actuator through a clevis attached to the beam 181 inches outboard from the finger joint centerline. The finger joints were placed so that full fingers were on the tension and compression faces of the box beam. The joints on the sides of the beam were essentially scarf joints. A circle of twenty 18-inch long steel studs were bonded into the root end of the beam with filled epoxy, to provide attachment to the steel support frame (Fig. 6).

Loads were applied perpendicular to the beam's long axis. The sinusoidal fatigue load was applied with a mean value of 3,587 lb and an alternating value of +/- 3,356 lb, creating a maximum load of 6,943 lb and a minimum of 230 lb. These loads produced a nominal maximum extreme fiber stress of 3,350 psi at the outboard finger tips and 3,570 psi at the inboard finger tips.

FINGER JOINT DESIGN

The specific design of the finger joint used in the fatigue test component is shown in Figure 7. This design was chosen as a result of numerous tests to determine the optimum geometry for a field joint in the very large sections of the Mod-5A wind turbine rotor. Wood industry experience in use of finger joints prompted the selection of the basic joint shape, but the size of the joint and the dimensions of joint details do not appear to have been used previously. The overall joint is based on a 10:1 scarf slope and a 0.207-in thick finger tip, with an overall finger length of about 11.5 inches. A bondline thickness of 0.015 inch was specified in this design. Bondline thickness is covered in detail in Appendices C and D of this report.

Strain gages were used to monitor the strain conditions on the exterior surface of the box beam near the finger joint at 32 positions as shown in

Figure 8. Gages are divided into three groups: (1) Pairs of gages on the tension and compression faces of the beam inboard and outboard of the joint that acted as load cells for measuring bending moment, (2) individual gages around the midsection of the finger joint that measured longitudinal strains near the middle of fingers, and (3) a set of gages clustered around a finger tip, to determine local concentrations of strain that might exist in the tip/valley area. Data from these strain gages were taken at 1, 10, 100 and 1,000 cycles of loading and at each 10,000 cycles thereafter. Additionally, the deflection at the tip of the beam and the applied load were recorded at those same intervals, to monitor any changes in compliance.

ANALYSIS OF TEST DATA

Fatigue loading was applied for a total of 570,000 cycles prior to failure of the finger joints on the face of the beam with a mean tensile stress. All the fingers were separated very cleanly on the tension face, as shown by the photographs in Figure 9. The failure surface deviated slightly from the finger joint bondline at the port side of the beam near the tension face and near the neutral axis.

Table 1 lists the activity of all the strain gages after 240,000 cycles of loading, in order to provide information about the strain distribution throughout the joint. Data are presented in the form of maximum, minimum, and alternating (one-half the range from maximum to minimum) moment unit loads and strains. Reference values are also included to aid in analyzing the significance of the measured data and to normalize the alternating loads and strains.

Examination of the bending moment data shows that the centerline moment loads measured by gages C(D) and I(J) were lower than those measured near the sides of the box beam. This would be the expected result of shear lag. Also, the average of the moment unit loads is approximately two percent less than the reference average, which indicates the calibration was slightly low but acceptable. The midsection gages showed the same shear lag effects. This was most apparent from the higher strains measured at gages M (tension face) and U (compression face) adjacent to the port side plate.

The gages in the tip region provide significant information on the flow of stress through the bond. For example, the alternating strain at gage AA is about 13 percent higher than the reference strain, but closer to the tip (at gage CC) the strain has dropped to only 30 percent of the reference value. This indicates that the blunt end of the tip was carrying little if any longitudinal stress. The stress flow was apparently around the blunt finger tip, as indicated by the high strains measured by gage GG. The subject of finger tip geometry was examined further in this study, and tip shapes with improved stress flow were identified.

Samples of the strain gage data collected during testing are presented graphically in Figure 10. Nine of the gages appeared to give some inconsistent results, but these same gages provide stable readings over a wide

part of the fatigue testing. This behavior is illustrated by the data in Figures 10(a), (b), and (c). Also, note that the compliance of the beam shown in Figure 11 increases significantly during testing from 300,000 to 480,000 cycles. This change was attributed to a shear crack near the root end of the beam. A repair was made at 480,000 cycles and testing was continued.

Analysis of the strain gage data indicates that some level of structural degradation occurred over the range of 480,000 to 570,000 (failure) cycles. The most active gages during that period are listed in Table 2 with the data changes recorded during this period of the test. The position and level of strain change generally indicates either a progressive tip disbonding or bondline creep or, more generally, a loss in load-carrying capability. Strain levels increased at the edge of the beam while those strains measured near the tip of the centerline finger decreased. Note especially in Table 2 the reversal in the direction of the minimum strain as measured by several gages. These reversals indicate that a permanent deformation has occurred which produces compressive strains under load conditions which initially produced tensile strains.

The most plausible failure scenario would be a disbonding at the finger tips which propagated along the bond line until the entire joint failed. This disbonding required a great deal of energy. When the beam was unloaded during each cycle, the unbonded tips of the fingers would have been placed in compression as they were forced back into their original positions. This compressive strain is evident in a number of the tip area strain gages during the last 90,000 cycles of loading, as shown in Figures 10(d) and (e).

SUMMARY OF THE INTERDISCIPLINARY INVESTIGATIONS

Analysis of the mechanical test data failed to conclusively show the cause of the test article joints premature fatigue failure. Thus, a broad investigation of the failed joint was initiated. The primary objectives of the investigation were to identify the failure mechanisms in the finger joint specimen and provide avenues for improvements in the joint's design and fabrication.

The interdisciplinary study of this structural component was completed at the following four distinct levels:

1. Fractographic analysis of the component's failure surface provided background information on the failure modes, microstructural characteristics of the adhesive joints, and quality of the bonding surfaces.

2. Chemical characterization of the adhesive along with its fillers, diluents, and the substrates (wood) fibers determined the compatibility of the various joint constituents and their curing characteristics.

3. Mechanical characteristics of the resin system were measured to quantify its axial, shear, and fracture toughness properties along with full-scale tests of the large finger configuration.

4. Mechanical analyses of the finger joint geometry were completed to quantify its stresses along with proposed redesigns of the joint to provide enhanced performance.

The results of the aforementioned irdepth investigations are presented in Appendices A through D. Review of the combined knowledge gained from these investigations has resulted in the identification of four major problem areas for this jointing system. These are summarized below, together with recommendations for solving each of these specific shortcomings.

Adhesive Void Content

Problem: Voids represented an average of 35 percent of the veneer bondline volume and an average of 28 percent of the finger joint bondline. These are excessive void contents which seriously degraded the strength, stiffness, and fracture toughness of the adhesive/adherend system.

Research during this investigation showed that these voids were not the result of the chemical reaction of either the resin components or the wood or asbestos present in the bondline. Rather, the major source of voids appears to be the mixing of the resin system, which contributed voids amounting to up to 20 percent of the resin volume. Surface roughness of the veneers and the machined fingers in the joint appeared to contribute the remaining voids. The inherent moisture or furfural alcohol (driven by the epoxy exotherm) may have contributed volatiles to form these voids.

Recommendations: A possible solution to the excessive void problem is to mix the resin components and fillers in an evacuated environment. This approach should remove a majority of the void volume from both the veneer and the finger joint bondlines. To induce the migration of entrapped air on the wood surface into the adhesive/adherend interface, the use of a precoating or primer is recommended, which (when fully cured) would seal the bonding surface. This primer may be chosen to enhance the epoxy's bondability as discussed next.

Limited Adhesion to the Wood Surface

Problem: Microscopic examination revealed the lack of either latewood failure or adhesive penetration into latewood surfaces, while shallow failures of earlywood were widely observed. Penetration of the adhesive was limited to the weaker earlywood, to damaged earlywood areas, and to lathe checks from the veneer peeling operation. Thus, the superior strength of the latewood was not fully exploited in the tested finger joint.

Recommendations: The principal suggestion for improving the penetration and bonding of the adhesive to the stronger latewood is the use of a primer or precoating of either phenol-resorcinol formaldehyde, aliphatic diepoxides, or poly(etheneimine). The primer should have a lower molecular weight than the epoxy, in order to lower its viscosity and thus penetrate and reinforce the weakened wood surfaces. The primer should also be formulated to bond well to the latewood substrate and to the gap-filling epoxy used in the bulk of the joint.

Finger Tip Geometry

Problem: The thick finger tips (0.206 inch) in the tested design produce an adhesive shear stress in excess of the elastic limit at less than 30 percent of the joint's potential strength. Under fatigue loading conditions this "overstress" into the inelastic/plastic region at the finger tips causes shear failure at the bondline which envelops the entire bonded joint, because there are no crack-arresting or low-stress locations. Supplementary full-scale tests of thick finger tip joints confirm this analysis. Static strength of joints with thick finger tips was found to be 40 percent less than the static strength of fully-scarfed (sharp) tips.

Recommendations: A better finger tip geometry would be one which is very thin or fully scarfed. Finger tip modifications such as undercutting of the tip, extending the thick tip, or producing a dual-slope tip were investigated, and all were found to be superior to the existing design. It is also recommended that crack-stopping and creep-resistant features be incorporated into the joint design.

Machining Quality

Problem: The aforementioned problems were all made more serious by either the limited quality or limited capability of the machining system used to fabricate the finger joints in the test specimen. Surface damage caused by sawing the fingers inhibited penetration of the epoxy into individual cells and resulted in a weakened interface, permitting failure to progress across these damaged fibers. Undesireable variations in the thickness of the bondline and the thickness of the finger tips are directly due to the limitations of using a circular saw to machine this finger joint.

Recommendations: A high-speed machine cutter is recommended for use as the final step in machining of the joint. A circular or band saw should be used only to bring the joint to its rough dimensions. The final machining of the surfaces should allow accurate control of the bondline thickness and production of a narrower tip, with more control of the tip configuration. These are essential for production of structural joints with consistently higher fatigue resistance than that of the finger joint splice in the test beam.

ACKNOWLEDGMENTS

The authors would like to acknowledge the considerable support provided by David A. Spera and Clinton Ensworth of NASA-Lewis, the Gougeon Brothers engineering staff, and Ronald Jokerst at the Forest Products Laboratory. We also thank the administrative and technical support staff at the Forest Products Laboratory for their assistance, including Vicki Claas, Shu Chi Liang, Arnie Okkonen, Wesley Rork, and Martin Wesolowski.

REFERENCES

1. Anonymous: Mod-5A Wind Turbine Generator Program Design Report, Volume I - Executive Summary. General Electric Company, DOE/NASA/0153-1, NASA CR-174734, 1984.

2. Stroebel, T.; Dechow, C.; and Zuteck, M.: Design of an Advanced Wood Composite Rotor and Development of Wood Composite Blade Technology. Gougeon Bros., Inc., DOE/NASA/0260-1, NASA CR-174713, 1984, pp. 13, 14, 64, and 65.

TABLE 1

STRAIN GAGE ACTIVITY AT 240,000 CYCLES OF LOADING

Gage	Maximum	Minimum	Alternating	Normalized alternating
(a) Bending moment gages (units = 1,000 in-lb/in, ref. moment = average moment unit load at midsection of joint).				
Ref.	-2.6	-78.9	38.1	1.000
A(B)	-3.8	-83.5	39.9	1.045
C(D)	-1.9	-74.7	36.4	0.955
E(F)	-3.1	-84.7	40.8	1.070
G(H)	-5.6	-77.8	36.1	0.946
I(J)	-4.4	-76.0	35.8	0.938
K(L)	-5.6	-79.7	37.0	0.971
			Weighted Aver.:	0.975
(b) Joint midsection gages (units = micro-in/in, ref. strain = average of gages N and P).				
Ref.	1075	95	490	1.000
M	1130	-70	600	1.224
N	1060	100	480	0.980
P	1090	90	500	1.020
Q	1290	160	565	1.153
R	62	42	10	0.020
S	0	-1000	500	1.020
T	0	-1160	580	1.184
U	-120	-1500	690	1.408
V	0	-12	6	0.012
(c) Tip region gages (units = micro-in/in, ref. strain = 1.033 times average of gages N and P).				
Ref.	1110	98	506	1.000
W	0	-100	50	0.099
X	1180	140	520	1.027
Y	1340	160	590	1.166
Z	870	70	400	0.790
AA	1310	170	570	1.126
BB	-50	-350	150	0.296
CC	300	-20	160	0.316
DD	230	0	115	0.227
EE	1150	50	550	1.087
FF	60	-120	90	0.178
GG	1430	70	680	1.343

TABLE 2

STRAIN GAGE ACTIVITY FROM 480,000 CYCLES TO FAILURE AT 570,000 CYCLES

Gage (s)	Level	480,000 cycles	570,000 cycles	Change
(a) Bending moment gages (units = 1,000 in-lb/in)				
C(D)	alt.	36.1	38.6	2.5
min. -87.9		-78.5	9.4	
E(F)	alt.	40.2	31.4	-8.8
	min.	-84.7	-66.2	18.5
(b) Joint midsection gages (units = micro-in/in)				
M	max.	1,250	1,550	300
	min.	75	410	335
N	max.	1,025	900	-125
	min.	50	0	-50
P	max.	1,085	950	-135
	min.	55	-40	-95
(c) Tip region gages (units = micro-in/in)				
BB	alt.	375	220	-155
CC	max.	260	-15	-275
	min.	-25	-300	-275
EE	max.	1,100	770	-330
	min.	20	-270	-290
GG	max.	1,390	1,050	-340
	min.	70	-220	-290

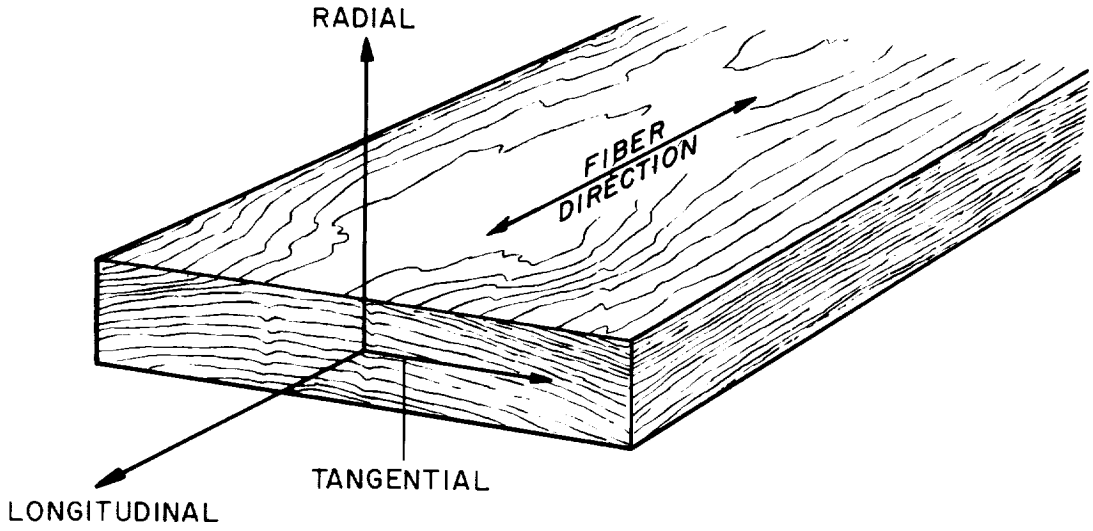

M 140 728

Figure 1--The three principal axes of wood with respect to grain direction and growth rings.

Figure 2--Cross-section of a ponderosa pine log showing growth rings: light bands are earlywood, dark bands are latewood. An annual growth ring is composed of the early wood ring and the latewood ring outside it.

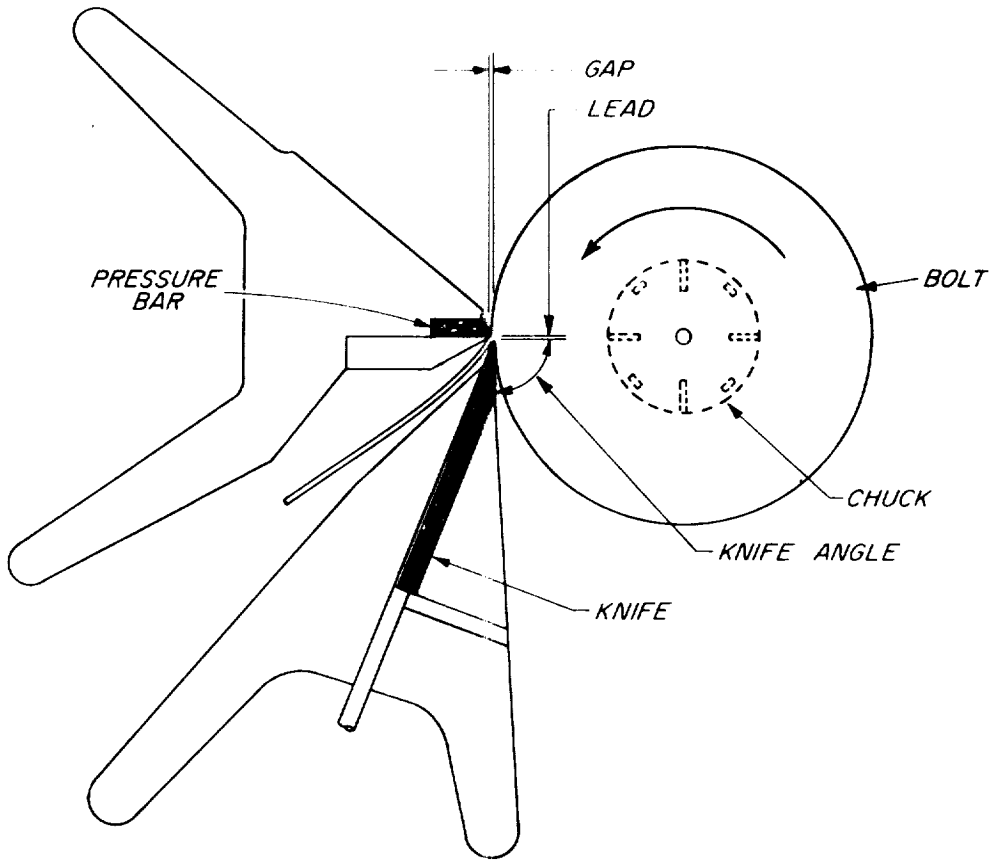

Figure 3--View of the veneer peeling process to produce rotary-cut veneer.

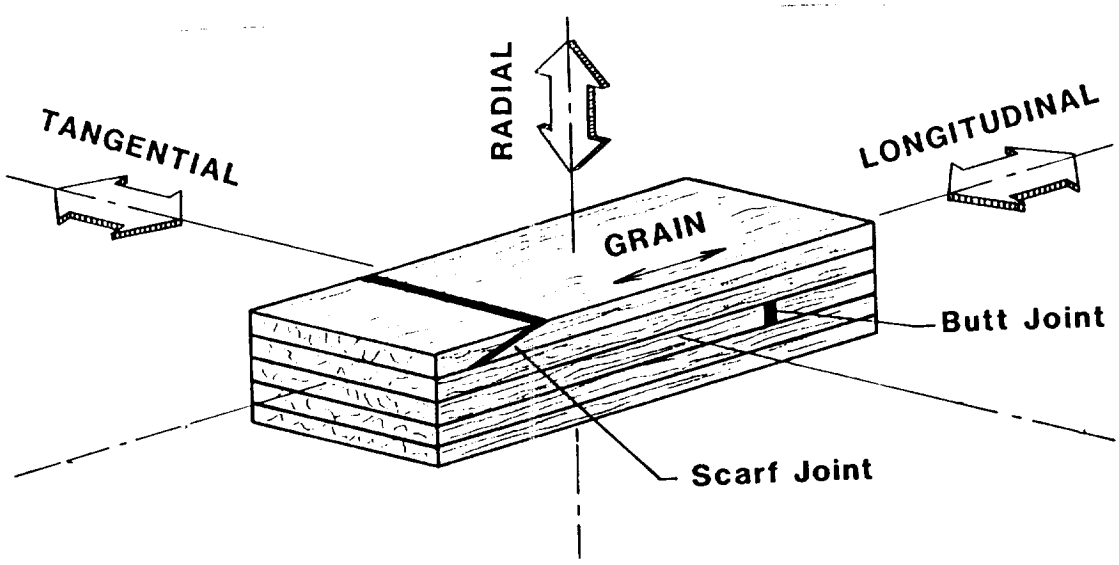

Figure 4--Laminate directional orientation. Note the orientation of the bondlines and veneer joints in the laminate.

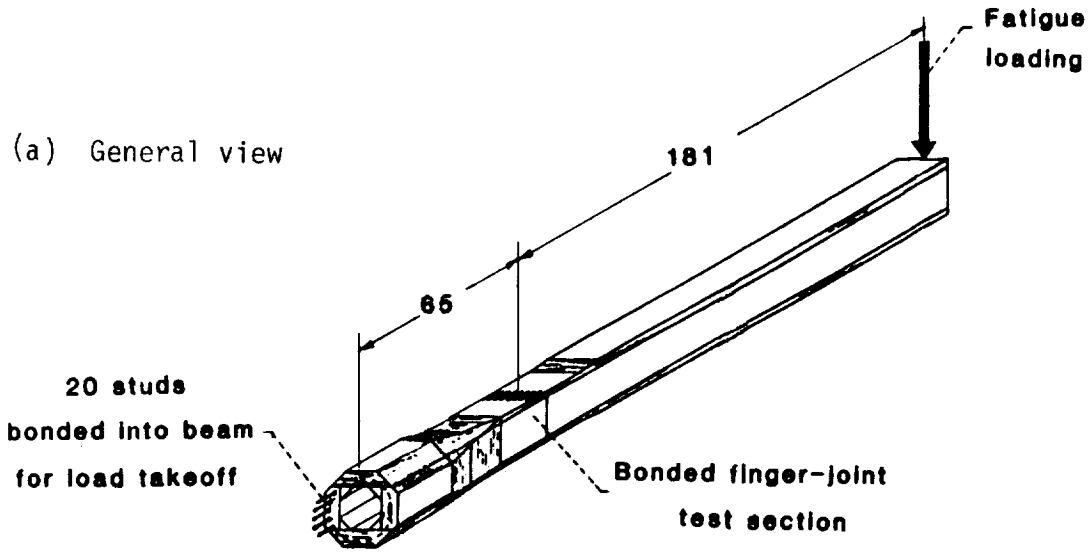

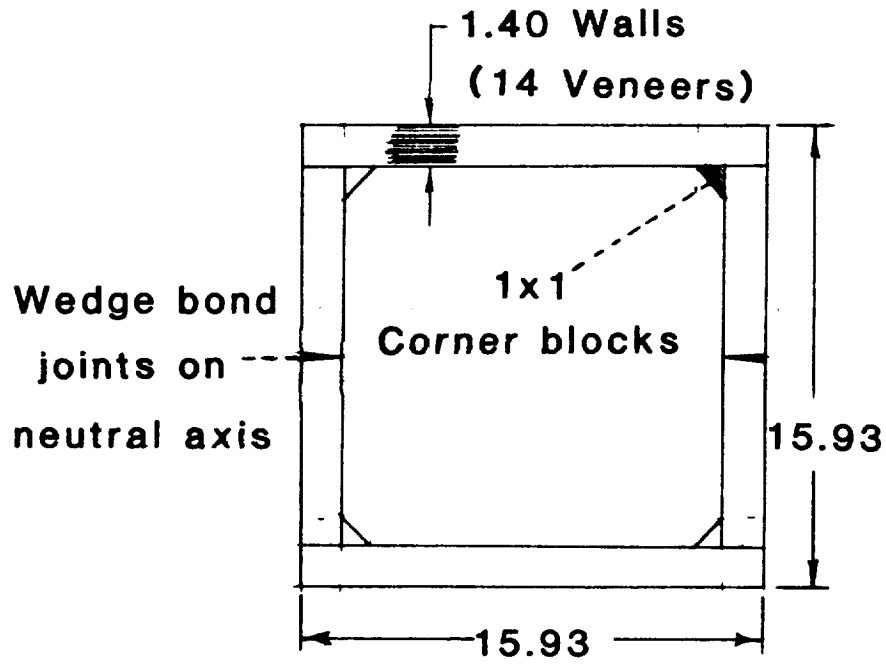

(b) Cross-sectional view at test section

Figure 5. - Cantilever beam fatigue test specimen containing bonded finger joint (all dimensions in inches).

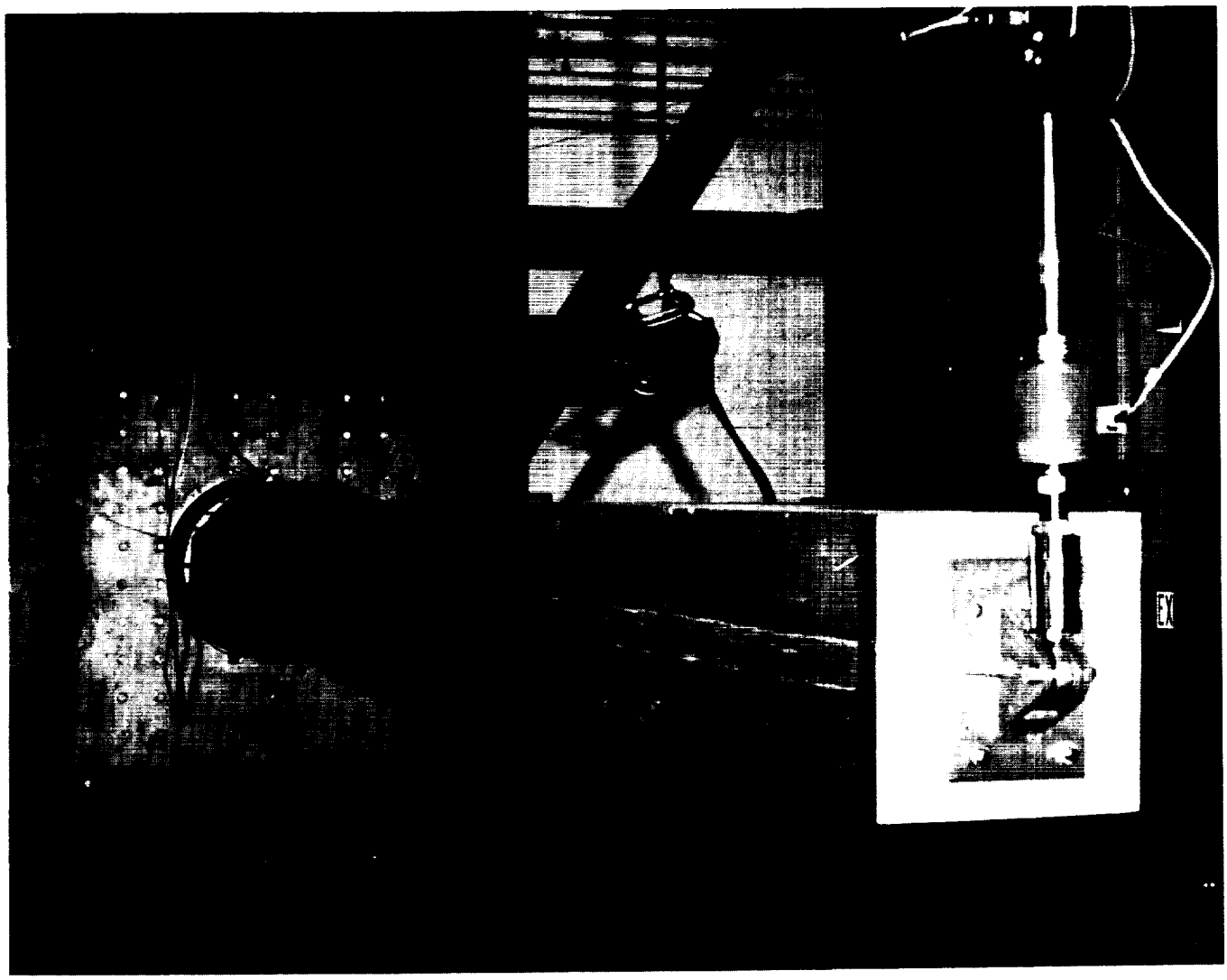

Figure 6 - Photograph of the fatigue test beam installed on a strongback (left) with hydraulic actuator attached (right), at the U.S. Army Research and Technology Laboratory, Ft. Eustis, Virginia.

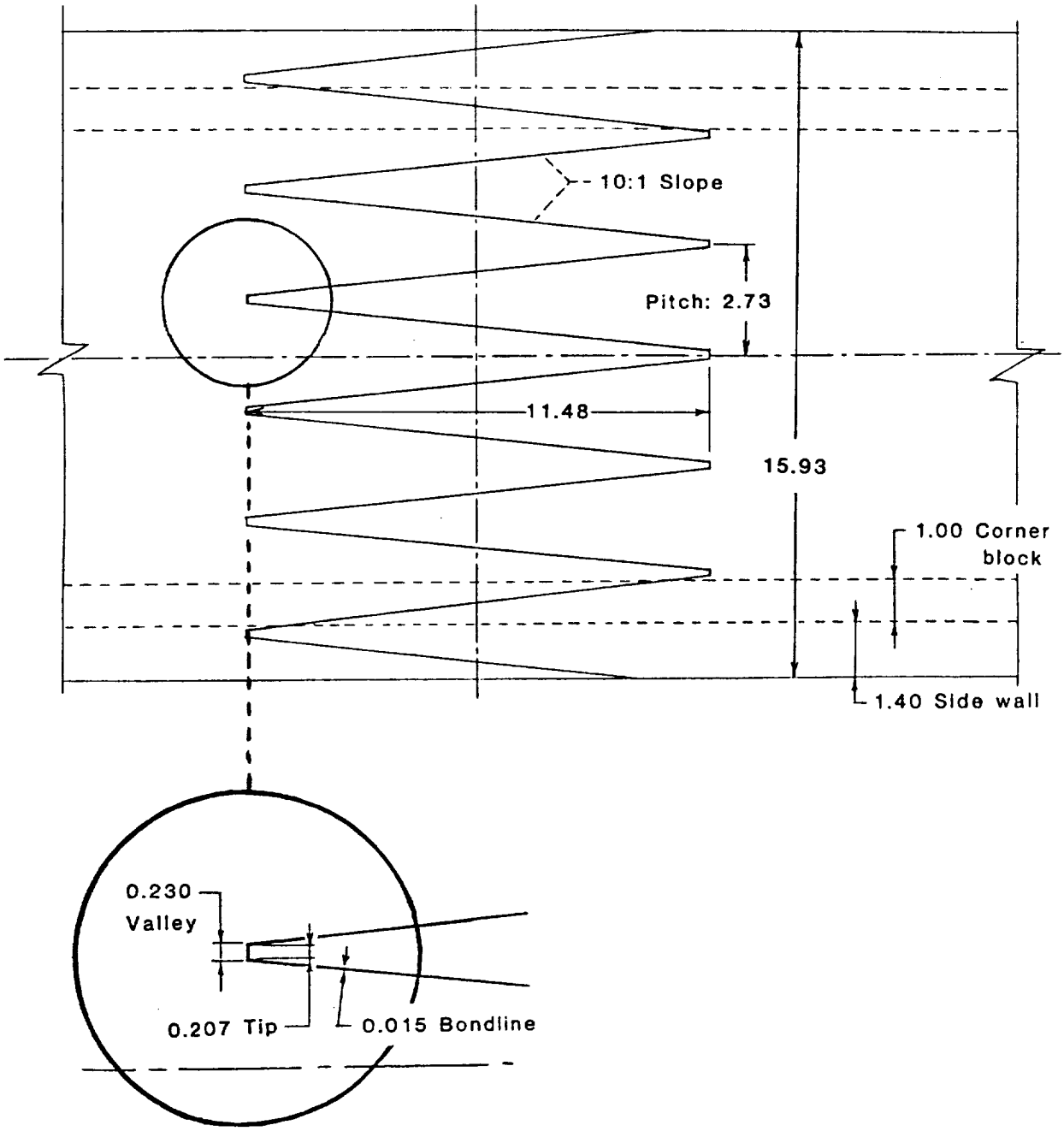

Figure 7. - Geometry of finger joint in fatigue test beam (all dimensions in inches).

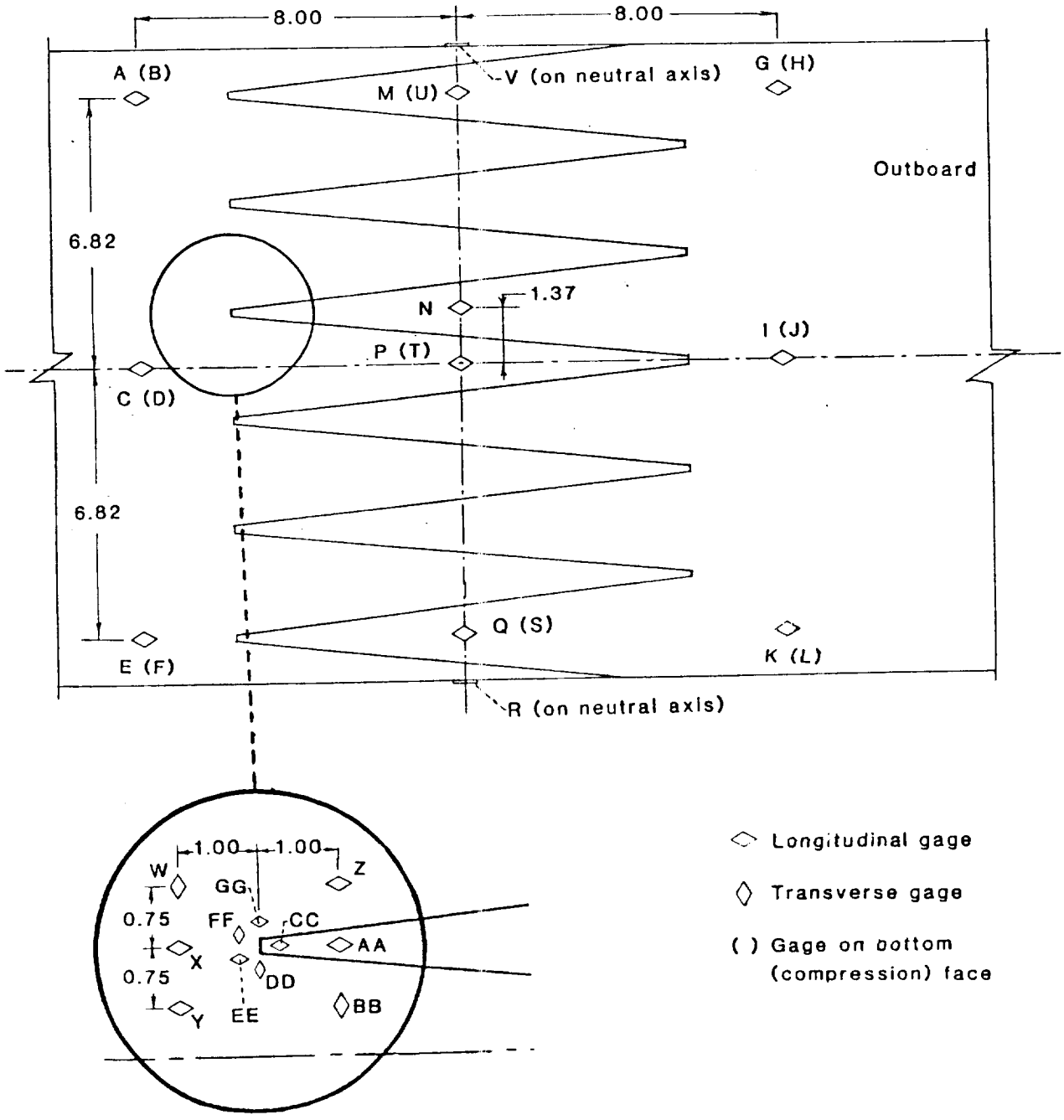

Figure 8. - Location of strain gages in test section (all dimensions in inches).

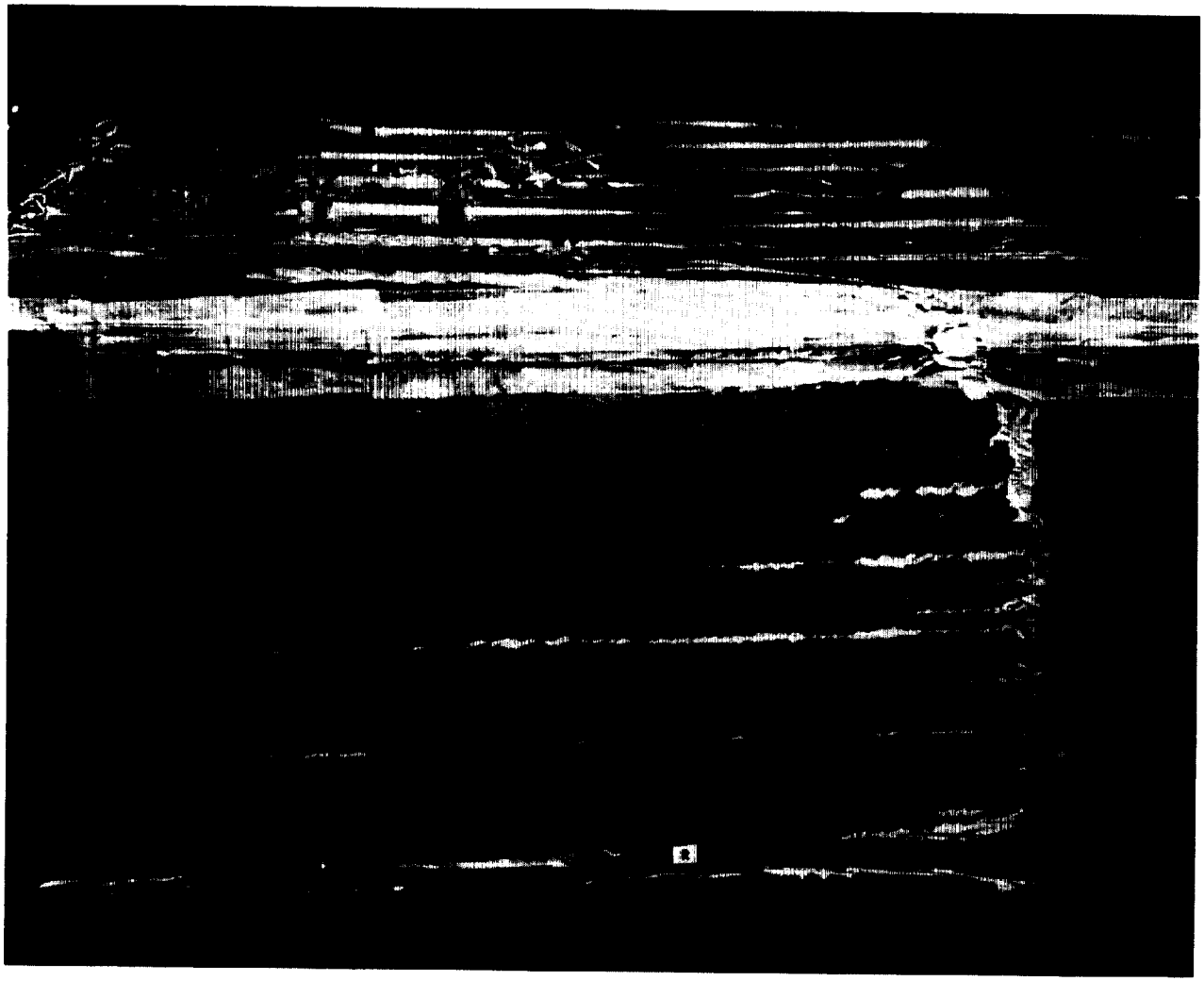

(a) Starboard side view, showing finger tips projecting above top (tension) surface.

Figure 9. - Photographs of the failed finger joint test section.

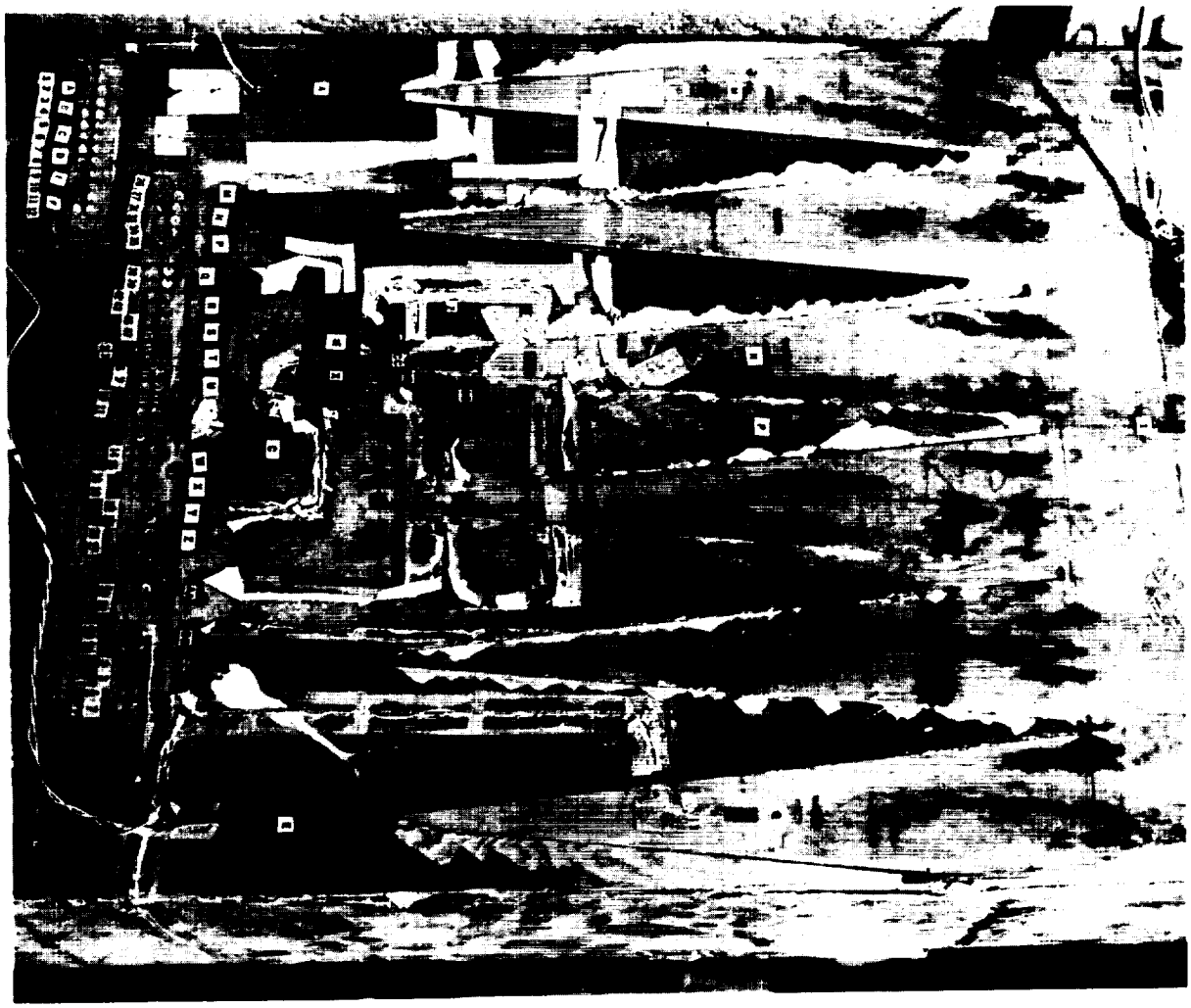

(b) Top (tension) face (outboard is to right).

Figure 9. - Continued. Photographs of failed finger joint test section.

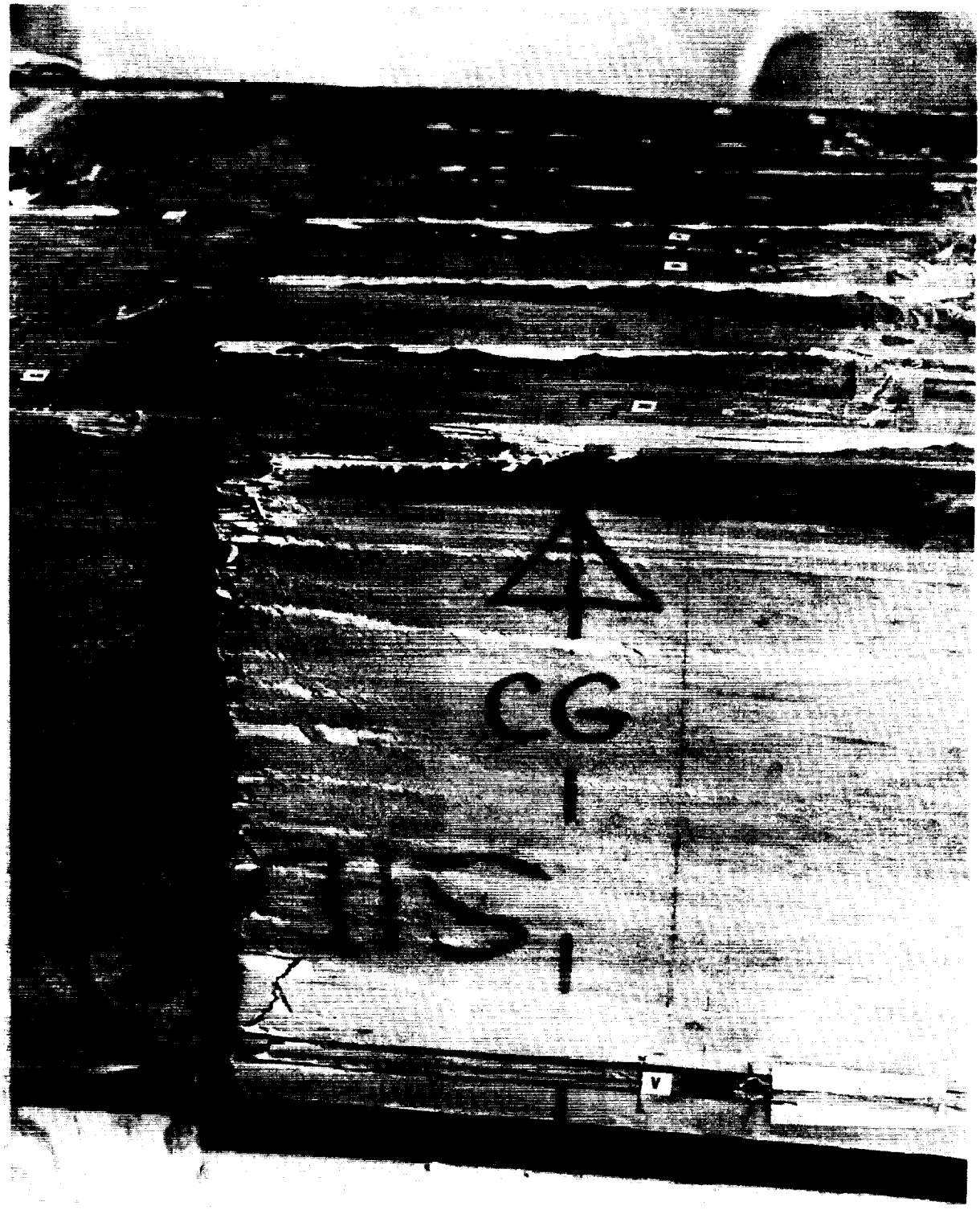

(c) Port side view showing failures on top, down port side, and parallel to neutral axis.

Figure 9. - Continued. Photographs of failed finger joint test section.

(d) Interior view of top side, showing failed surface on port side parallel to neutral axis.

Figure 9. - Concluded. Photographs of failed finger joint test section.

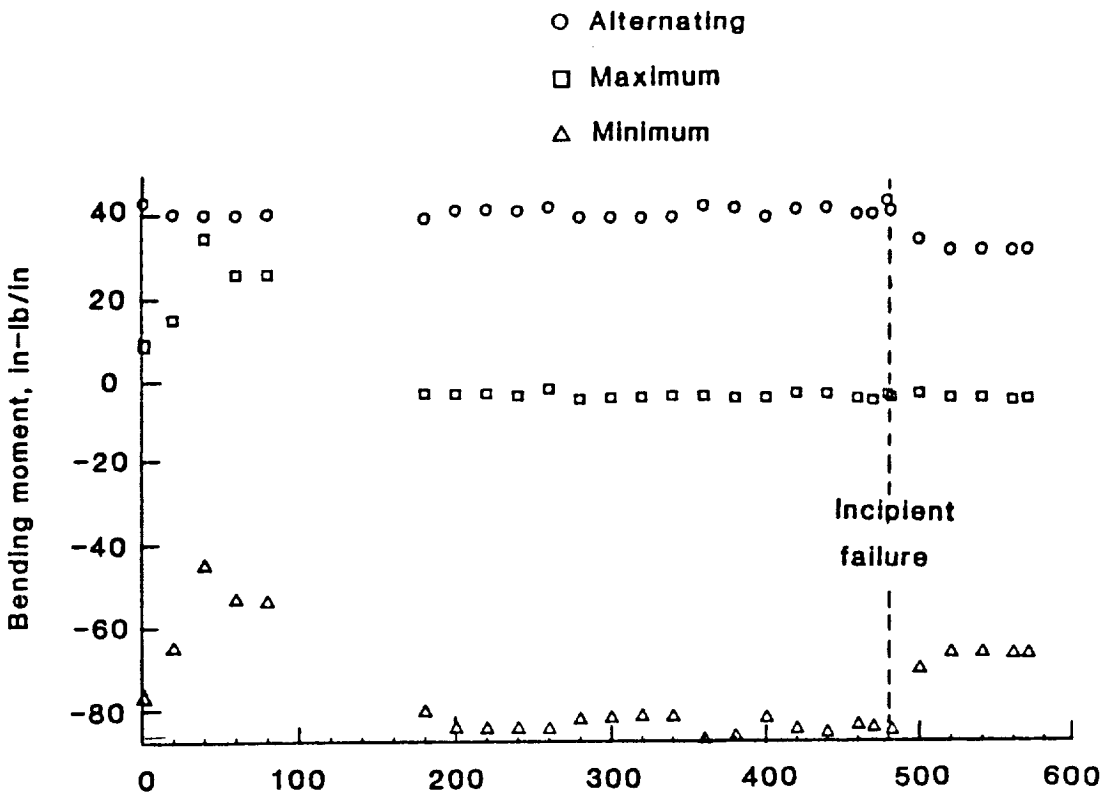

(a) Bending moment gages E(F).

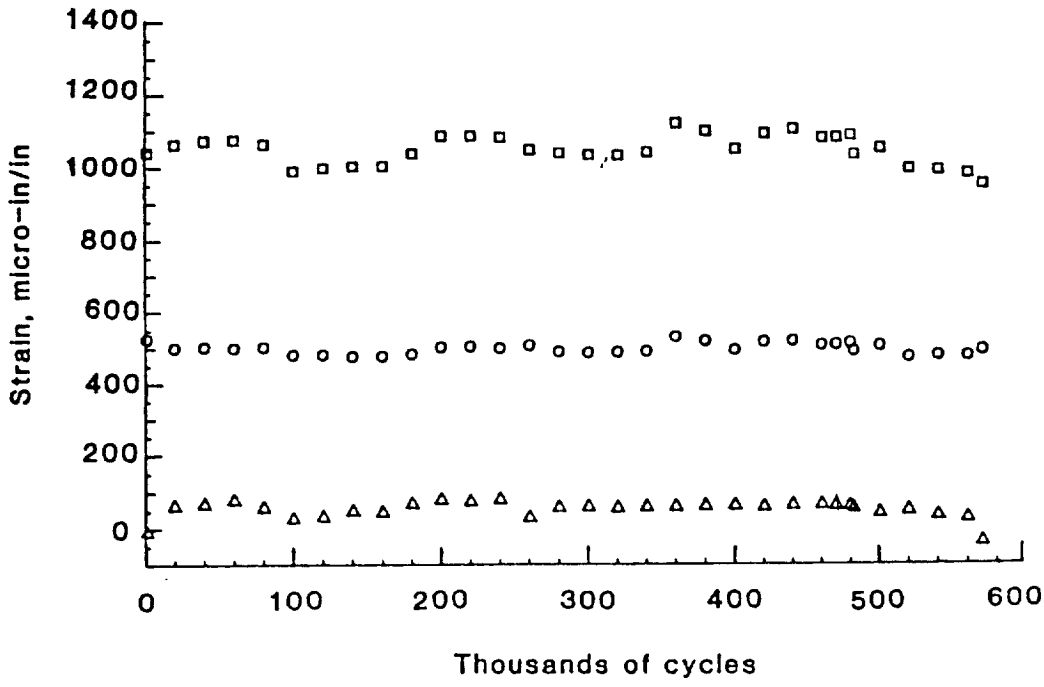

(b) Midsection strain gage P.

Figure 10.- Samples of strain gage data.

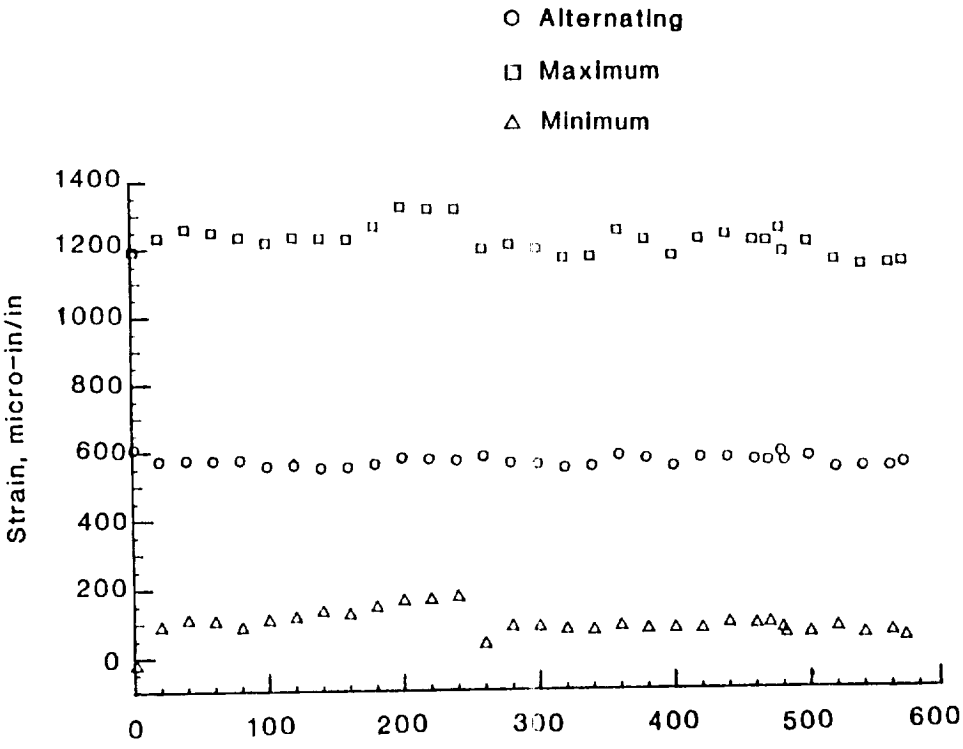

(c) Tip region strain gage AA.

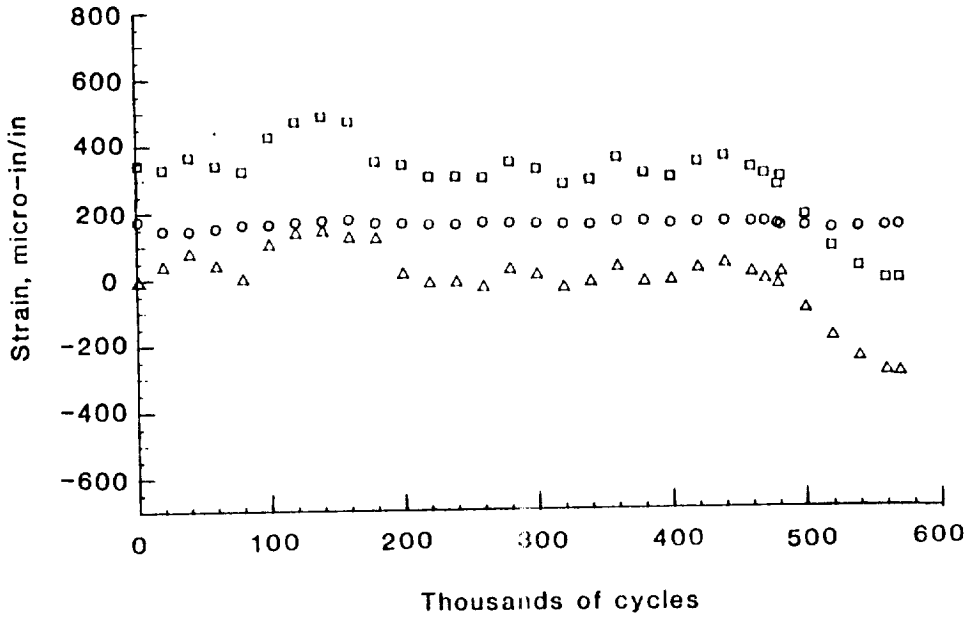

(d) Tip region strain gage CC.

Figure 10. - Continued. Samples of strain gage data.

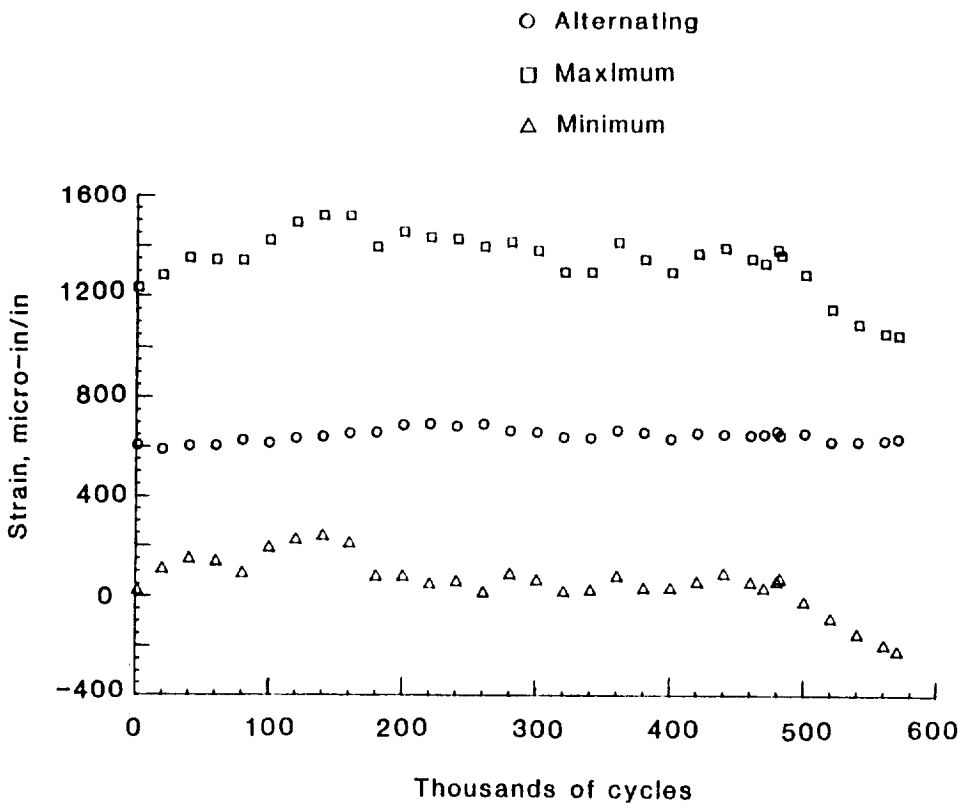

(e) Tip region gage GG.

Figure 10. - Concluded. Samples of strain gage data.

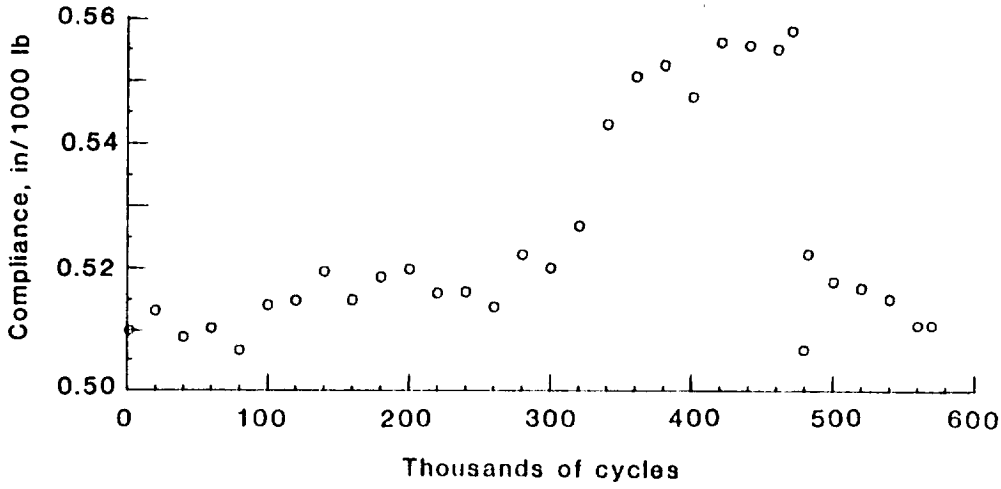

Figure 11. - Variation in beam compliance during fatigue testing (tip deflection range/load range).

APPENDIX A

MICROSCOPIC EXAMINATION

Microscopic techniques were used to study this wood-adhesive joint at a microstructural level. In evaluating failures in bonded wood structures, it is difficult to judge where and what type of failure has occurred. Both FM and SEM have been proven to be fast and efficient ways of examining fracture surfaces and the quality of gluelines.

The wood/epoxy composite material was examined using fluorescence microscopy (FM) and scanning electron microscopy (SEM). Observations were made on samples from both the unfailed compression face and the failed tension face of the cantilever-beam fatigue test specimen, in the area of the finger joint splice.

Material and Methods

The material examined was part of a large box beam made from parallel laminated Douglas-fir veneer, bonded using an epoxy resin system. Of primary importance in this study were the large jointed fingers fabricated on the faces of the beam in the wood/epoxy composite material.

The fracture surfaces were examined by FM utilizing a reflected ultraviolet (300-400 nm) radiation. This was obtained by inserting a UG-1 filter in the light path of a mercury lamp in a Leitz Ortholux microscope. Wood exhibits a natural bluish autofluorescence in ultra-violet radiation, while epoxy resin has a white or yellow-green fluorescence. The color differences allow the exposed areas of wood to be distinguished from those covered with the resin.

In addition to fracture surfaces, finger joint gluelines from the unfailed part of the specimen, and gluelines between the veneers from the failed and unfailed parts were examined. For examination of gluelines, small blocks with about 1 cm^2 of transverse surface, including a bondline, were smoothed with a sliding microtome.

Light microscopy techniques provide only limited means for studying the type of failure since the smallest discernible structures are too large for detailed analysis. Wood seldom fractures in a single plane, and the separated surfaces consist of three-dimensional structures with dimensions which are beyond the range of the light microscope focal depth. This can be solved by using a scanning electron microscope.

For scanning electron microscopy, small blocks containing fracture surfaces, approximately 8 mm on a side, were mounted on standard aluminum stubs with silver paint and coated with gold in a sputter-coater. The microscope was the Cambridge Stereoscan, type 2 A.

Finger tips in the Unfailed Compression Face

The gap at the end of finger tips is fully wetted with epoxy and averages 0.040 inch in thickness. Entrained air in the epoxy approaches 20 percent of the bondline volume with an average void diameter of 0.006 inch (Fig. A-1). The finger tip displays a crushing wood failure, termed brooming, which involves an average 0.008 inch of wood fiber cell length. In this view, a compression-induced crack is apparent at the edge of the finger tip which includes a shear-slip zone into two large voids.

Close examination of the brooming failure at the finger tip revealed that the extent of failure is limited to the length of fiber that is impregnated by epoxy. The epoxy was drawn into the cell lumen by capillary action or was pushed in by the forced closure of the joint. A network of matrix cracking was apparent at the wood-epoxy interface and especially at the voids where strain concentrations occurred.

Sloped Area of Finger Joints in the Unfailed Compression Face

The portion of the finger joint that is bonded along the 1:10 sloped wood grain has a bondline thickness that varies from 0.002 to 0.009 inch as compared to the design bondline thickness of 0.015 inch. Again, porosity of the bondline is high, averaging 12 to 45 percent in the samples examined. Noticeable amounts of crushing or damaged wood surfaces are seen (Fig. A-2), located predominately in the low density earlywood (the wood formed during the early part of the growing season). The machining operation is responsible for the majority of this damage, which is evidenced as a compressed mass of cells in the cross-sectional view shown in Figure A-3. Latewood (the wood formed after the fast growing earlywood) rarely displayed any machining damage because of its higher density and its thicker cell walls.

Localized areas of cell compression due to the hydraulic pressure of the bonding operation are also apparent (Fig. A-4). These areas are characterized by buckling of the cell walls perpendicular to the bondline. Cell wall compression or damage was rarely observed for latewood. Breakage of middle lamella between the latewood tracheids is frequently seen (Fig. A-5). These radial fractures are commonly attributed to veneer checking caused by the rotary peeling process. The lack of both machining damage and hydraulic crushing in latewood typically resulted in thin bondlines where two latewood bands met (e.g. 0.002 in thick in Fig. A-5).

Machining damage was also seen in the form of deep fractures in the veneer surface. Most of these areas were filled by the epoxy during the finger joint bonding operation. These fractures are of small dimension (0.003 in wide). Thus, the epoxy was drawn into the damaged areas by capillary action. Some fraction of the porosity in the bondlines could be attributed to the release of entrapped air in these fractures after the joints are assembled.

Inter-Veneer Bondlines in the Unfailed Compression Face

A typical inter-veneer bondline is shown in Figure A-6. Bondlines between veneers range from 0.002 to 0.021 inch in thickness. Porosity is high, ranging from 25 to 45 percent where adequate adhesive is present to form the spherical voids shown in Figure A-6. Larger irregular voids (Figs. A-7 and A-8) are evident where inadequate adhesive was retained to form spherical voids. Adhesive penetration into damaged wood surfaces, veneer checks, or open-ended cells was seen to take up the adhesive at the bondline. Damaged earlywood surfaces use a great deal of adhesive to "heal" the damage (Figs. A-6, A-7, and A-8), whereas latewood surfaces absorb little adhesive (Fig. A-6).

Damage of earlywood appears to be caused only by the rotary peeling operation, not by hydraulic pressures, as was seen in the finger tip region. Earlywood surfaces are quite rough in comparison with latewood surfaces (Fig. A-6). The roughness produces elevation differentials up to 0.006 inch on a single veneer surface. Masses of damaged earlywood cells are also found in the bond-line (Fig. A-8), usually attached by several cell walls to the parent wood surface.

Finger Joint Failure Surfaces on the Tension Face

On the basis of visual examination, wood failure was estimated to constitute between 5 and 40 percent of the fracture area of each sloped finger surface. An average for all failure surfaces is estimated at 20 percent. Failure was dominated by adhesive and cohesive failures. In adhesive failures, impressions (castings) of the opposite wood surface are discernible (Fig. A-9). Cohesive failure is characterized by failure within the adhesive layer with the exposed layers being amorphous (Fig. A-10).

At no point on the failure surfaces was wood failure more than 0.15 inch away from the bondline. Some of the wood failure could be associated with veneer lathe checks (the fractures produced by the rotary peeling process). These lathe-check failures (or intra-wall failures) are distinguished by a failure surface which follows the wood grain without deviation.

Brash wood failures (i.e. unsplintered, low-strain failures) were observed (Fig. A-11), characterized by trans-wall failures in which earlywood tracheids were broken across their long axes. This is typical of brittle wood. A large percentage of the trans-wall failures included epoxy-impregnated material. Thus, with the epoxy acting as a "cell stiffener," trans-wall failures had a more brash appearance (Fig. A-12). Trans-wall failure of earlywood accounted for over 95 percent of all trans-wall failures. Damaged bonding surfaces and subsurface layers have been linked to inferior bonded joint performance (River and Miniutti, 1975; Jokerst and Stewart, 1976; and River et al, 1981).

Bondline voids were important contributors to the failure surface. Inter-veneer bondline voids provided the opportunity for casting of their

impressions and formation of mechanical locks during the finger joint bonding. Adhesive failure surfaces over inter-veneer bondlines displayed a glassy-type failure (Fig. A-13). Large voids in the finger joint bondline represented a low-resistance path in failures propagating cohesively or adhesively.

Summary

Both the finger joint and the inter-veneer bondlines are high in void content. These voids were caused by entrapped air in the mixed resin, resin components volatilizing, or air displaced from the wood fiber surfaces or cell cavities. They amount to an average of 35 percent of the bondline volume for inter-veneer bondlines and 28 percent for finger joint bondlines. These voids are prominent features in both the cohesive and adhesive failure surfaces of the finger joint.

On the average, wood failure accounted for about 20 percent of the failed surface in the finger joint. Earlywood intra-wall and trans-wall failures were the primary modes of wood failure. Lathe checks provided low-energy failure paths for intra-wall failures. Additionally, the brash wood failure of the fractured wood surface suggests that the wood was brittle, a consequence of the machining damage and subsequent epoxy impregnation of the bonding surface. These damaged areas played a prominent role in the failure surfaces, contributing to the porosity of the bondline and the weakened wood substrate.

Literature Cited

Jokerst, R. W.; Stewart, H. A.: Knife- versus abrasive-planed wood: Quality of adhesive bonds. Wood Fiber 8(2): 107-113; 1976.

River, B. H.; Miniutti, V. P.: Surface damage before gluing weak joints. Wood and Wood Products; July 1975.

River, B. H.; Murmanis, L.; Stewart, H. A.: Effect of abrasive-planing stock removal rate on adhesive-bonded joint performance. In: Proceedings, Wood adhesives--research, application, and needs, symposium sponsored by the Forest Products Laboratory and Washington State University; 1980, September 23-25; Madison, WI; 1980.

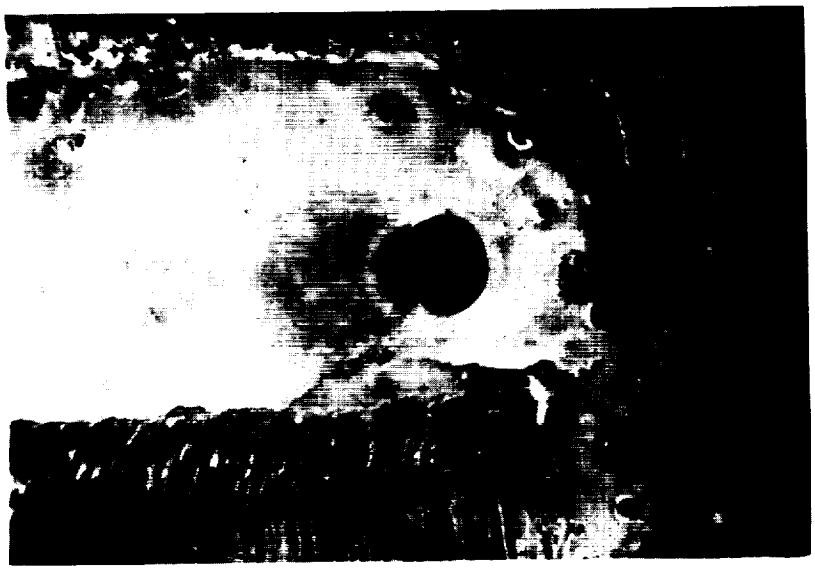

Figure A-1. - Typical finger tip from the "unfailed" compression face. Note the broom-type failure at the finger tip, void formation, and epoxy macro- and micro-cracking (70X; longitudinal-tangential (L-T) plane).

Figure A-2. - Finger joint bondline intersecting two slightly offset inter-veneer bondlines. Note earlywood crushing along the finger joint and veneer bondline wood surfaces (82X; radial-tangential (R-T) plane).

Figure A-3. - Finger joint bondline showing damaged earlywood (200X; R-T plane).

Figure A-4. - Finger joint bondline with hydraulically-induced earlywood damage (190X; R-T plane).

Figure A-5. - Finger joint bondline between latewood bands, showing the fractures between tracheids and a typically thin bondline (207X; R-T plane).

Figure A-6. - Inter-veneer bondline having 45 percent porosity. Note the extensive penetration of epoxy into earlywood areas (82X; R-T plane).

Figure A-7. - Inter-veneer bondline with inadequate epoxy available for spherical void formation (75X; R-T plane).

Figure A-8. - Inter-veneer bondline with extensive earlywood surface damage which serves to starve the bondline (75X; R-T plane).

Figure A-9. - Adhesive failure of the finger joint surface (69X; L-R plane).

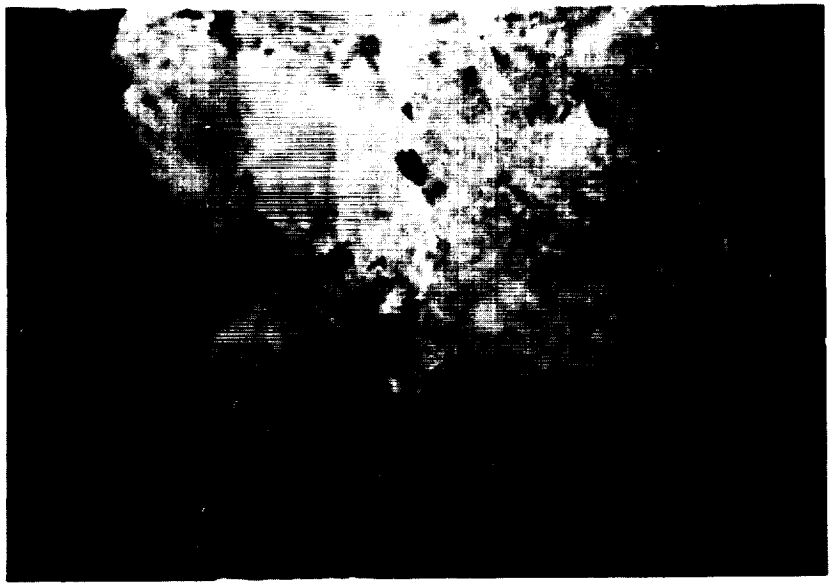

Figure A-10.- Cohesive finger joint bondline failure (75X; L-R plane).

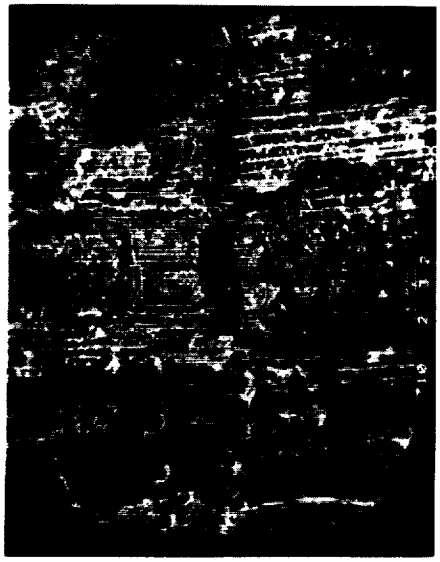

Figure A-11.- Trans-wall wood failures along finger joint bondline (SEM, 54X; L-R plane).

Figure A-12.- Trans-wall wood failures showing effects of epoxy impregnation (SEM, 500X; L-R plane).

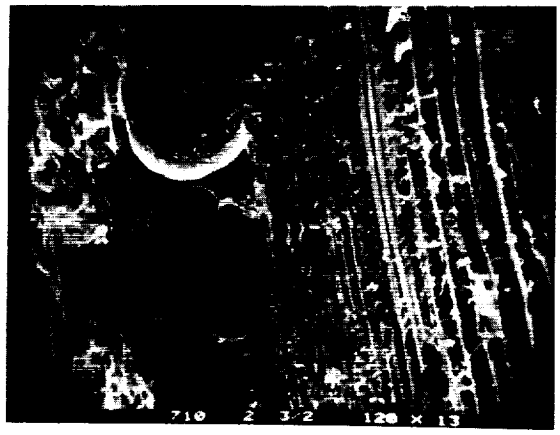

Figure A-13.- Glassy-type failure over an inter-veneer bondline on the finger joint failure surface (SEM, 120X; L-R plane).

APPENDIX B

ADHESIVE/INTERFACE CHEMICAL CHARACTERIZATION

The objectives of this work were (1) to determine whether the reactivity of the epoxy resin was affected by interaction with wood or asbestos, (2) to characterize the chemical constituents, and (3) to detect any possible interferences with bonding.

Adhesive Materials

WEST System Epoxy 105 from Gougeon Brothers Inc. (GBI) Resin 105 is an essentially monomeric form of the diglycidyl ether of bisphenol A containing furfuryl alcohol. The viscosity of the unfilled resin is stated by the manufacturer to be 500 to 700 cP, and for the 9 percent asbestos-filled resin the viscosity is 118,000 cP. Gel time of the resin with hardener 206 at 21 °C (70 °F) is 35 to 40 minutes.

WEST System Hardener 206 from GBI Hardener 206 is a proprietary aliphatic polyamine mixture, including amine components such as diethylene-triamine and triethylenetetramine. The viscosity of the neat hardener is stated to be 250 to 350 cP, and for the 9 percent asbestos-filled hardener the viscosity is 80,000 cP.

Douglas-fir Wood Flour Wood flour, used as a resin filler in the unextracted and dried condition, had been ground by vibratory ball milling. This provides the finest particle size that can be routinely obtained.

Asbestos Fiber The asbestos fiber in the epoxy components is expected to be the chrysotile type occurring in North America, processed into mineral fibers. This material (Streib, 1978) has the chemical composition $Mg_3(Si_2O_5)(OH)_4$, and has a polar, alkaline surface. Although bundles of fibrils are normally seen, the individual fibrils seen by electron microscopy would be cylinders or fibers with 0.02 to 0.03 micrometer diameters. These have very high tensile strength, alkali and heat resistance, and absorb only 2% to 3% moisture from saturated air.

Adhesive components were measured in the ratio 5 pphr resin to 1 pphr hardener by weight for both the filled and the unfilled adhesives. The resin and hardener were mixed by hand with a small spatula in small aluminum dishes. The adhesive was usually prepared in 10- to 25-gram batches.

Test Methods

The test methods used to evaluate the chemical/adhesive characteristics were adapted to provide the information needed for this study. The following are brief descriptions of three of the test methods used.

Differential Scanning Calorimetry The reactivity of the mixed resins was evaluated by differential scanning calorimetry using a Perkin-Elmer DSC-2 calorimeter. Five parts, by weight, of the resin were vigorously hand mixed with one part of the hardener (and where appropriate one part of the wood flour), then droplet samples of 2 to 24 mg were put into either aluminum capsules or stainless steel large volume capsules (LVC) and sealed. The aluminum capsules were used at first because the heat transfer is faster and it was assumed there was little to volatilize in an epoxy resin. The stainless steel LVCs, which withstand 200 to 300 lb/in^2 (1.4 to 2.1 MPa) vapor pressure and have capacities of 75 ?l, were used later when volatilization endotherms were found to be a confusing factor.

The samples were heated at a constant scanning rate of 5, 10, 20, or 40 °C per minute from room temperature to near 500 K (227 °C), after which point they were cooled off quickly back to room temperature. They were then rescanned under the previous conditions. At the end they were weighed to detect any weight losses of more than 0.1 mg. The temperatures corresponding to the peaks of the exotherms were taken as characteristic of the curing reaction for purposes of kinetic analysis. Temperatures were corrected in accordance with results on an indium melting point standard.

The data can be plotted as the reciprocal of the peak temperature (degrees Kelvin) against the logarithm of the heating rate (°C/min). A linear equation was fit to the corrected data with a least squares technique, and the slope was used in an equation formulated by Duswalt (1974) for determining the activation energies of reactions: $E_a(kJ/mol) = -0.0182 \times slope$. Prime (1981) finds that the simple equation based on change of peak temperature with heating rates gives activation energies to an accuracy of ±10 percent for simple reactions.

Fourier-Transform Infrared Spectroscopy Infrared analyses of the resin, hardener, and mixtures of these (with and without wood flour) were obtained by spreading the viscous fluids on KBr crystals and scanning these in a Nicolet 6000 Fourier-transform infrared spectrometer. Data were recorded on magnetic disk, allowing later manipulation to transform the spectra to either absorbance units (for quantitation) or transmittance units for comparison with available reference spectra. Samples of resin mixtures made for several DSC experiments were transferred to the spectrometer within 0.5 hour of mixing. Subsequently, scans were taken at intervals of time to follow the progress of cure over periods of weeks.

Using the Fourier-transform capabilities of the machine it is possible to mathematically subtract one spectrum from another to produce a difference spectrum, which will show which peaks have changed and in which direction. In spreading the wood-filled mixture thinly enough on the crystal to get sufficient transmission, it was hard to see spectral evidence of the wood particles.

Viscosity The viscosities of the neat Resin 105 and Hardener 206 were determined in a Brookfield LVTDCP digital cone-and-plate viscometer at 25 °C.

Differential Scanning Calorimetry Results

The differential scanning calorimetry (DSC) data in Table B-1 show that Douglas-fir wood flour, added as one part per six parts mixed resin, did not have an effect on peak temperatures, and thus did not by itself reduce reactivity. Asbestos, however, lowered the temperatures at which maximum reaction occurred, especially at the lower heating rates. The temperature dependence of reactivity was not affected greatly. Activation energies (in kcal/mol) were 54.8 for the mixture of just resin and hardener, 57.6 for wood flour added to the mixture, and 52.3 for the mixture of asbestos-filled resin and hardener. These are in the range seen in many previous studies of diglycidyl ether of bisphenol A (DGEBA) reactions with amines (see Dutta, 1979). However, there has been some recent criticism of constant temperature rate-increase experiments to evaluate epoxy cure (Schiraldi, 1983).

The Douglas-fir wood flour was essentially dry. According to Stark et al (1985), water in some epoxies can accelerate the curing reaction, and Mahoney (1986) has found that high moisture contents in uncured epoxy components can lower modulus and glass transition values of eventual (higher temperature) cured resins. The laminated veneer used to make the wood/epoxy composite should not have had a high moisture content.

Fourier-Transform Infrared Spectroscopy Results

The infrared spectrum of Resin 105 is shown in Figure B-1, and that of Hardener 206 is shown in Figure B-2. A series of difference spectra from an epoxy mixture of the resin and hardener compared between sequential cure times showed changes of intensity for several bands over a 22-day period. Bands with center wavenumbers at 750, 850, 1,010, and 1,150 cm^{-1} decreased primarily during the first hour, while bands at 865, 916, and 1,030 cm^{-1} decreased at a decelerating rate over the first day. The most dramatic changes were increases of bands at wavenumbers 1,180, 1,250, and 1,510 cm^{-1}, developing over a period of weeks. Two bands, at 830 and 1,610 cm^{-1}, did not show substantial increases until after 3 days. At the other end of the spectrum of the epoxy mixture, a broad peak at 3,400 cm^{-1} started increasing after 3 hours.

The spectra from the mixture originally containing about 14 percent wood flour (Fig. B-3) did not show any bands that were not seen in the epoxy. In this case, in which the sample and mount were moved as a unit, the difference spectra show the greatest intensity decreases (in order) at wavenumbers 850, 916, 750, 1,010, 1,030, and 1,150 cm^{-1}. Smaller absolute, broader changes occurred in the 3,000 to 3,700 cm^{-1} N-H and O-H stretching region. In this case the changes at 1,510 and 1,250 cm^{-1} were much smaller.

The transmission infrared spectroscopy results show that the oxirane ring peak at 916 cm^{-1} (O'Brien, 1968), characteristic of an unreacted epoxy, decreases substantially with cure time, compared to the constancy of the phenyl aromatic ring peak at 1,582 cm^{-1}. The plot in Figure B-4 shows the ratio of these two absorbances (A_{916}/A_{1582}) versus the logarithm of cure

time for the mixture which originally contained wood. From the spectra of Resin 105 and Hardener 206 (Figs. B-1 and B-2), the ratios (A_{916}/A_{1582}) in those components were 1.784 and 0.948, respectively. By a simple law of mixtures, these should give an unreacted (time = 0) mixture ratio of 1.645. This reaction was effectively finished within 24 hours, but there was still a noticeable peak at 916 cm^{-1}, indicating that epoxy groups were not all reacted.

Viscosity Test Results

The measured viscosities of the epoxy components were 502 cP for Resin 105 and 355 cP for Hardener 206. The measured resin viscosity was at the bottom of the manufacturer's stated range while the hardener viscosity was slightly above the top of its stated range.

Summary of Chemical Reaction Characterization

1. Wood, in the form of a dry flour dispersed in resin within a capsule, does not affect the curing reactivity of the epoxy resin during a temperature-scanning curing procedure.

2. Asbestos has a slight accelerating effect on cure rate, for the already viscous asbestos-filled resin. This very viscous system would not allow air bubbles to move out of the resin quickly.

3. The reaction of the epoxy oxirane rings has effectively ceased by the end of the first 24 hours, but some other reactions continue for many days afterward.

Recommendations

1. Effect of Moisture on Cure

The effect of moisture on cure was not checked. Moisture in the much more massive wood members could diffuse into the epoxy resin nearest the wood and interfere with cure there. The possibility of cure inhibition could be checked by conditioning wood to several different moisture contents, bonding, and then determining the bond strengths. Curing epoxy films in controlled humidity chambers for set periods of time and then determining their level of cure by DSC scanning experiments could also show moisture inhibition of cure.

2. Reinforcement of Weakened Wood Surfaces

Some researchers have considered it essential to phenolic wood bonding that the phenolic molecules penetrate to a depth of 4 to 8 cell wall diameters. This penetration serves to provide a mechanical interlocking grip on the wood and to reinforce the wood cells that are inevitably damaged when the wood surface is created or later prepared. It may be that the bulky,

mostly hydrophobic epoxy molecules do not penetrate the cell walls and, therefore, cannot perform as do the phenolics. This might be corrected by first applying a primer of a low-molecular-weight room-temperature curing phenol-resorcinol-formaldehyde resin to penetrate the cell walls and start curing before the bondline-filling epoxy is applied. One must be cautious, however, in using these low-molecular-weight components because of potential health hazards.

A low-molecular-weight aliphatic diepoxide could also be tried as a primer. The previous use of poly (ethyleneimine) as a primer may be an attempt to find a hydrophilic material which can penetrate into and hydrogen-bond well to wood, while still having the amine structures with which epoxy groups can react easily.

There is no information, at least of which we are aware, on whether epoxy resin has been shown to penetrate into the cell walls of wood fibers. Research by Roger Rowell at the Forest Products Laboratory has shown that the lowest molecular weight (gaseous) epoxides (alkylene oxides) will go into the cell wall and react there. However, in working with isocyanates Rowell found that only the lowest molecular weight species diffuse readily into the cell wall, not the species containing an aromatic ring, especially as more groups are attached to that ring. It might be worth while to determine whether epoxy molecules, usually based on the much larger starting molecule bisphenol A, do actually penetrate the wood cell walls. It might be necessary to use a "tagged" model epoxy molecule, e.g., one containing a chlorine atom, so that these molecules can be detected by EDXA (energy dispersive x-ray analysis) during electron microscopy of microtomed wood sections previously impregnated.

It is possible that viscosity increase of the epoxy mixture hinders penetration of the mixture into the cell walls, if penetration is at all possible. A way to get at the effect of viscosity changes with time could be to apply resin and quickly bond a number of wood samples at various intervals after an epoxy is mixed. Subsequently, these could be mechanically tested and analyzed for penetration to determine bonding time limitations.

To get a better handle on cure at room temperature and normal moisture contents, reactivity studies could be performed on samples which are mixed early in the day and from which samples are quickly taken for separate DSC capsules. As cure progresses in the epoxy during the day, capsules can be selected at various curing times for testing in the differential scanning calorimeter. The area of the exotherm will be a measure of residual reactivity, which should decrease with increasing room temperature cure time. The literature indicates that room temperature will never give as full a cure as an elevated temperature, but an asymptote should be reached. If the DSC can be run at temperatures well below freezing, one could start at a low temperature for each sample and detect the glass transition (glassy-to-rubbery transition) too, which is also a function of cure.

Literature Cited

Duswalt, A. A.: The practice of obtaining kinetic data by differential scanning calorimetry. Thermochim. Acta 8: 57-68; 1974.

Dutta, A.; Ryan, M. E.: Effect of fillers on kinetics of epoxy cure. J. Appl. Polym. Sci. 24: 635-649; 1979.

Mahoney, C. L.: Design of moisture resistant adhesives. Presented at the Ninth Annual Adhesion Society Meeting, Hilton Head, SC, February 9-12, 1986.

O'Brien, R. N.; Hartman, K.: An ATR infrared spectroscopy study of the epoxy-cellulose interface. Proc. Am. Chem. Soc., Div. Org. Coat. Plast. Chem. 28(2): 236-45; 1968.

Prime, R. B.: Thermosets, in Turi, E. (ed.) Thermal characterization of Polymeric Materials. New York: Academic Press; 1981: 435-569.

Schiraldi, A.; Baldini, P.: Epoxy polymers. Use and misuse of nonisothermal DTA and DSC in the study of the curing process. J. Therm. Anal. 28: 295-302; 1983.

Stark, E. B.; Ibrahim, A. M.; Munns, T. E.; Seferis, J. C.: Moisture effects during cure of high-performance epoxy matrices. J. Appl. Polym. Sci. 30: 1717-31; 1985.

Streib, W. C.: Asbestos. In: Kirk-Othmer Encyclopedia of Chemical Technology. 3d ed. Vol. 3. New York: John Wiley & Sons; 267-283; 1978.

Table B-1--Calorimetric analysis of the epoxy curing reaction

Heating rate	Peak temperature (corrected)	Correlation coefficient	Activation energy
°C min^{-1}	°C		KJ mol^{-1}
	Epoxy 105 + 206 (Aluminum Capsules)		
10	99		
20	113	1.000	54.8
40	129		
	Epoxy Plus Wood Flour (Aluminum Capsules)		
10	100		
20	113	0.999	57.6
40	129		
	Epoxy Plus Asbestos (LVCs)		
5	83		
10	93		
20	109	0.992	52.3
40	127		

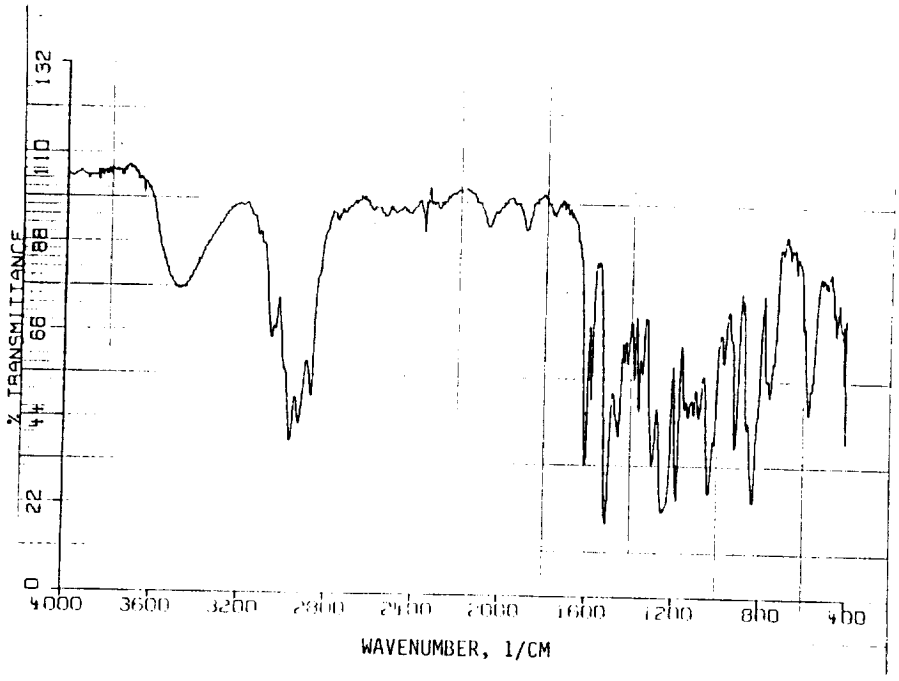

Figure B-1. - Infrared spectrum of Epoxy Resin 105, neat, on a KBr crystal.

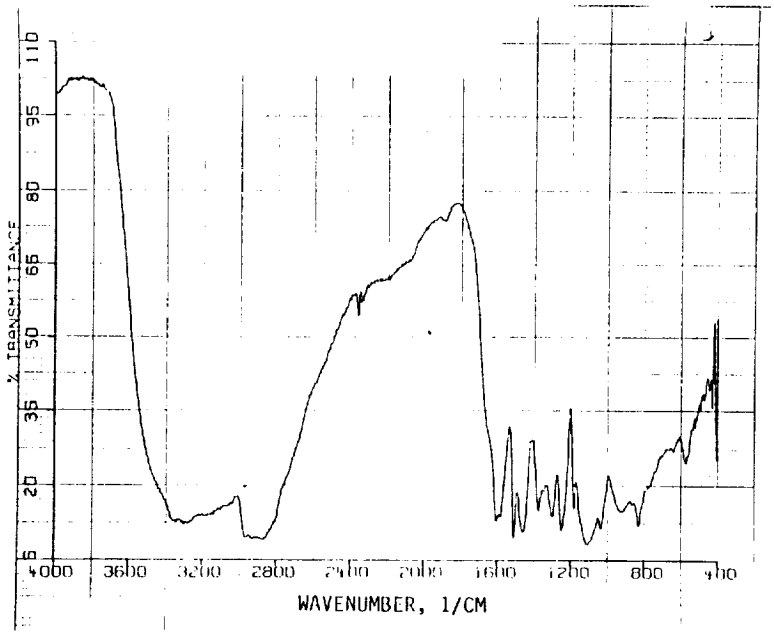

Figure B-2. - Infrared spectrum Epoxy Hardener 206, neat, on a KBr crystal.

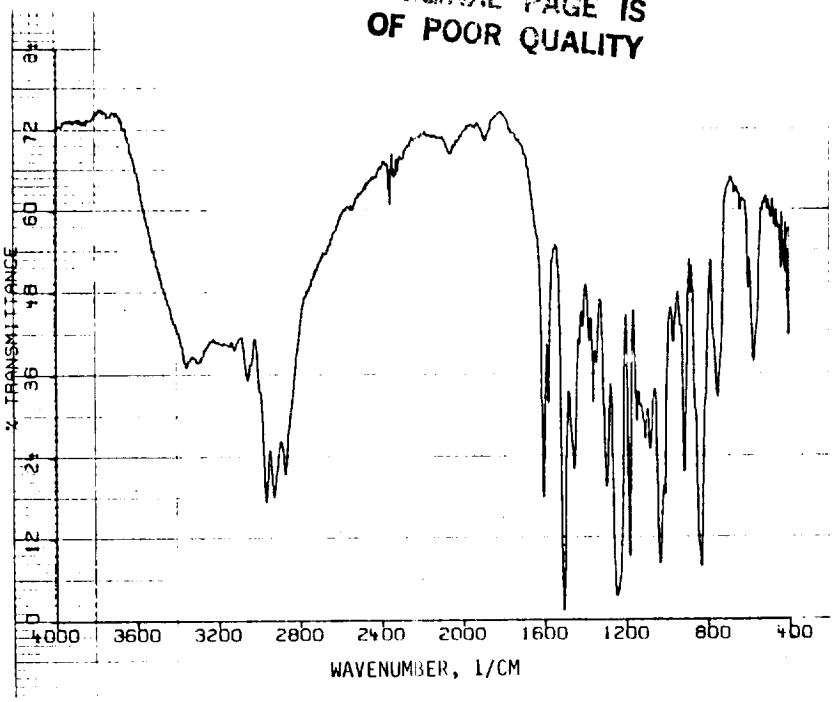

Figure B-3. - Infrared spectrum of a resin/hardener epoxy mixture containing 14 percent wood flour.

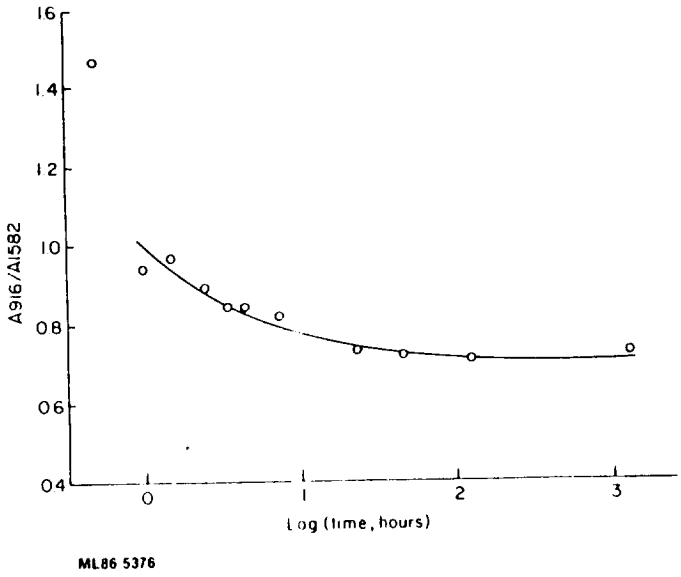

Figure B-4. - Effect of the logarithm of cure time on the ratio of infrared absorbances corresponding to an oxirane ring band and an internal thickness band.

APPENDIX C

ADHESIVE/ADHEREND MECHANICAL PROPERTY CHARACTERIZATION

Introduction

Seven types of mechanical tests were conducted to gain information about the mechanical properties of the WEST epoxy and the interaction of this epoxy with the Douglas-fir laminate used in the fatigue test article. Most of the tests were adaptations of existing ASTM standard tests. Some were innovative tests designed to challenge hypotheses about the Douglas-fir/WEST epoxy material or the 12-inch 1:10-slope finger joint. The following list summarizes the seven test types and the specimens tested within each type:

1. Mode I Fracture Toughness (Tapered Double-Cantilever Beam)
   a. Aluminum-to-aluminum (ASTM D 3433)
   b. Wood-to-Wood, 90 deg grain angle (adapted from ASTM D 3433)
   c. Wood-to-Wood, 6 deg grain angle (adapted from ASTM D 3433)

2. Mode I Fracture Toughness (Compact Tension)
   a. 90 deg grain angle (adapted from ASTM D 399)
   b. 6 deg grain angle (adapted from ASTM D 399)

3. Mode II Fracture Toughness
   a. Notched short beam, 6 deg grain angle
   b. Modified-rail, 6 deg grain angle (adapted from ASTM D 4027)

4. Tensile Strength and Modulus (Cast Film)
   a. Thin film (adapted from ASTM D 638)
   b. Thick film (adapted from ASTM D 638)

5. Tensile Strength and Modulus (Bondline)
   a. Metal-to-metal
   b. Wood-to-wood

6. Shear Strength and Modulus
   a. Thick adherend, steel (adapted from ASTM D 3983)
   b. Thick adherend, Douglas-fir parallel laminated veneer (adapted from ASTM D 3983)
   c. Thick adherend, hard maple (adapted from ASTM D 3983)

7. Combined Shear and Tension in Scarf Joints
   a. Scarf joint, feathered tips
   b. Scarf joint, 1.6-mm tip
   c. Scarf joint, 3.2-mm tip

The geometry of these test specimens is illustrated in Figure C-1, showing grain direction where important. Each test series is discussed separately in

the following sections, and conclusions and recommendations are then given, based on all the test results.

Test Series 1. - Mode I Fracture Toughness (Tapered Double-Cantilever Beam)

The wood-to-wood tapered double cantilever beam specimens in this test series were made by bonding two 6- by 13- by 280-mm pieces of Douglas-fir laminate with the WEST epoxy (Fig. C-2). The edges of the veneer (the 13- by 280-mm surfaces) were bonded. Bondline thickness was controlled at approximately 0.5 mm by the use of shims placed at the ends of the bondline. This double laminate was then bonded between two tapered hard maple beams to form the tapered double cantilever beam specimen (Ebewele et al. 1980).

The strain energy release rate of the WEST epoxy bondlines was determined by the equation:

$$G_{I_c} = \frac{P_c^2}{2b} (dC/da)$$

in which

G_{I_c} strain energy release rate at crack propagation load

P_c load at crack propagation

b thickness perpendicular to directions of crack growth and load

dC/da rate of change of specimen compliance, C, with respect to crack length, a

The compliance (load point displacement/load) and rate of change of compliance were determined at several crack lengths during the progress of each test. The average dC/da for the specimens tested was 0.0000115 mm/N for 6 deg grain-angle specimens and 0.0000098 mm/N for 90 deg grain-angle specimens. Table C-1 lists the strain energy release rates of joints bonded with the WEST epoxy, based on the calibration values for dC/da and the average loads at crack propagation.

Table C-1

Strain Energy Release Rates of WEST Epoxy Bondlines

Joined Materials	Grain/bondline angle, deg	Strain energy release rate, J/m^2
Aluminum	---	366
Douglas fir laminate	6	382
Douglas fir laminate	90	264

A tearing type of load-deflection curve was obtained with all three types of joints. A tearing failure is characterized by little difference between the crack initiation and crack arrest loads. This indicates that the WEST epoxy is not a brittle adhesive, in comparison to phenol-resorcinol which has quite large differences in crack initiation and arrest loads. The 6 deg grain-angle wood-to-wood joints and the aluminum-to-aluminum joints produced approximately the same toughness values (366 and 382 J/m^2), although the types of failure were quite different. The fracture surfaces of 6 deg grain-angle wood specimens included quite a lot of fractured wood (Fig. C-2(a)). The aluminum joint failure surfaces were at the metal/epoxy interface (or in the epoxy adhesive very near the interface) with no cohesion failure in the bulk adhesive layer.

The 90 deg grain-angle wood-to-wood joints produced lower toughness values. No wood failure occurred nor was any expected. Fracture occurred at the interface, but the fracture surface jumped back and forth from one adherend to the other. This erratic crack growth path was related to the crack tip encountering the changing density of earlywood and latewood as it progressed (Fig. C-2(b)).

The observed values obtained for WEST epoxy joints are within the range of 100 to 1,000 J/m^2 reported for another wood-epoxy system (Sasaki and Walsh, 1977; Takatani and Sasaki, 1980; and Hamada and Takatani, 1980). The fracture toughness of an unmodified (brittle) room-temperature cured system was 200 J/m^2. The addition of 20 parts of a flexibilizer (toughening agent) raised the toughness to 300 J/m^2, which is within the same range as that measured for the WEST epoxy. This suggests that the WEST epoxy is a toughened formulation. Takatani and Sasaki found that toughness was not dependent on bondline thickness at 20 parts flexibilizer. But at 40 and 60 parts of flexibilizer, toughness was strongly dependent upon bondline thickness, increasing from about 300 J/m^2 at 0.1 mm thickness to 1,000 J/m^2 at 1.5 mm thickness.

Hamada and Takatani found that the addition of 20 parts of flexibilizer increased bending fatigue life in thin bondlines (compared to joints made with unflexibilized epoxy) but reduced it somewhat in thicker (0.75 to 1.5 mm) bondlines. Higher levels of flexibilizer reduced fatigue life in all bondline thicknesses (again compared to joints made with unflexibilized epoxy), and the

effect increased with the amount of flexibilizer. The relationships revealed by Takatani and Sasaki, i.e. greater toughness with increasing flexibility and bondline thickness, seem in contradiction to the shorter fatigue life under the same conditions found by Hamada and Takatani. Nevertheless it is evident that crack-growth resistance of wood epoxy joints is quite dependent upon the amount of flexibilizer and bondline thickness.

The fatigue test beam was intended to have a bondline thickness of 0.38 mm in the finger joints, but the actual bondline thickness was in the range of 0.05 to 0.22 mm, as reported in Appendix A. It is possible that better performance could be obtained in the test-article finger joints after careful study of the interactions of the flexibilizer level and bondline thickness in the Douglas-fir/WEST epoxy laminate system.

Test Series 2. - Mode I Fracture Toughness (Compact Tension Specimen)

Compact tension specimens were cut from 13-mm by 25-mm by 250-mm panels of the Douglas-fir laminate (Fig. C-3). The surface for bonding was the 13-mm by 250-mm edge of the panel, which is formed by the edges of the veneers. In one set of specimens these edges are the radial-longitudinal wood surface (side grain), while in the second set of specimens the edges are the radial-tangential surface (end grain). Pieces of polyvinylidene fluoride film were placed in the bondline at specific locations to act as crack starters. Three specimens were cut from each bonded panel. Specimens were made with ratios of crack length to bond length, a/w, of 0.4, 0.5, 0.7, and 0.8.

The critical stress intensity factor of the compact tension specimens was calculated by the following equations:

$$K_{I_c} = \frac{P_c}{b\, w^{0.5}}\, Y$$

and

$$Y = 29.6 - 185.5(a/w) + 655.7(a/w)^2 - 1{,}017(a/w)^3 + 639.8(a/w)^4$$

in which

K_{I_c} critical stress intensity factor
P_c load at crack propagation
b specimen thickness
w distance from the load point to the end of the specimen
Y factor for load and specimen geometry
a crack length measured from the point of loading.

Table C-2 summarizes the critical stress intensity factors determined by averaging the results for two specimens at each of several crack lengths.

Table C-2

Critical Stress Intensity Factors for WEST Epoxy Bondlines

Specimen type	K_{I_c}, $(N/mm^2)\ mm^{0.5}$			
	Crack length, mm			
	20	25	36	41
Side grain (6 deg grain angle)	15.0	15.9	12.3	12.0
End grain (90 deg grain angle)	19.2	22.5	26.8	18.5

In the side-grain orientation, specimens with small cracks had higher fracture toughness than those with large cracks, while in the end-grain orientation the middle-size cracks produced the highest toughness. The values obtained with these compact tension tests are comparable to values reported by Ruedy and Johnson (1978, Fig. 13). These investigators showed critical stress intensity factors for Southern pine/epoxy bondlines of 0.5 $kPa\text{-}m^{0.5}$ for edge-grain joints and 0.9 $kPa\text{-}m^{0.5}$ for end-grain joints. These values convert to 15.8 and 28.4 $(N/mm^2)\ mm^{0.5}$ for edge- and end-grain joints, respectively.

Test Series 3. - Mode II Fracture Toughness

Neither the short beam shear nor the modified-rail shear tests were successful. Lathe checks in the veneer caused the specimens to fail outside the bondline, so valid critical loads were not obtained. Further work is suggested in this area with improved specimen designs, possibly using sawn veneers instead of rotary peeled veneers.

Test Series 4. - Tensile Strength and Modulus (Cast Film)

Twelve dogbone-shaped specimens in two thicknesses were made in the shape of the standard ASTM D 638 specimen for the measurement of the tensile properties of plastics. The thickness of the thin specimens tested averaged 0.20 mm. The thick specimens had an average thickness of 2.6 mm. Tensile elongation was measured with an LVDT extensometer over a 25.4-mm gage length centered in the necked-down portion of each specimen. No plastic deformation was evident in any of the tensile load-elongation curves. An attempt was made to determine the Poisson's ratio of the WEST epoxy on two of the thick specimens by measuring lateral strain using foil strain gages attached at the center of the longitudinal extensometer gage length. However, this procedure did not work satisfactorily.

Table C-3 summarizes the results of the modulus and tensile strength measurements made with cast film specimens of the WEST epoxy. Both average properties and ranges of the experimental data are given.

Table C-3

Tensile Properties of Cast WEST Epoxy Film

Specimen thickness, mm	Cross-sectional area (aver.) mm^2	Tensile modulus MPa (a)	Tensile strength MPa
0.20 (0.15-0.25)	0.20	2,590 (1,380-3,800)	29 (20-44)
2.54 (2.3-2.9)	32.3	3,030 (2,110-3,800)	33 (29-36)

(a) Convert MPa to psi by multiplying by 145.

The thin film tensile properties were more variable than the thick film properties due to poorer control of thin film thickness during casting and a greater sensitivity of the adhesive to flaws in the thin films.

The average measured tensile modulus values are somewhat lower than the value of 3,230 MPa given in the GBI WEST epoxy data sheet. The measured tensile strengths are much lower than the data sheet value of 62 MPa. These differences are probably due to greater porosity in the specimens in this test series. Adhesive film strength is sensitive to the effect of bubbles or flaws which were prevalent in these specimens. In each thick specimen the fracture passed through (and possibly originated at) a bubble that was much larger than the background matrix of bubbles. Only fine bubbles were observed in the unmixed resin, so it is probable that the large bubbles were introduced when the hardener was mixed in.

Test Series 5. - Tensile Strength (Bondline)

Cross-lap maple specimens were made by bonding the intersection of the 25- by 50-mm faces of two maple blocks (Fig. C-4(a)). Maple block surfaces were lightly sanded with 320 grit before bonding. One set of maple blocks was bonded with the standard unfilled epoxy precoat, and one set was bonded without the precoat. Bondline thickness was controlled by shims to about 0.5 mm.

Metal-to-metal specimens were made by bonding 25-mm aluminum cubes or 16- by 25- by 50-mm maple blocks (Fig. C-4(b)). The bonding surfaces of the aluminum cubes were masked to limit the bonded area to 12.5 mm by 12.5 mm.

The WEST epoxy bondlines were cured for 6 days at room temperature before testing. The aluminum specimens were pulled apart by loads applied through

shear pins passing through the cubes. The maple specimens were pulled apart by fixtures which hook the ends of the blocks extending beyond the bonded lap area.

Table C-4 gives the average bondline tensile strengths of 4 metal-to-metal and 10 wood-to-wood test specimens.

Table C-4

Tensile Strength of WEST Epoxy Bondlines

Specimen Type	Tensile strength MPa
Aluminum-to-aluminum	11.5
Maple-to-maple, with precoat	3.7
Maple-to-maple without precoat	3.6

By comparing the results given in Tables C-3 and C-4, it can be seen that the tensile strength of the WEST epoxy adhesive in an aluminum-to-aluminum bondline is only 35 to 40 percent of the tensile strength of the adhesive in film form. Failure was at or near the aluminum/epoxy interface. There was no appreciable cohesive failure. The tensile strength of WEST epoxy bond lines in wood specimens was found to be roughly one-third of the tensile strength of bondlines in the metal specimens and about 12 percent of the tensile strength of WEST epoxy film.

Some bondlines in wood specimens exhibited slight amounts of shallow wood failure (less than 10 percent), but there was no appreciable cohesive failure in the epoxy in any of the three types of specimens. The predominate mode of failure was separation either at the interface between the wood and the adhesive or in weak boundary layer in the adhesive very near this interface (Fig. C-4(a)). Differences in tensile strength among the three specimen types are due to differences in adhesion, boundary layer effects, specimen geometry, and methods of loading. However, the type of failure observed in the maple specimens is typical of epoxy butt joints in dense wood. Such joints will not develop the tensile strength of the adhesive and certainly not the tensile strength of the wood.

Test Series 6. - Shear Strength and Modulus

Three types of thick adherend specimens were prepared for measuring the shear strength and modulus of the WEST epoxy adhesive: (1) Steel, (2) Douglas-fir laminate, and (3) solid hard maple. A Douglas-fir laminate specimen is shown in Figure C-5(a). Bondline thicknesses were measured with a linear traversing recording microscope and ranged from 0.5 to 1.0 mm. Most of

the specimens were made with a 10-mm overlap, and a few wood specimens were made with 20-mm and 30-mm overlaps. Specimens were loaded at a 1 mm/min crosshead speed. The measured shear properties are summarized in Table C-5 and typical fracture surfaces are shown in Figures C-5(b) and (c).

Table C-5

Average Shear Properties of WEST Epoxy Bondlines in Thick Adherends

Adherend (cure time)	Specimen thickness, mm	Overlap mm	Bond area, mm^2	Shear modulus, MPa	Shear strength MPa	Failure strain Δ	Failure type (a) (Δ)
Steel (6 days)	0.70	10	200	790	25	19	C(75)
Steel (20 days)	0.66	10	200	1,010	31	16	A(60)
Douglas fir laminate (6 days)	0.62	10	200	130	9.2	10	W(47)
Douglas fir laminate (20 days)	0.81	10	200	120	8.7	11	W(65)
Hard maple (6 days)	0.88	10	200	210	9.0	6	A(97)
Hard maple (6 days)	0.59	20	400	153	7.3	7	A(100)
Hard maple (6 days)	0.74	30	600	217	6.0	6	A(100)

(a) A = adhesive failure at epoxy/adherend interface
C = cohesive failure within epoxy
W = wood failure
Percentages are estimates based on visual examination.

Shear modulus and strength measured with the steel specimens increased with increasing cure time while failure strain decreased somewhat. The failure type after 6 days of cure was predominately cohesive within the epoxy layer (Fig. C-5(c)), while the failure type after 20 days was predominately adhesive. The stress-strain curves at both cure times exhibited a great deal of plastic strain before failure. A different effect of cure time is noted in Table C-5 with specimens made of Douglas-fir laminate. Both modulus and strength decreased with longer cure time, but only slightly.

The significant fact is that the shear modulus and strength of the WEST epoxy adhesive layer measured by means of the Douglas-fir laminate specimens are much lower than those measured by means of the steel specimens. Shear modulus is 84 to 88 percent lower, depending on cure time, while shear strength is 63 to 72 percent lower. The difference in modulus could be an artifact caused by deformation of the wood adherends. Deformation of the adherends, when added to the deformation of the adhesive layer, would make the adhesive appear less rigid.

The shear modulus test method is thought to be accurate (according to the theory upon which it is based) as long as the tensile modulus of the adherends exceeds the shear modulus of the adhesive by a factor of 300. In the present case, if the adhesive shear modulus actually is 1,000 MPa (as measured by the steel adherends) then accurate results cannot be expected using Douglas-fir or maple adherends because the ratio of the two moduli is only about 13.

The differences in strength could be due to the relative weakness of the Douglas-fir laminate. The failure surface of the Douglas-fir specimens was typically 50 percent or more wood (Fig. C-5(b)). However, there are other possi- bilities. First, it is possible that the adhesive does not adhere to the wood as well as to the steel, and second, the wood may somehow inhibit the curing reaction of the epoxy.

Specimens were made with hard maple adherends to study the effects of lathe checks, adherend properties, and stress concentrations upon the measured adhesive properties. The tensile modulus of the maple is about the same as that of the Douglas-fir laminate, but maple's shear strength is about 60 percent higher. Thus, the adhesive can be stressed to a higher level with maple than with Douglas-fir laminate adherends. The maple adherends were sawn from solid wood rather than laminated veneer, to eliminate lathe check effects. Specimens were made with 10-, 20-, and 30-mm lap lengths to vary the stress concentration at the ends of the laps. As shown in Table C-5, maple specimens produce the same shear strength as the Douglas-fir specimens (about 9 MPa) with the same 10-mm lap length. The failure surface of the strongest maple specimen was more than 50 percent in the wood.

Maple specimens with longer lap lengths produced progressively lower strengths, as expected from knowledge of the behavior of single lap joints, with little or no wood failure. This indicates the sensitivity of the wood/adhesive interface or the boundary layer of the adhesive to the increased stress concentration in the longer lap specimens. Adhesive modulus did not change significantly with increasing lap length, and it should not if the specimen is properly designed. However, the modulus values measured with the maple specimens were 56 percent higher than the values measured with the Douglas-fir laminate specimens. Since the two woods have about the same stiffness it is unlikely that the adherend stiffness causes this difference. Maple is much stronger in shear but since modulus is measured at stress levels well below failure it is unlikely that difference in wood strength causes this difference. The results suggest (but do not prove) there is a species effect on epoxy bond strength and modulus. They suggest (but do not prove) that the

inferior shear strength and shear modulus, as measured with wood adherends, is due to the wood interfering with the cure of the WEST epoxy.

The results of the chemical characterization (Appendix B) do not support the results of the mechanical tests which show some species- and wood-related changes. These thoughts are offered to explain this inconsistency:

1. The bulk wood used for the mechanical studies, with its moisture and greater reservoir of extractives, could be affecting the cure of epoxy in a way that the Douglas-fir wood flour, in a smaller mass ratio to resin, did not in the chemical characterization tests.

2. The maple might be more receptive to resin than Douglas-fir and thus allow more impregnation. Perhaps this stiffens the interfacial region between the two different adherends and transfers stress more effectively.

3. Maybe there is a difference because of the type of test itself, a factor which has not been encountered before.

Test Series 7.- Combined Shear and Tension in Scarf Joints

Tensile strip specimens (Fig. C-1(b)) were made with Douglas-fir laminate to represent one side of a full scale finger in the splice in the fatigue test beam. The finished specimens were 12.5 mm by 35 mm in cross section by approximately 700 mm long. Length varied slightly with the geometry of the tips of the scarf joint. The joints ran diagonally across the 35- by 700-mm face with a 1:10 slope.

Three tip geometries were used to evaluate tip shape effects on the strength of the joint. The first set of joints was made with the scarf drawn out to a feathered tip. The second set was made with a blunt tip 1.6-mm wide, which is one-half the proportionate width of the finger tips in the actual test beam. The third set of specimens was made with blunt tips 3.2-mm wide, in the same proportions as the test beam. In addition to the different finger tip geometries, some specimens were made with a bit of polyvinylidene fluoride film at the tips to act as an initial flaw or crack starter. The specimens were loaded in tension through a Templin wedge-action grip, at a cross head speed of 1.0 mm/min. The results of these tension tests are given in Table C-6.

Table C-6

Tensile Strength of Scarf Joint Specimens

Tip width mm	No of specimens	Average strength MPa	Std. deviation MPa	Joint efficiency (b) percent
a. Without crack starters				
Feathered	1(a)	75	---	80
1.6	3	56	8.9	60
3.2	6(a)	42	5.7	45
b. With crack starters				
Feathered	3(a)	50	2.1	53
1.6	4	51	5.3	54
3.2	8	34	5.0	36

(a) Failure in one specimen initiated at grip in response to crushing by grip (Fig. C-10).
(b) Based on an unjointed laminate strength of 94 MPa (unpublished data from GBI).

The effectiveness of a finger joint is typically expressed as a joint efficiency, which is the percentage of the unjointed-wood strength which can be obtained with the finger joint. There are numerous factors determining the efficiency of finger joints, including the length of the fingers, the thickness of the base (pitch), the slope of the bond, and the thickness of the tip. Satisfactory joints are usually obtained if the effective bond area determined by the pitch and the length is 8 to 10 times the cross-sectional area of the member, and if the slope is less than 1:10. Tip thickness should be as small as possible for maximum performance (Selbo, 1963; Jokerst, 1982). With these guidelines and under proper bonding conditions finger jointed wood can achieve 70 percent of the strength of the unjointed wood.

Unpublished test data from Gougeon Brothers Inc. (GBI) gives an average tensile strength of about 94 MPa for unjointed Douglas fir/epoxy laminated material when the tested volume is the same as that of the scarf-jointed specimens in this test series. As shown in Table C-6, using 94 MPa as a basis, average joint efficiencies for the scarf-jointed specimens ranged from a high of 80 percent for feathered tips without crack starters to a low of 36 percent for wide tips with crack starters. For tests without artificial crack starters, the joints with fully-feathered tips met or exceeded the 70 percent efficiency level typical of acceptable finger joints. However, specimens with tips proportional to those in the fatigue test beam (3.2-mm wide) had joint efficiencies that averaged only 45 percent. This is well below the 70 percent which is considered acceptable.

The dimensions of the fingers in the splice in the fatigue test beam appear to have been scaled up from the dimensions of smaller joints commonly used in the manufacture of glued and laminated structural beams. The scaled-up joint satisfies the criteria for bond area ratio (8:1 to 10:1) and for slope (less than 1:10), but it has very wide finger tips (6 or 7 mm compared to 1 mm in commercial laminated beams). This test series demonstrated the very strong effect of tip thickness upon the strength of the joints. The introduction of a 3.2-mm tip reduced average efficiency by 35 percent from that of a fully-feathered tip. It is certainly not sufficient to simply scale up a conventional finger joint to a very large size. Even when the area ratio and the slope are maintained in their acceptable ranges, tip thickness is a controlling factor in joint strength and must be maintained at a minimum level (Jokerst, 1982).

The large stress concentration at a broad tip causes it to be the point of crack initiation, as was observed in tests sponsored by GBI at the University of Dayton (Anonymous 1983). It should be noted that the specimens tested at the University of Dayton had a maximum tip thickness of only 2 mm, much narrower than the 6- or 7-mm wide tips in the fatigue test beam. Once a crack starts it easily travels along the wood-adhesive interface (or weak adhesive boundary layer) as was observed in the failed full-scale test beam (Fig. C-6(a)) and in the present half-finger tests. The insertion of a crack starter lowers strength regardless of the finger tip geometry, but it has the most pronounced effect on the strength of specimens with fully-feathered tips, as shown in Table C-6.

Analysis of Fractured Surfaces

Douglas-fir is a coarse-textured softwood, meaning that it has zones of tissue differing greatly in density. These zones are the earlywood and latewood. Although the average specific density for the species is 0.48, the specific densities of the two tissues are in the range of 0.28 to 0.39 for earlywood and 0.84 to 1.09 for latewood (in the oven-dry state; Quirk, 1984). With common wood bonding adhesives, both the joint strength and percentage of wood failure decline when the specific gravity increases above 0.80 (Chow and Chunsi, 1979). The WEST epoxy adhesive (and epoxy adhesives in general) develops enough adhesion strength to fail the lower density earlywood but not enough to fail the high density latewood.

A typical epoxy joint fracture surface in high density wood, regardless of the specimen geometry or mode of loading, consists of fractured earlywood cells and adhesion or boundary layer failure in the adhesive adjacent to the latewood cells (Fig. C-6(b)). Of course with rotary-cut veneer such as that used in the GBI Douglas-fir laminate, there are latewood failures where the wood has been prefractured during the veneer cutting operation (lathe checks) or where the earlywood underlying the latewood is fractured. In all of the mechanical property tests conducted in this investigation, cohesive failure of the WEST epoxy was the principal failure mode only in the steel thick-adherend shear tests (Fig. C-5(c)) and, of course, in the tensile film tests. The bubbles characteristically observed in the adhesive layer may reduce the

bondline stiffness, but they do not manifest themselves as a major component on the fractured surfaces.

Conclusions

Based on these results it appears that the premature failure of the finger joints in the large test beam under fatigue loading was due to two factors:

1. High stress concentrations at the blunt finger tips.

2. Limited adhesion to, or limited adhesive strength development adjacent to the wood surface, particularly the latewood surface. This ensured joint failure at stress levels below the bulk adhesive's yield stress. When failure occurs below the yield stress, the adhesive's ability to arrest crack growth through the absorption of plastic strain energy is minimized.

Recommendations

1. Redesign fingers to a shorter length and narrower finger tips (no wider than 1.6 mm), while maintaining the proper bond area and slope (Jokerst, 1982; Selbo, 1963).

2. Experiment with wood surface primers other than the unfilled WEST epoxy previously used as a precoat, to improve adhesion to the dense latewood. Good success has been obtained using a polyethyleneimine solution as a primer for Douglas-fir before bonding with epoxy (Caster, 1980).

Literature Cited

American Society for Testing and Materials.: Standard practice for preparation of metal surfaces for adhesive bonding. Designation D 2651-79, Annual Book of ASTM Standards, Volume 15.06; 1985a.

American Society for Testing and Materials.: Test method for tensile properties of plastics. Designation D 638-82a, Annual Book of ASTM Standards, Volume 08.01; 1985b.

Anonymous.: An evaluation of the static and cyclic performance of finger joints in Douglas-fir/epoxy laminate material. Report No. UDR-TR-83-49. Report to Gougeon Bros. Inc. by Structural Test Laboratory Group, Experimental and Applied Mechanics Division, University of Dayton Research Institute, Dayton, Ohio; 1983.

Caster, D.: Correlation between exterior exposure and automatic boil test results. In: Proceedings of symposium "Wood Adhesives--Research, Application, and Needs," Madison, WI. Sponsored by the U.S. Forest Products Laboratory, Madison, WI, and Washington State University, Pullman, WA; 1980.

Chow, S.; Chunsi, K. S.: Adhesion strength and wood-failure relationship in wood-glue bonds. Mokuzai Gakkaishi 25(2): 125-131; 1979.

Ebewele, R. O.; River, B. H.; Koutsky, J. A.: Tapered double cantilever beam fracture tests of phenolic-wood adhesive joints. Wood and Fiber 12(1): 40-65; 1980.

Hamada, R.; Takatani, M.: Studies on epoxy resin adhesives for wood. Kinki Daigaku Nogakubu Kiyo 14: 127-136; 1980.

Jokerst, R. W.: The effect of geometry on the performance of structural finger joints. In: Prins, C.F.L., ed. Production, marketing and use of finger jointed sawnwood: Proc. of an International Seminar Organized by the Timber Committee of the United Nations Economic Commission for Europe, Hamar, Norway, Sept. 15-19. Boston, MA: Martinus Nijhof; 1982.

Quirk, J. T.: Shrinkage and related properties of Douglas-fir cell walls. Wood and Fiber Science 16(1): 115-133; 1984.

Ruedy, T. C.; Johnson, J. A.: Glueline fracture of wood adhesive compact- tension specimens at various grain orientation configurations. Proceedings First International Conference on Wood Fracture, Banff, Alberta, Canada. Sponsored by the Western Forest Products Laboratory, Forintek Canada Corp., Vancouver, British Columbia; 1978.

Sasaki, H.; Walsh, P. F.: Cleavage fracture toughness of wood-epoxy resin bond system. J. Soc. Materials Science, Japan 26(284): 453-459; 1977.

Selbo, M. L.: Effect of joint geometry on tensile strength of finger joints. Forest Products Journal 13(9): 390-400; 1963.

Suzuki, M. A.; Schniewind, A. P.: Fracture toughness of wood-adhesives joints by a tapered double-cantilever beam. Mokuzai Gakkaishi 30(1): 60-67; 1984.

Takatani, M.; Sasaki, H.: Effect of glue-line flexibility on cleavage fracture toughness of wood-epoxy resin bond system. Wood Research (Bull. Wood Research Institute, Kyoto Univ.) 66: 30-51; 1980.

(a) Fracture

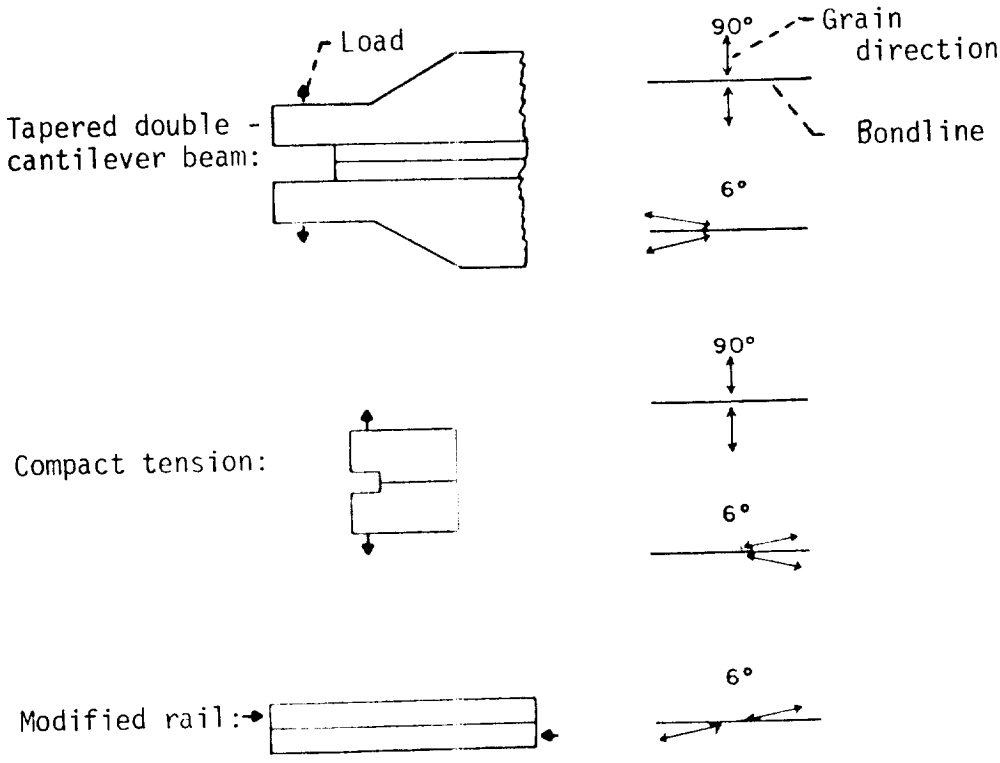

(b) Combined shear and tension

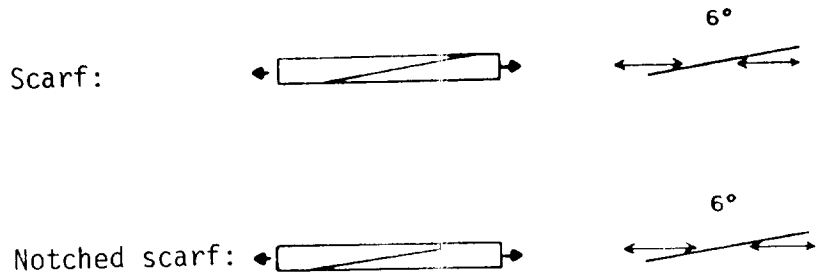

(c) Shear:

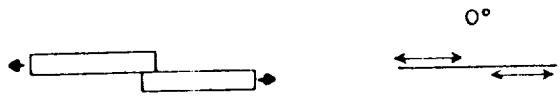

Figure C-1. - Schematic drawings of wood specimen geometry and loading, showing the relationship between glue line, grain direction, and loading.

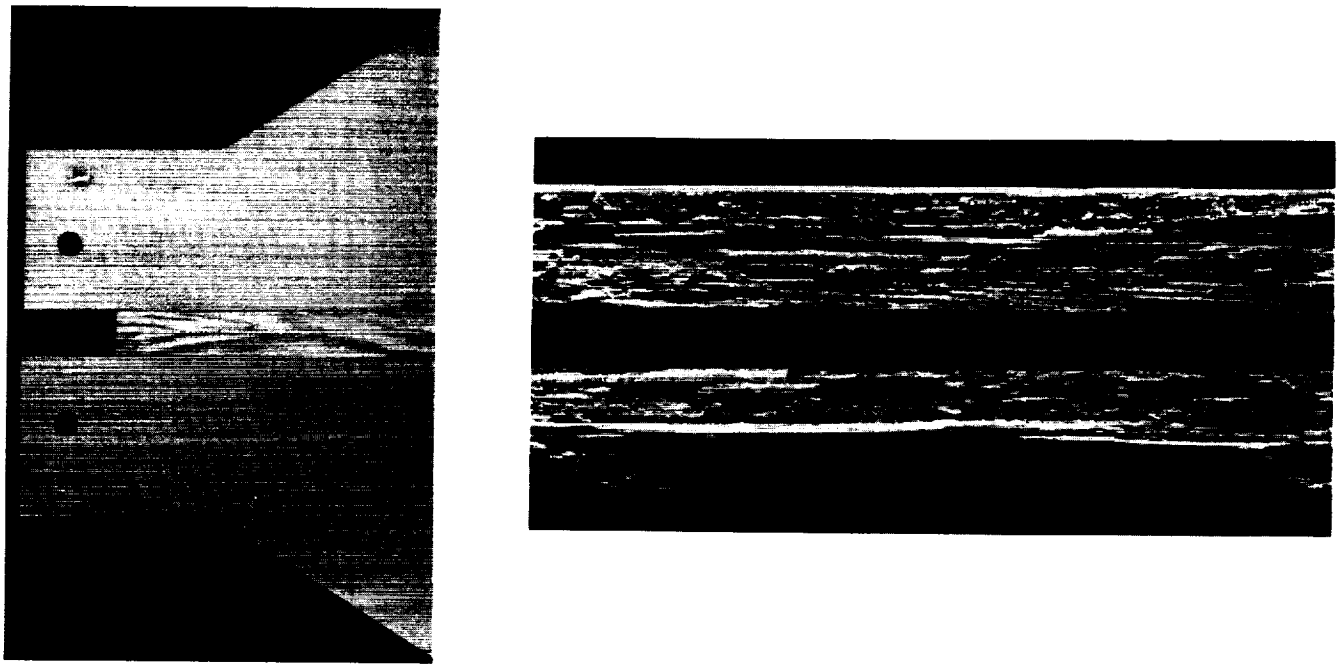

(a) 6 deg grain-to-bondline angle. Fracture surfaces show considerable wood failure.

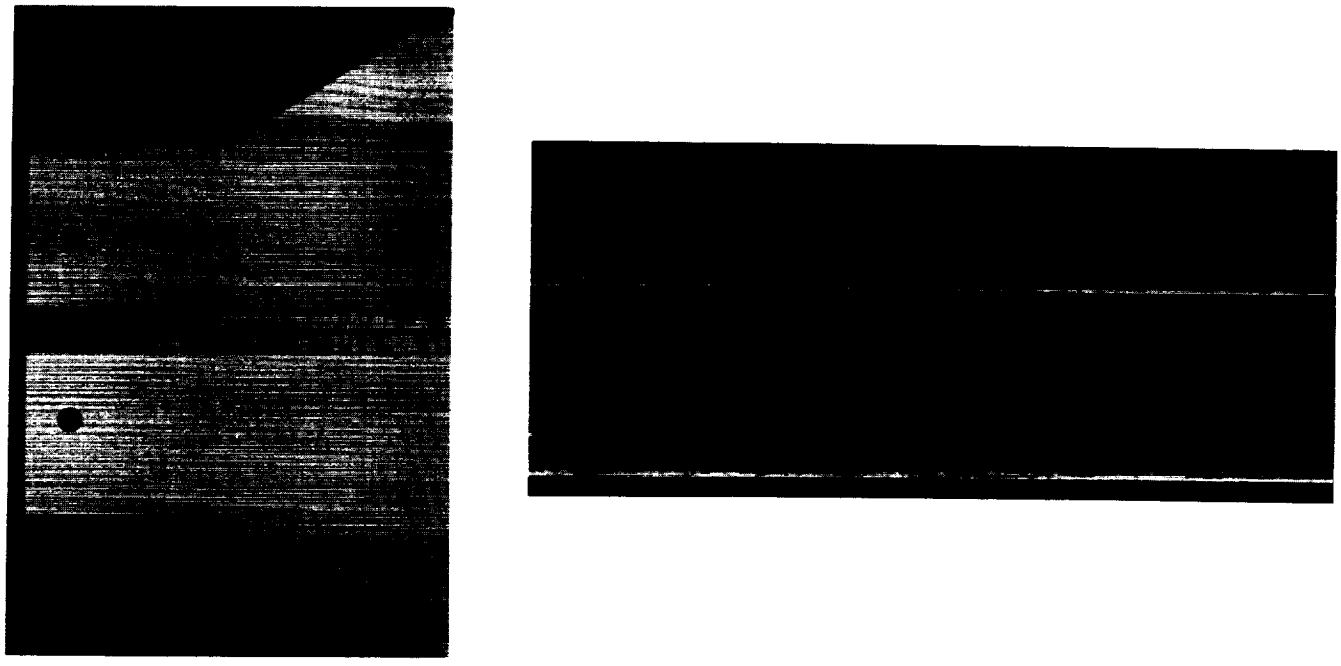

(b) 90 deg grain-to-bondline angle. Fracture surfaces show no wood failure and an adhesive failure following the latewood bands (growth rings).

Figure C-2. - Tapered double-cantilever beam fracture specimens.

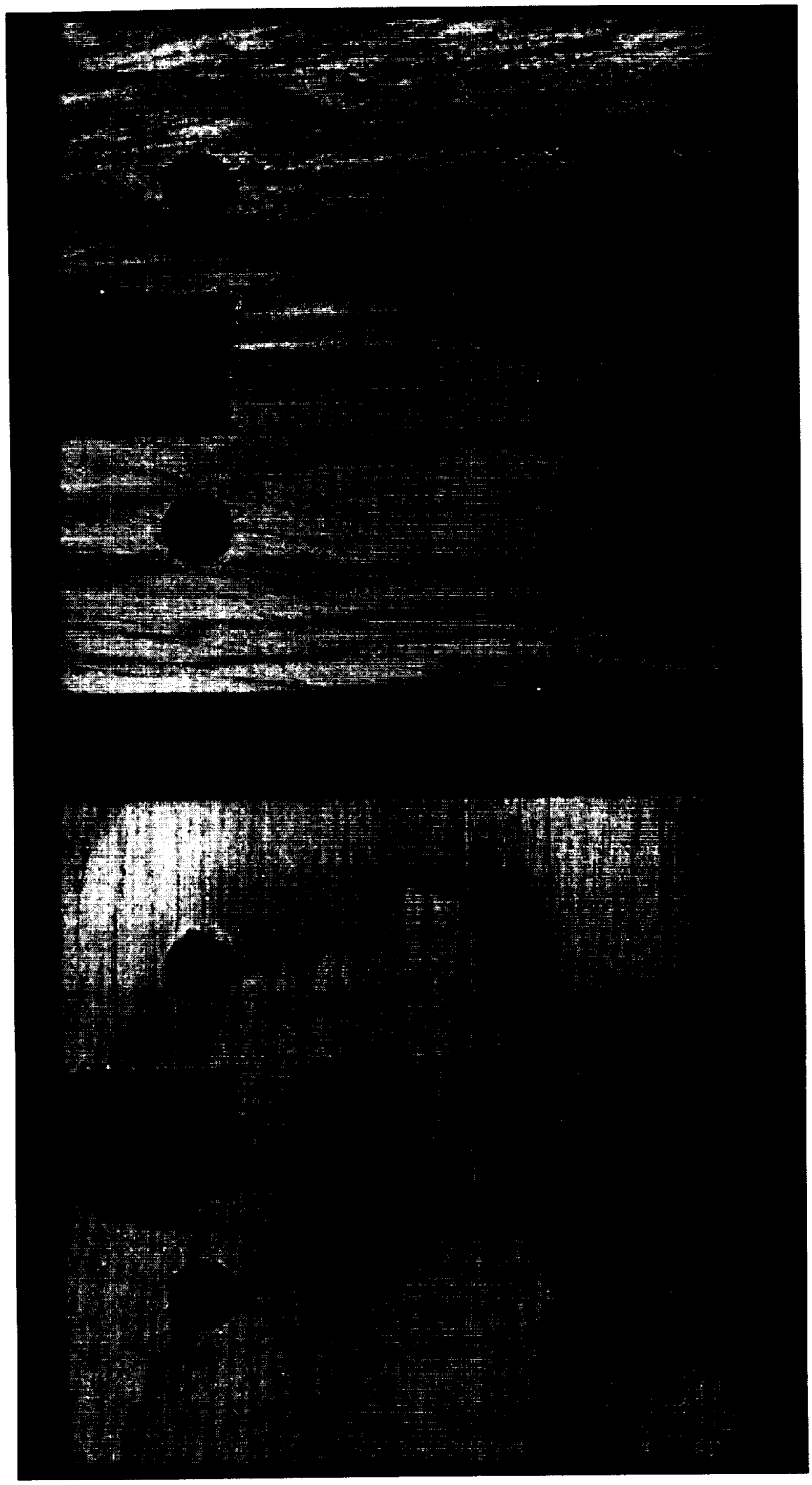

(a) 6 deg grain-to-bondline angle.

(b) 90 deg grain-to-bondline angle.

Figure C-3. - Compact tension fracture specimens.

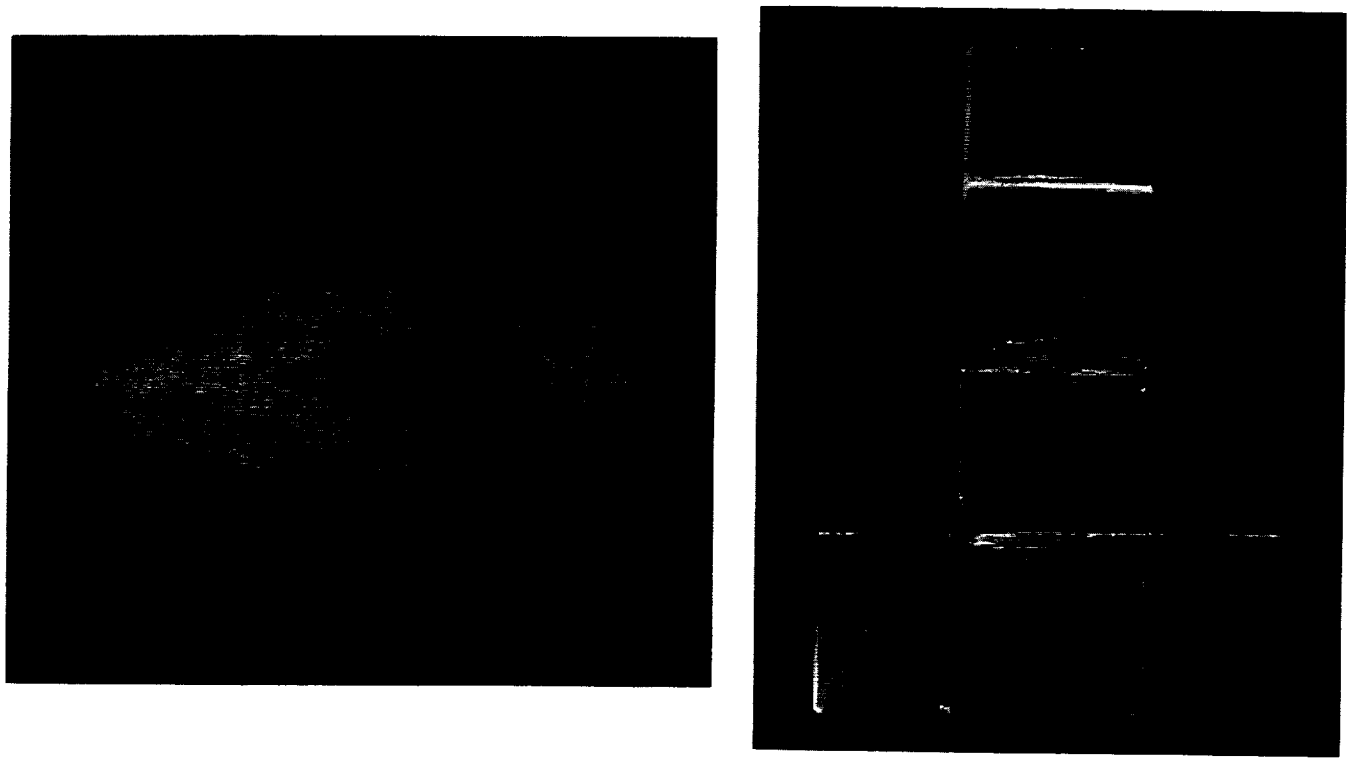

(a) Maple cross-lap specimen, showing low or absent cohesive failure of adhesive or wood.

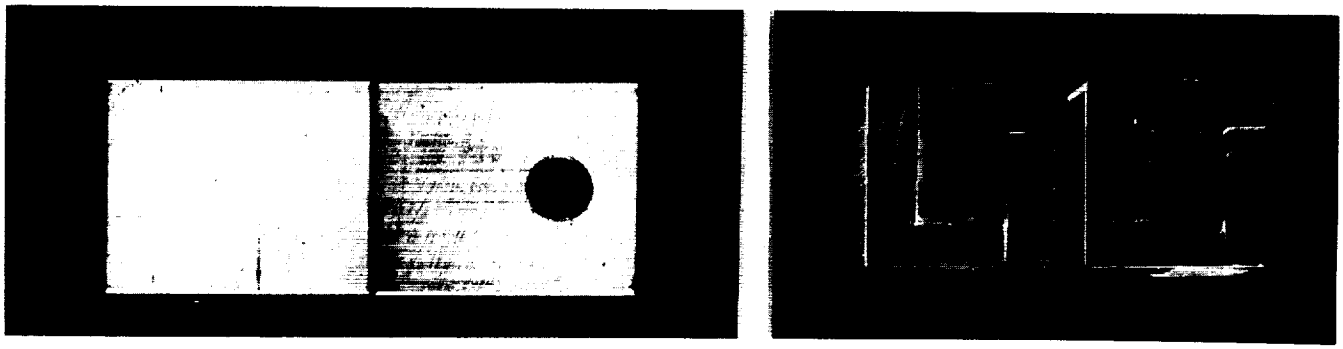

(b) Aluminum-to-aluminum butt joint specimen, showing absence of cohesive failure in adhesive.

Figure C-4. - Specimens for measuring bond tensile strength perpendicular to the bondline.

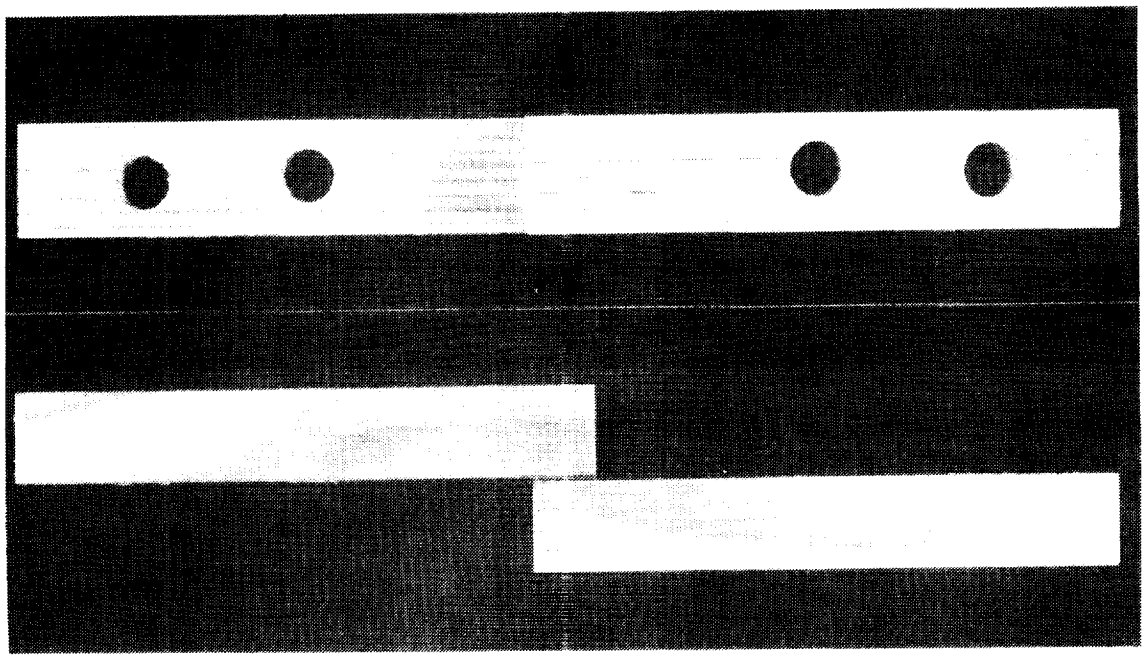

(a) Specimen geometry

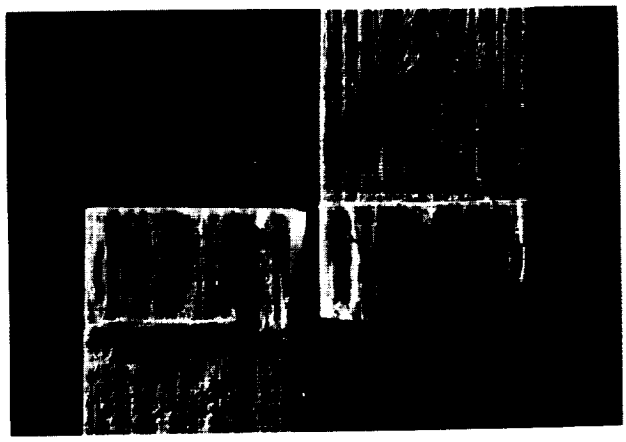

(b) Douglas-fir specimen, with wood failure predominantly in earlywood and bondline failure next to latewood.

(c) Steel specimen, with mixed cohesive/adhesive failure in the epoxy.

Figure C-5. - Thick adherend shear specimens.

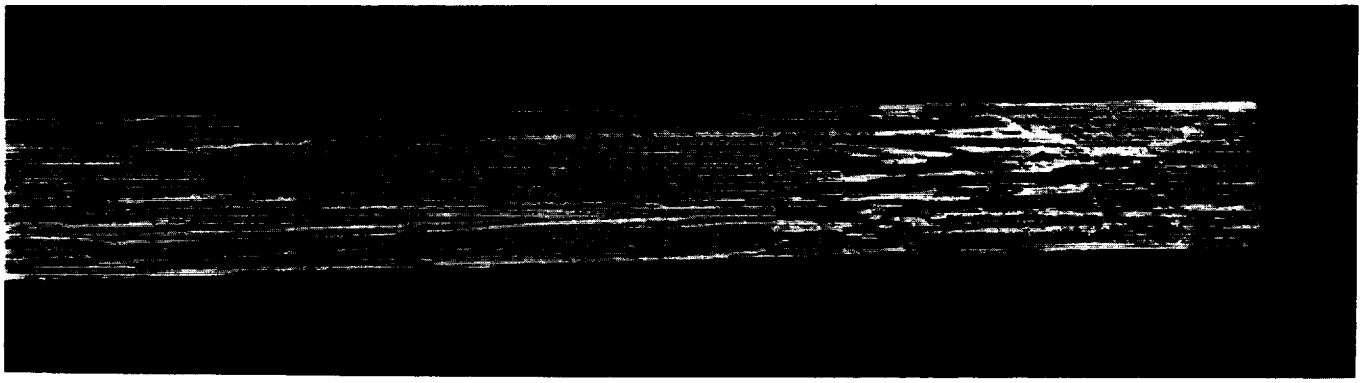

(a) General view showing fracture surface dominated by failure at the interface between wood and adhesive. Coarse surface area at right shows failure in weaker earlywood.

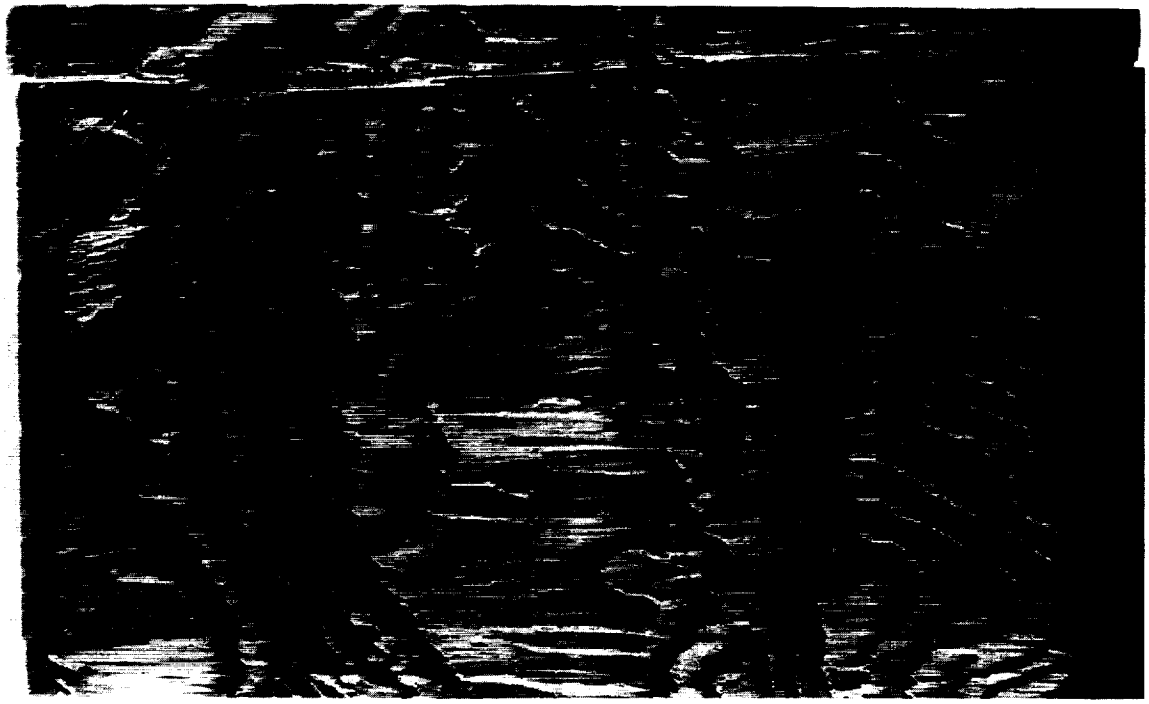

(b) Closeup view of wood failure pattern related to earlywood/latewood layers in opposing finger. Shear fractures in the adhesive were marked by faint diagonal lines from lower left to upper right in this view.

Figure C-6. - Fracture surface of a finger taken from the fatigue test beam.

APPENDIX D

MECHANICAL ANALYSIS OF FINGER JOINT DESIGNS

Measurement of adhesive mechanical properties suggests a change in the adhesive's characteristics when cured in the presence of wood. However, chemical analysis indicates that the wood has little effect on the epoxy. The microscopic evidence clearly indicates that failure is dominated primarily by the adhesive/boundary layer and secondarily by the relatively weak earlywood near the bondline. Additionally, simulated finger joints indicate that failure load for a unit width of blunt-tip finger joint is less than half that found for a sharp-tip finger joint. Thus, the analysis which is described in this section attempted to define and control the high strain regions of the existing design.

Mechanical analysis of the finger joint was used to: (a) provide substantiation of experimentally determined results with full-scale finger joints, (b) assess sensitivity of the existing joint to changes in adhesive layer properties, and (c) investigate improved designs of the large finger joint.

Survey of Available Analysis Methods

Theoretical analyses of bonded joints in metallic substrates, based on the classical analytical methods of continuum mechanics, were presented almost 40 years ago. The methods have been modified for application to composite materials because of their anisotropic and environmentally sensitive nature. Widespread use of the digital computer has resulted in development of the finite element method which allows solution of problems which are virtually unsolvable by classical analytical methods.

All analyses assume loading on bonded joints of large width. This assumption results in identical stress distributions at all sections of the joint and permits one to neglect edge effects. Critical to the strength of these joints is the stress distribution within the joint. This distribution of stress is dependent on the geometry of the joint and the mechanical properties of the adhesive and the adherends. From classical solutions of bonded joint behavior, the following physical parameters can be of significance: (1) length of adherend overlap, (2) adherend strength and stiffness, (3) adhesive thickness, (4) strength, and (5)stress/strain characteristics. No attempt has been made to analyze the adhesive as anything but an isotropic material.

Failures of adhesively bonded metal structure may be identified by one of several failure modes. Adherends may fail in tension or shear, or the bond may fail within the bondline or at the adherend/adhesive interface. In composites, the adherends may display interlaminar or transverse failures near the bonded surface. An adherend/adhesive interface failure usually indicates an improperly prepared joint which may fail at significantly lower loads than high quality joints.

Single lap joints loaded in tension have been the basis of most analytical work. Solution of these analyses usually implies simplifications. The correlation between the theoretical and experimental results is critically dependent on which factors are omitted from the analysis. The simplest approach (and the first) is due to Volkersen (1938), with the simple "shear-lag" analysis. In this analysis the only factors considered are the shear deformation of the adhesive and the elongation of the adherends. It is more of a double-lap than a single-lap joint since in the latter, overall bending of the adherends will occur.

The bending effects which occur in single-lap joints were first considered in detail by Goland and Reissner (1944) and de Bruyne (1944). The result of adherend bending is the introduction of direct stresses into the adhesive, in the through-thickness direction. These are termed "peel" stresses because of their tendency to peel apart the single-lap adherends. In addition to the peel and shear stresses, Goland and Reissner also accounted for the longitudinal stress in the adhesive. All these stresses were assumed constant across the adhesive thickness which, as in most analyses, is assumed small compared to the adherend thickness. The bending moment and shear force in the adherends at the ends of the joint (caused by the eccentric load path) are obtained by considering the adherends to be cylindrically bent plates.

In common with most analyses, the joint is considered to be wide, which produces a plane-strain condition. The magnitudes of the maximum peel and shear stresses do increase with load. It is further shown that these stress maxima reach asymptotic values at large overlaps. Typical adhesive stress distribution calculations using this simple analysis have non-zero shear stress at the ends of the joint. This result violates the stress-free boundary condition and, as pointed out by Benson (1954), is a consequence of ignoring the variation of peel stress through the thickness of the adhesive. The through-thickness adhesive stress variation is included in analyses by a number of authors (Kelsey and Benson, 1956; Pahoja, 1971; Pirvics, 1974; Allman, 1976). The main effect of including this in the analysis is to move the peak shear stress to a position about one adherend thickness from the joint ends. Ojalvo and Eidinoff (1978) present experimental evidence of this result.

All the analyses mentioned so far considered the adherends as thin beams and ignored the through-thickness shear and normal deformations in the adherends. As shown by Srinivas (1975) this only causes significant error if the lap length is small or the adhesive stiffness is large. However, the variation of stress through the adhesive thickness was neglected in that analysis. A similar analysis was performed by Renton and Vinson (1975). As the situation considered is made more general, the governing equations become increasingly complicated, and their solution requires the use of a computer.

A number of authors have performed parametric studies to identify the factors that influence the peak stresses in bonded joints in metals. Some general conclusions that may be made for minimizing the peak stresses are (a) adherends should be identical, (b) adherends should have equal bending and in-plane stiffnesses, (c) adherends should have as high an in-plane stiffness

as possible, (d) overlap should be as large as possible, (e) the adhesive should have low tensile and shear moduli.

A low modulus adhesive can produce undesirable creep in a joint. Thus, some investigators have advocated the use of a low modulus adhesive only at the ends of the joint with a higher-stiffness adhesive in the central region to afford creep resistance. However, varying the thickness of the bondline along the length of the joint will achieve the same desirable result (Srivanas, 1975; Ojalvo and Eidinoff, 1978; Cherry and Harrison, 1970; Thamm, 1976).

Finite width of a structural bonded joint has been discussed in only one instance. The corners of the overlap have been shown to have a peak stress due to Poisson effects. Some special joints receiving study are the scarf joint by Lubkin (1957) and Wah (1976) and a tubular lap joint by Lubkin and Reissner (1956).

Although most early investigations looked only at an elastic adhesive in analysis, most of the synthetic adhesives are quite elastic-plastic. The stress/strain nonlinearity of "ductile" adhesives was studied by Adams et al (1976). Adhesive nonlinearity information is presented by Grant (1976), Grimes (1972), and by Lubkin (1954) for tubular joints.

Stepped and scarf joints between orthotropic and isotropic plates were studied using plane stress and plane strain assumptions (Erdogan and Ratwani,1971; Reddy and Sinha, 1975). It is shown that the maximum adhesive shear stress is less in the scarf joint and the highest adherend direct stress always occurs on the stiffer side of a joint with nonidentical adherends. Properties of the adhesive are the primary determinates of the stress within the joint.

The normal laminate constitutive equations are used by Wah (1973) to describe the cylindrical bending behavior of the adherends in a single lap joint. Stresses in the adhesive are allowed to vary across the thickness. Fictitious stresses are imposed to allow satisfaction of all boundary conditions. There appear to be computational difficulties in obtaining accurate stress values at the joint ends, arising from the solution of coupled second- and fourth-order differential equations.

In support of an experimental program, Grimes (1971) used a shear-lag analysis in conjunction with classical lamination theory. Sinha and Reddy (1976) included the effect of stresses induced by the curing process. It was shown that a residual shear stress will exist in the adhesive making the critical end of the joint dependent on the direction of the applied load.

General works such as Allman (1976), Srinivas (1975), and Renton and Vinson (1975) include analysis of joints with composite adherends. However, they do not account for stress variation through the adhesive thickness. Dickson et al (1973) compared a general approach with that of Goland and Reissner (1944) and showed that neglecting through-thickness direct strains is likely to be most significant. The Goland and Reissner results are

conservative. It is also shown that residual thermal strains can cause a large increase in adhesive shear stress.

Parametric studies indicate the same trends in joint stresses in composites as were previously outlined for metals. The adhesive stresses are reduced and become more uniform as the adhesive modulus is reduced, the adherend stiffness is increased, and the overlap length is increased. For composite adherends the ply lay-up and stacking sequence are additional variables. It appears that the lay-up has more influence on the adhesive peel stress than on the shear stress.

Several authors have shown that nonlinearity effects are generally so much more significant than those due to through-thickness strains, that the latter may usually be ignored. An analysis which includes through-thickness adherend strains as well as the nonlinear character of the adhesive would be very cumbersome. Dootson and Grant (1975) and Grant (1978) neglected adherend bending in a simplified shear-lag analysis but allowed nonlinear adhesive elastic properties. Governing equations were written in finite-difference form and solved iteratively with a prediction of a failure based on the maximum adhesive shear strain. Corvelli (1972) used a simple linear analysis, modifying the results by using the secant shear modulus at failure, to establish a stress concentration factor for determining the maximum adhesive shear stress. Grimes et al (1975) considered adhesive nonlinearity, adherend bending, and adherend nonlinear elasticity in a package of nonlinear analyses. Nonlinear elasticity was characterized with secant modulus and a Ramberg-Osgood approximation for a stress-strain law.

Hart-Smith (1974) analyzed double-lap, single-lap, scarf, and stepped joints. Nonlinearity of the adhesive was characterized by an elastic-perfectly plastic model of the stress-strain curve. For double-lap joints it was shown that the adhesive strain energy in shear is the only significant quantity affecting joint strength. By adjusting the elastic strain limit and keeping the maximum plastic strain limit fixed the idealized adhesive stress-strain behavior may be matched to the actual behavior. This assures the same strain energy in both cases. With the same adherends, all adhesives having the same strain energy, failure strain, and failure stress will produce joints with identical strength, provided that the interfacial bond strength is unchanged. Increasing the plastic strain limit will increase the strength of the joint, while the stress-strain behavior affects only the stress distribution along the joint. Scarf joint analysis using similar approaches showed the adhesive stress to be uniform if the adherends are identical. For nonidentical adherends, the distribution of stresses becomes increasingly nonuniform as the mismatch becomes greater. Because the thermal mismatch is independent of the stiffness mismatch, the critical end of the joint is determined by the interaction of the thermal, stiffness, and loading characteristics of the joint.

Computerized finite element analysis presents one with the possibility of studying adhesive bonded joints without the assumptions that are usually part of simplified classical analyses. Basically, one can choose between a large number of primitive elements or a smaller number of more sophisticated

elements. The only practical restriction on this type of analysis is the amount of computer time/memory available. The rapidly varying stress fields in adhesive/adherends require significantly higher densities of elements than may be encountered in typical finite element analyses.

An assumed strain field is generated in conventional finite elements, and hence these only satisfy equilibrium in an overall sense. This means that the method will not satisfy conditions at a stress-free boundary. This condition can only be met exactly by the use of elements that also specify stress variation (Spiker and Chou, 1980). As with classical methods, one can perform linear or nonlinear analyses, with either material or geometric nonlinearities.

Linear strain elements were used by Thongcharoen (1977) in a parametric study to optimize the geometry of metal single- and double-lap joints. Adams and Peppiatt (1974) and Chan and Sun (1980) used these simple elements to demonstrate the usefulness of the finite element method to treat problems that are effectively insoluble by classical methods. Consideration of the adhesive spew fillet showed that it causes significant reductions in the maximum shear and direct stresses in the adhesive. Further work (Adams and Peppiatt, 1977) dealt with tubular lap and scarf joints under tensile and torsional loading.

Finite element analyses which utilize the nonlinearity of materials or geometries of the bonded joint are extremely expensive in terms of computer time. Thus, most works utilize a preliminary linear analysis to provide first estimates of strain levels. Cooper and Sawyer (1979) used elements with an assumed linear stress field, thus giving the possibility of satisfying equilibrium on a stress-free boundary. Though they assumed a linear elastic material, their analysis included the nonlinear effects of joint rotation.

As part of an extensive parametric study, Liu (1976) used quadratic linear strain elements in analysis of metal single-lap joints. Wright (1980) used triangular linear strain elements to model double-butt and scarf joints of a graphite composite. Adams et al (1978) studied double lap, bevel, and scarf joints including the adhesive spew fillet. The adhesive was represented as elastic-perfectly plastic in these works.

Joint Design Guidelines

Design of bonded joints is the subject of numerous papers dealing on the qualitative level. Experimental and theoretical investigations which can provide quantitative design information and parametric evaluations will be noted here. A detailed discussion of possible failure modes was presented by Grimes and Greimann (1975) and Hart-Smith (1974). Efficient joints are said to be easier to design in metals than in composite materials, according to Hart-Smith. This is due to the brittle nature of the latter. Strength of double-lap joints is limited by the adherend thickness, because when the adherends become too thick, tensile failure will occur through the thickness of the adherends. Adherends that are thick and highly loaded should be

stepped or scarfed. Joint strength is improved in composite materials if the zero-degree plies are placed next to the adhesive layer.

An adhesive shear strength approaching 50 percent greater than that of the adherends is recommended for reliability of the bonded joint. The bonded joint should contain areas that are stressed to less than 30 percent of their capacity to assure creep resistance of the system. Many of the ductile adhesives have ultimate shear strains exceeding 200 percent of their elastic strain limit. Limiting the plastic zone to less than 50 percent of the joint length will allow unstressed creep resisting areas.

Although fatigue loading will require limiting of maximum strain levels (and hence not allow the full load capacity of a ductile adhesive to be realized), a ductile adhesive should still be used in preference to a stronger brittle adhesive. Ductile adhesives provide superior fatigue resistance and greater margins of safety in bonded joints than the stronger but more brittle adhesives. Hart-Smith (1974) recommended the reduction of maximum shear strength by 20 percent to account for incomplete wetting of large production-type bondlines.

Analysis Methodology Used in this Study

Symbols

A,B,C,D	integration constants
E	Young's modulus (longitudinal) for adherend
G	adhesive shear modulus for elastic-plastic representation
L	overlap (length of bond)
T	direct stress resultants in adherends
t	thickness of adherend
x	axial (longitudinal) coordinate parallel to direction of load
γ	adhesive shear strain
γ_e	elastic adhesive shear strain
γ_p	plastic adhesive shear strain
δ	axial (longitudinal) displacement of adherend
η	thickness of adhesive layer
τ	adhesive shear stress
τ_p	plastic (maximum) adhesive shear stress

Subscripts

e,p	elastic and plastic values
1,2	different adherends of joint

The analysis of the Douglas fir/epoxy bonded finger joints in this study will follow the basic derivations by Hart-Smith (1974). Adhesive behavior in shear is considered to be elastic perfectly-plastic (Fig. D-1). This is in close agreement with experimentally measured shear behavior. An accurate continuous characterization of the adhesive shear stress-strain behavior is deemed to be less important than the accurate representation of the shear strain energy, maximum shear stress, and maximum shear strain.

A usual problem for bonded joints possessing a finite-tip thickness or a thick nontapered adherend is the initiation of peel stresses at the joint end. Due to the fully symmetric nature of the fatigue test beam and the feathering of a partial finger (essentially a scarf joint) at the edge of this box beam, no peel stresses can develop. Thus, only adhesive shear stresses were addressed in this analysis.

An element of the adherend/adhesive/adherend system (Fig. D-2) and the finite-tip scarf joint (Fig. D-3) may be modeled with some basic mechanical property information for the adherends and adhesive. The equilibrium equations for a differential element of length dx (Fig. D-2) may be written as

$$\frac{dT_1}{dx} - \tau = 0, \quad \frac{dT_2}{dx} + \tau = 0 \tag{1}$$

The elastic relations for the adherends are

$$\frac{d\delta_1}{dx} = \frac{T_1}{E_1 t_1}, \quad \frac{d\delta_2}{dx} = \frac{T_2}{E_2 t_2} \tag{2}$$

The adhesive shear strain, for tensile lap shear loading, is

$$\gamma = (\delta_1 - \delta_2)/\eta \tag{3}$$

Elastic adhesive shear stress is related to the shear strain by

$$\tau = G\gamma = G(\delta_1 - \delta_2)/\eta \tag{4}$$

A solution follows as

$$\frac{d\tau}{dx} = \frac{G}{\eta}\left(\frac{d\delta_1}{dx} - \frac{d\delta_2}{dx}\right) = \frac{G}{\eta}\left(\frac{T_1}{E_1 t_1} - \frac{T_2}{E_2 t_2}\right) \tag{5}$$

$$\frac{d\tau^2}{dx^2} = \frac{G}{\eta}\left(\frac{2}{E_1 t_1} + \frac{2}{E_2 t_2}\right)\tau = \lambda^2 \tau \tag{6}$$

The solution of equation (6) is

$$\tau = A \cosh(\lambda x) + B \sinh(\lambda x) \tag{7}$$

where the integration constants A and B are to be determined by boundary conditions for each step. Substitution into equation (1) yields:

$$T_1 = T_{1'} + \frac{A}{\lambda} \sinh(\lambda x) + \frac{B}{\lambda} [\cosh(\lambda x) - 1] \tag{8}$$

and

$$T_2 = T_{2'} - \frac{A}{\lambda} \sinh(\lambda x) - \frac{B}{\lambda} [\cosh(\lambda x) - 1] \tag{9}$$

The values of $T_{1'}$ and $T_{2'}$ are reference values that depend upon the origin of the coordinate x. It is convenient to adopt the start of each step as the reference for the step. Integrating again, using equation (2)

$$\delta_1 = \delta_{1'} + \frac{1}{E_1 t_1} \left[T_{1'} X + \frac{A}{\lambda^2} \cosh(\lambda x) + \frac{B}{\lambda^2} \left\{ \sinh(\lambda x) - \lambda x \right\} \right] \tag{10}$$

$$\delta_2 = \delta_{2'} + \frac{1}{E_2 t_2} \left[T_{2'} x - \frac{A}{\lambda^2} \cosh(\lambda x) - \frac{B}{\lambda^2} \left\{ \sin(\lambda x) - \lambda x \right\} \right] \tag{11}$$

A FORTRAN computer program was used to solve Equations (10) and (11) for the elastic stepped-lap joint. The analysis proceeds one joint step at a time, beginning with assumed values of load and adhesive shear strain. When calculating the maximum load to be carried under elastic conditions, the maximum adhesive shear strain is set at the most critical location in the joint. The integration constants A and B are evaluated at the beginning of each step as

$$A = \tau, \text{ at } x = 0 \tag{12}$$

and from equation (5)

$$B = \frac{G}{\eta\lambda} \left[\frac{T_1}{E_1 t_1} - \frac{T_2}{E_2 t_2} \right], \text{ at } x = 0 \tag{13}$$

All other values are determined from Equations (7) to (11). Adjustments to initial assumptions are made if adherend or adhesive allowable stresses are exceeded at any point in the joint. Computational iterations proceed until all boundary and internal conditions are met to a specified tolerance.

For full consideration of the adhesive's potential, the elastic-plastic analysis of a joint requires that

$$\tau = G\gamma \text{ for } \gamma < \gamma_e \tag{14}$$

and

$$\tau = \tau_p \text{ for } \gamma \geq \gamma_e \tag{15}$$

In the zones where the adhesive is plastic ($\gamma \geq \gamma_e$), Equations (2) and (3) give

$$\frac{d\gamma}{dx} = \frac{1}{\eta}\left(\frac{d\delta_1}{dx} - \frac{d\delta_2}{dx}\right) = \frac{1}{\eta}\left(\frac{T_1}{E_1 t_1} - \frac{T_2}{E_2 t_2}\right) \tag{16}$$

and from Equation (1)

$$\frac{d^2\gamma}{dx^2} = \frac{1}{\eta}\left(\frac{1}{E_1 t_1} + \frac{1}{E_2 t_2}\right)\tau_p = \frac{\lambda^2}{G}\tau_p \tag{17}$$

Thus in the plastic zone of the joint,

$$\gamma = \frac{\lambda^2}{2G}\tau_p x^2 + C_x + D \tag{18}$$

and

$$T_1 = T_1' + \tau_p x \tag{19}$$

$$T_2 = T_2' - \tau_p x \tag{20}$$

and

$$\delta_1 = \delta_1' + \frac{1}{E_1 t_1} T_1' x + \tau_p x^2 \tag{21}$$

$$\delta_2 = \delta_{2'} + \frac{1}{E_2 t_2} T_{2'} x - \tau_p x^2 \qquad (22)$$

Solution of Equation (18) proceeds by setting D equal to γ at the beginning of the step ($x = 0$) and C is evaluated from Equations (16) and (18), as follows:

$$C = \left.\frac{d\gamma}{dx}\right|_{x=0} = \frac{1}{\eta}\left[\frac{T_1}{E_1 t_1} - \frac{T_2}{E_2 t_2}\right]_{x=0} \qquad (23)$$

Numerical analysis of the elastic-plastic joints required the computer to keep an accounting of the transitions between the elastic and plastic adhesive conditions. Computationally, the analyses of elastic and elastic-plastic joints are quite similar in logic. However, iteration to solutions with a given level of accuracy requires substantially more time for the elastic-plastic cases.

An additional feature of the elastic-plastic analysis is the capability to analyze joint strength utilizing the adhesive's full plastic strain potential. This is achieved by artificially increasing the adherend strength to force the ultimate failure condition to be the maximum plastic strain in the adhesive.

Results of Analysis of Fatigue Test Beam Finger Joint

The analysis method presented earlier was applied to a parametric study of the joint design used in the fatigue test beam. Major variables selected for study were the following:

1. Adhesive thickness, η
2. Maximum adhesive shear strain, γ_{max}
3. Adhesive shear stiffness, G
4. Adhesive shear strength, τ_{max}

A "baseline" analysis, which represented the median geometric and mechanical properties assessed from the previous phases of work was designated AT005. This joint model had adhesive and adherend properties as follows:

Property	Adhesive	Adherend
Thickness	0.005 in.	1:10 slope
Strength	1,450 psi (shear)	10,000 psi (tension)
Stiffness	18,130 psi (shear)	2.5×10^6 psi (tension)
Failure strain	0.11 in./in. (shear)	0.004 in./in. (tension)

In addition to the parameter analyses, individual analyses of the joint with adhesive properties as determined from the mechanical testing of steel, Douglas-fir, and maple adherends were used to illustrate the wide range of joint strengths possible when using experimentally determined adhesive

properties. The input data for the analyses as well as the predicted elastic and elastic-plastic joint strengths are given in Table D-1.

Table D-1

Summary of Parametric Analysis of Fatigue Test Beam Joint

Analysis case	η	G	γ_{max}	τ_{max}	$\gamma_{elastic}$	Elastic joint strength	Elastic-plastic joint strength
	in.	psi	in/in	psi	in/in	psi	psi
AT003	0.003	18,130	0.11	1,450	0.080	2,390	3,150
AT005	0.005	18,130	0.11	1,450	0.080	2,960	3,890
AT009	0.009	18,130	0.11	1,450	0.080	3,740	4,900
G200	0.005	29,010	0.11	1,450	0.050	2,430	4,360
G900	0.005	130,500	0.11	1,450	0.011	1,250	4,900
GM090	0.005	18,130	0.09	1,450	0.080	2,960	3,310
GM175	0.005	18,130	0.175	1,450	0.080	2,960	5,240
TM6.5	0.005	18,130	0.11	943	0.052	1,920	3,350
TM13	0.005	18,130	0.11	1,885	0.104	3,850	4,060
STEEL	0.005	130,500	0.175	4,060	0.031	3,510	9,240
DOUGFR	0.005	18,130	0.11	1,450	0.080	2,960	3,890
MAPLE	0.005	29,010	0.06	1,070	0.037	1,800	2,660

The results of the baseline analysis (AT005) should be directly comparable to the results obtained in the experimental strength determination (Appendix C), in which the of the finger tip thickness was 3.2-mm. The average experimental cross-sectional strength was 6,090 psi while the predicted elastic-plastic joint strength is 3,890 psi. As with the full-scale test beam (stressed near 3,500 psi), no control was exercised over the bondline thickness in the half-scale experimental joints. The analysis is based on a bondline thickness of 0.005 inch. This represents an average

bondline thickness observed microscopically on the unfailed finger joints in the full-scale fatigue test beam.

The tabulated results indicate that all the adhesive variables chosen in the parametric study have significant effects upon predicted strengths, both elastic and elastic-plastic. An insightful presentation of the results of this study are the graphical plots of adhesive shear stress and location referenced from the finger tip (Figs. D-4 to D-8).

Clearly the controlling factor in all the joint analyses is the behavior at the finger tip. The tip behavior creates varying levels of stress (or strain) concentration depending upon adhesive properties used in the analysis. Note that the elastic joint strength is significantly lower than the elastic-plastic analysis. This plastic or ductile behavior can "absorb" some of the stress concentration effects. If the adhesive layer were modeled to be "perfectly plastic" or had elastic-plastic behavior to very large plastic strains, the joint strength would utilize all the adhesive layer strength. That is, if τ_{max} is equal to 1,450 psi, joint strength would be equal to (11.5 in.) x (1,450 psi)/ (1.35 in.), or 12,350 psi, regardless of strain concentrations in the joint or adhesive properties (except strength).

Typical bonded joint design utilizes only elastic behavior of the adhesive to preclude fatigue or creep problems within the joint. Note that over the wide range of adhesive layer properties represented in the Table D-1 (excluding adhesive shear strength), the elastic joint strength covers a fairly narrow range (1,250 to 3,740 psi). Thus, with the present tip design, elastic joint efficiencies are calculated to range from 10 percent (1,250 psi/12,350 psi) to 30 percent (3,740 psi/12,350 psi).

The elastic-plastic behavior of the adhesive creates a great deal of ductility at the finger tip. This allowed up to a four-fold increase from the elastic strength limit for one parameter case (G900). Joint efficiencies based on elastic-plastic behavior range from 26 percent to 42 percent.

Analysis of Modified Geometries

Three simple variants of the finger joint design in the fatigue test beam were evaluated to determine their relative effect on efficiency in transmitting load. These variants in geometry were chosen by GBI as geometries that represented minimal manufacturing and assembly problems (Fig. D-9) and had potential for improved joint performance. However, a finger tip with a 1:10 slope was included to illustrate both the potential of this idealized geometry and its inherent problems.

As with the previous analyses, the baseline results and adhesive properties of analysis case AT005 are used to provide a common reference for the alternate geometries. The analysis cases, geometry modifications, and joint strengths are listed in Table D-2 below.

Table D-2

Summary of Analysis of Modified Finger Joint Geometries

Analysis case	Modification	Elastic joint strength psi	Elastic-plastic joint strength psi	Potential bond strength psi
AT005	Baseline	2,960	3,890	--
A	Extend tip 0.25 in.	3,300	4,350	--
B	Extend tip 0.50 in.	3,510	4,640	--
C	Extend tip 1.0 in.	3,640	4,820	--
D	Modify slope to 1:2.5	3,680	4,540	--
E	Modify slope to 1:5	15	15	77
F	Modify slope to 1:10	5,725	5,725	10,260
G	Reduce tip 0.5 in.	4,170	4,170	5,990
H	Reduce tip 1.0 in.	5,300	5,860	9,320
I	Reduce tip 2.0 in.	6,090	6,220	7,900

Extended Tip.--The extension of the existing tip thickness up to 1 inch into the finger valley yields only modest improvements in joint capacity. As before, the behavior at the tip controls the joint performance (Fig. D-10). A positive change from previous performance is the generation of a low stress "trough" along the 0.1-inch-thick tip which becomes evident for the 1.0-inch case.

Modified Slope.--Changes in the tip slope were accomplished by holding the joint length constant (11.5 in.). The 1:2.5 slope tip was strong enough to resist tip breakage, whereas the 1:5 and 1:10 slope tips failed in tension at approximately 0.2 inch from the tip. This is evidenced in the analyses as neither of these slope cases reached the adhesive shear strength of 1,450 psi (Fig. D-11). However, by assuming that adherend strength does not limit the joint strength, the potential bond strength for the 1:10 slope joint 10,260 psi, closely matching the experimentally determined value of 10,900 psi (feathered tip/no crack starter, Appendix C).

Note that a joint efficiency of 83 percent (10,260 psi/12,350 psi) is predicted for the 1:10 slope joint due to the large "stress spikes" in the solution (Fig. D-11b) caused by the finite step sizes. Theoretically, both the elastic and the elastic-plastic analyses should produce 100 percent adhesive efficiency for a scarf joint when the adherend possesses adequate strength. Thus, the maximum efficiency that can be achieved with the joint is limited not by adhesive strength, but by the wood material strength (i.e. 10,000 psi or 81 percent efficiency) in these analyses.

Reduced Tip.--The reduction in tip thickness, and therefore stiffness and strength, resulted in the failure of the tips from all of the undercut tip analyses. However, the joint performances are significantly better than the baseline results for the 1.0- and 2.0-inch-long undercut tips. The efficiency of the elastic behavior for the 2.0-inch undercut reaches 49 percent (6,090 psi/12,350 psi) which represents more than twice the capacity of the baseline joint.

As with the modified slope analyses, the reduction in tip stiffness and strength has caused tip failures to occur. However, unlike the modified slope, an optimum solution to the reduction in tip thickness can be achieved by tapering the gullet of the undercut at a shallow slope. This slope, say 1:5, will improve the performance of the joint and keep the highly stressed portion of the bondline (Fig. D-12) away from the tip areas.

Regardless of the method for controlling the peak stress at the end of the undercut, the 2.0-inch undercut (Analysis Case I) represents the highest performing elastic joint analyzed.

Recommendations

1. Accurate analysis of bonded joints requires that the mechanical characteristics of the adhesive and adherend be measured under closely controlled conditions. To this end, better control of bondline thickness and adhesive porosity is needed. Bondline thicknesses in the fatigue test beam were observed microscopically to range from 0.002 to 0.009 inch, resulting in significant joint strength losses from the target bondline thickness of 0.015 in. Likewise, stiffness loss due to the high void content of the adhesive manifests itself in permitting greater flexibility of the bondline. The voids also introduce microstress risers. This reduction of stiffness permitted an increased elastic capability for the joint, but may have decreased the strength of the adhesive layer and forced failure to occur near the interface. Methods for reducing porosity should be thoroughly investigated in future joints.

2. Elimination of the blunt finger tip is essential to achieving adequate capacity in the finger joint. A satisfactory joint design should have the highest stress at an interior location so that the plastic strain condition will not be close to the joint boundary. This dual-sided stress field gives the joint additional capacity. The interior location for maximum stress condition also assures stability in crack growth conditions. An

example of this is the undercut tip geometry (Fig. D-12) which should display controlled crack growth near the failure condition with good crack-stopping ability under cyclic loading conditions.

3. Of the candidate joint modifications evaluated, features of two joints are recommended for further research. First the reduced thickness tip obtained by bifurcating the tip provides a highly-stressed interior region in the joint. However, the valley of the bifurcation undercut should have a gradual transition to reduce the stiffness (or strain) concentration. This could be accomplished by sloping the undercut valley floor or increasing the feathered tip stiffness with synthetic fiber materials.

Second, the 1:10 slope joint with a sharp tip would be the most efficient joint for carrying loads, but its failure modes are usually catastrophic. Thus, the difficulty in fabricating the sharp tip is not justified. A known stress riser in the interior of the joint provides the crack-stopping capability desired. At the same time, the areas removed from the highly stressed bond- line act as creep arrestors. Though the creep characteristics of the epoxy are not well quantified, thermally-induced creep may be of concern in this cyclic loading environment.

4. During the redesign of the finger joint, a sensitivity analysis should be performed to evaluate the feasibility of each new redesign. Bondline thickness, local reinforcements, voids in the bondline, adhesive behavior, and geometric discontinuities should all be evaluated to assess their effects upon joint strength and stress distribution. The analysis presented in this Appendix can accommodate all of these variables.

5. The cantilever box beam employed to test the joint design should be modified to produce a uniform tensile stress field. A reduction in stress across the tension and compression faces of the beam (caused by shear lag) amounts to approximately 7 percent. The stress may be made approximately uniform by forming the top and bottom plates of the beam in a convex parabolic curve. A rise at the beam's center of 1.1 inches would be necessary for the 16-inch square cross-section used previously in this box beam.

6. Any large scale joint test specimens should be designed to preclude failure initiation due to Poisson effects at the specimen's side edges. The scarf joints on the fatigue test beam served this purpose, to a limited degree. The use of additional reinforcement, such as a fiberglass cloth overlay bonded at the edge or side of the beam over these scarf joints, would ensure failure over the continuous portion of the joint. Another option is to use a 1:15 or 1:20 slope on these outer scarf joints.

Literature Cited

Adams, R. D.; Peppiatt, N. A.: Stress analysis of adhesive bonded lap joints. J. Strain Anal. 9(3): 185; 1974.

Adams, R. D.; Coppendale, J.; Peppiatt, N. A.: Failure Analysis of aluminum-aluminum bonded joints. Adhesion 2, K. W. Allen (editor), Applied Science Publishers, Chap. 7; 1976.

Adams, R. D.; Peppiatt, N. A.: Stress analysis of adhesive bonded tubular lap joints. J. Adhesion 9: 1; 1977.

Adams, R. D.; Peppiatt, N. A.; Coppendale, J.: Prediction of strength of joints between composite materials. Symp. on Jointing in Fiber Reinforced Plastics, Imperial College, IPC Press, London; 1978.

Allman, D. J.: A theory of elastic stresses in adhesive bonded lap joints. RAE Tech. Rep. 76024; 1976.

Benson, N. K.: Influence of stress distribution on the strength of bonded joints. Int. Conf. Adhesion, Fundamentals and Practice, Nottingham; 1954.

Chan, W. W.; Sun, C. R.: Interfacial stresses and strength of lap joints. 21st Conf. Structures, Struct. Dynam. and Materials, AIAA/ASCE/ASME/AHS, Seattle, May 1980.

Cherry, B. W.; Harrison, N. L.: Optimum profile for a lap joint. J. Adhesion 2: 125; April 1970.

Cooper, P. A.; Sawyer, J. W.: A critical examination of stresses in an elastic single lap joint. NASA TP-1507, September 1979.

Corvelli, N.: Design of bonded joints in composite materials. Symp. Welding, Bonding and Fastening, NASA TM-X-70269, Williamsburg, Virginia; 1972.

de Bruyne, N. A.: The strength of glued joints. Aircraft Engineering 16: 115; April 1944.

Dickson J. N.; Hsu, T.; McKinney, J. M.: Development of an understanding of the fatigue phenomena of bonded and bolted joints in advanced filamentary composite materials. Rep. No. AFFDL-TR-72-64, U.S. Air Force; June 1973.

Dootson, M.; Grant, P. J.: Bonded joints in aircraft structures. Conf. Plastics Design Eng., Cranfield Inst. of Tech.; 1975.

Erdogan, F.; Ratwani, M.: Stress distribution in bonded joints. J. Composite Materials 5(3): 378; July 1971.

Goland, M.; Reissner, E.: Stresses in cemented joints. J. Appl. Mech. 11: 115; March 1944.

Grant, P. J.: Strength and stress analysis of bonded joints. Rep. No. SOR(P) 109, British Aerospace, Warton, England; 1976.

Grant, P. J.: Analysis of adhesive stresses in bonded joints. Symp. Jointing in Fiber Reinforced Plastics, Imperial Coll., IPC Press; 1978.

Grimes, G. C.: Stress distribution in adhesive bonded lap joints. SAE Trans. 710107, p. 370; 1971.

Grimes, G. C.; Greimann, L. F.; Wah, T.: The development of nonlinear analysis methods for bonded joints in advanced filamentary composite structures. Tech. Rep. AFFDL-TR-72-97, U.S. Air Force; September 1972.

Grimes, G. C.; Greimann, L. F.: Analysis of discontinuous edge effects and joints. Composite Materials and Structures, Design and Analysis. Part II, C. C. Chamis (editor), Academic Press; 1975.

Hart-Smith, L. J.: Analysis and design of advanced composite bonded joints. NASA CR-2218; April 1974.

Kelsey, S.; Benson, N. K.: ISD Rep. No. 10 (Inst. fur Statik und Dynamik der Luft- und Raumfahrkonstruktionen), Univ. of Stuttgart; 1956.

Liu, A. T.: Linear elastic and elasto-plastic stress analysis for adhesive lap joints. Ph. D. Thesis, Univ. of Illinois; 1976.

Lubkin, J. L.: Stress distribution in adhesive joints. Final Rep. Contr. No. Nord 13383, Mid-West Res. Inst. Eng. Div. Kansas City, Missouri; August 1954.

Lubkin, J. L.; Reissner, E.: Stress distribution and design data for adhesive lap joints between circular tubes. Trans. ASME; August 1956, p. 1213.

Lubkin, J. L.: A theory of adhesive scarf joints. J. Appl. Mech.; June 1957, p. 255.

Ojalvo, I. U.; Eidinoff, H. L.: Bond thickness effects upon stressed in single lap joints. AIAA J. 16(3): 204; March 1978.

Pahoja, M. H.: Stress analysis of an adhesive lap joint subjected to tension, shear force and bending moments. T and AM Rep. No. 361; 1971.

Pirvics, J.: Two-dimensional displacement stress distributions in adhesive bonded composite structures. J. Adhesion 6(3): 207; 1974.

Reddy, M. N.; Sinha, P. K.: Stresses in adhesive bonded joints for composites. Fiber Sci. and Tech. 8: 33; 1975.

Renton, W. J.; Vinson, J. R.: On the behavior of bonded joints in composite material structures. Eng. Fracture Mech. 7: 41; 1975.

Renton, W. J.; Vinson, J. R.: The efficient design of adhesive bonded joints. J. Adhesion 7: 175; 1975.

Sinha, P. K.; Reddy, M. N.: Thermal analysis of composite bonded joints. Fiber Sci. and Tech. 9: 153; 1976.

Spiker, R. L.; Chou, S. C.: Edge effects in symmetric composite laminates. Importance of satisfying the traction free-edge condition. J. Composite Materials 14(1): 2; January 1980.

Srinivas, S.: Analysis of bonded joints. NASA TN D-7855; April 1975.

Thamm, F.: Stress distribution in lap joints with partially thinned adherends. J. Adhesion 7: 301; 1976.

Thongcharoen, V.: Optimization of bonded joints by finite element and photoelasticity methods. Ph. D. Thesis, Iowa State Univ.; 1977.

Volkersen, O.: Die Nietkraftoerteilung in Zubeanspruchten Nietverbindunge mit Konstanten Loschonquerschnitten. Luftfartforschung 15; 1938.

Wah, T.: Stress distribution in a bonded anisotropic lap joints. Trans. ASME, J. Eng. Mater. and Tech. 95(3); July 1973.

Wah, T.: The adhesive scarf joint in pure bending. Int. J. Mech. Sci. 18(5): 223; May 1976.

Wright, M. D.: Stress distribution in carbon fibre-reinforced plastic joints. Composites 9(1): 46; January 1980.

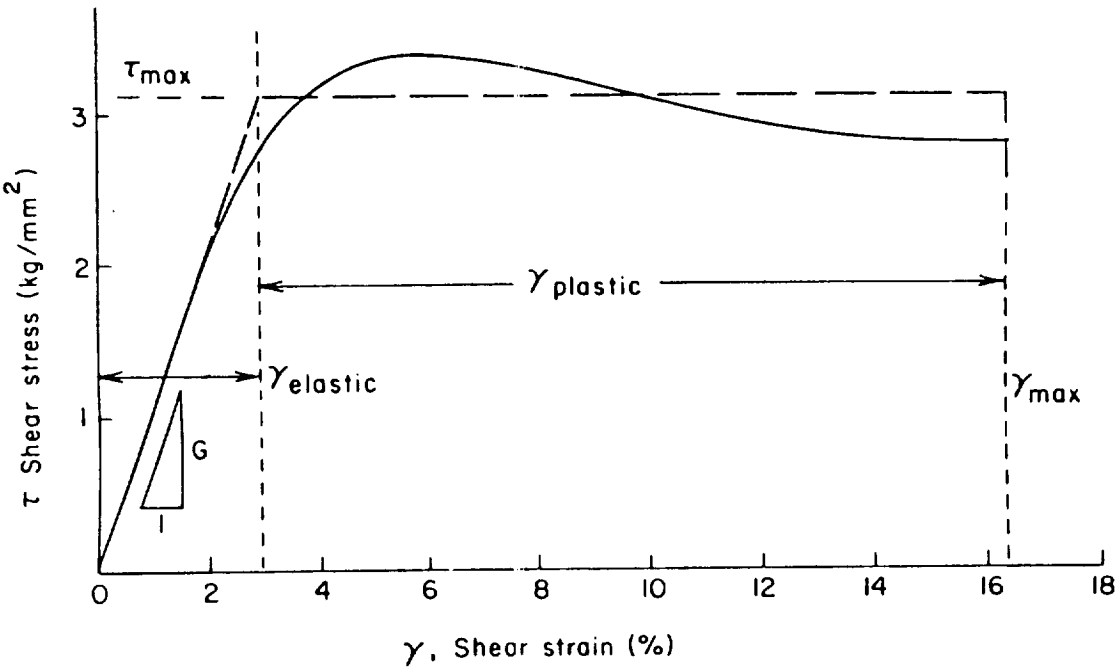

ML86 5377

Figure D-1. - Shear stress/strain behavior of the epoxy adhesive, with an idealized elastic-plastic characterization.

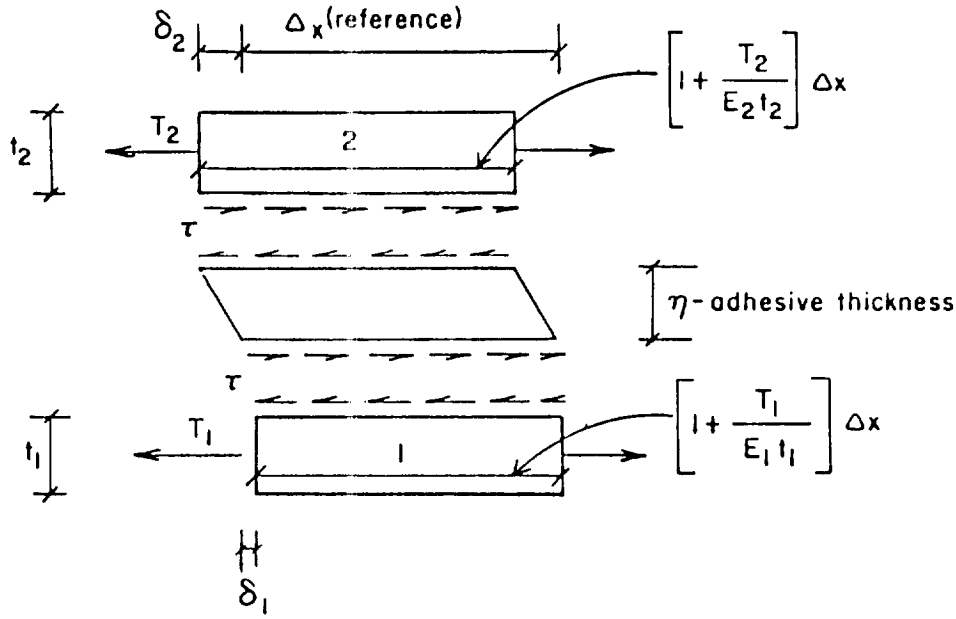

ML86 5378

Figure D-2. - Dimensions, forces, and deformations of an element of the adherend/adhesive/adherend system.

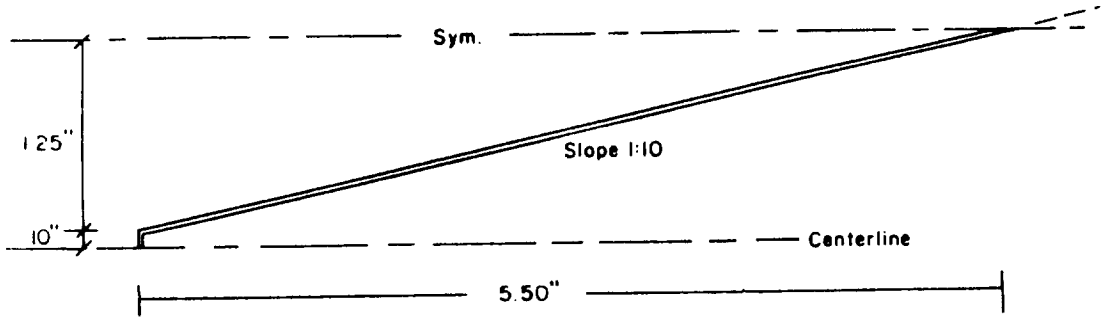

(a) Plan view of finger.

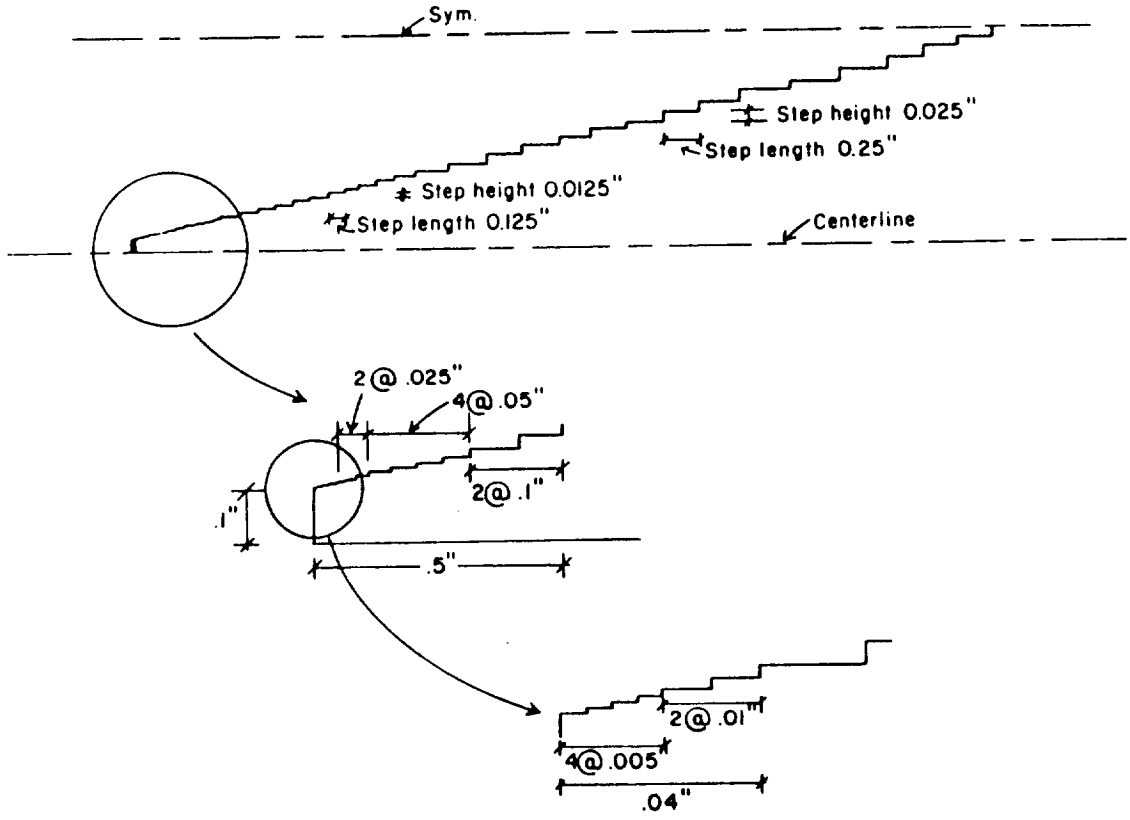

ML86 5372

(b) Idealized FEM model of finite-tip scarf.

Figure D-3. - Geometry of finger joint in the fatigue test beam as used for stress analysis and its idealization with step elements.

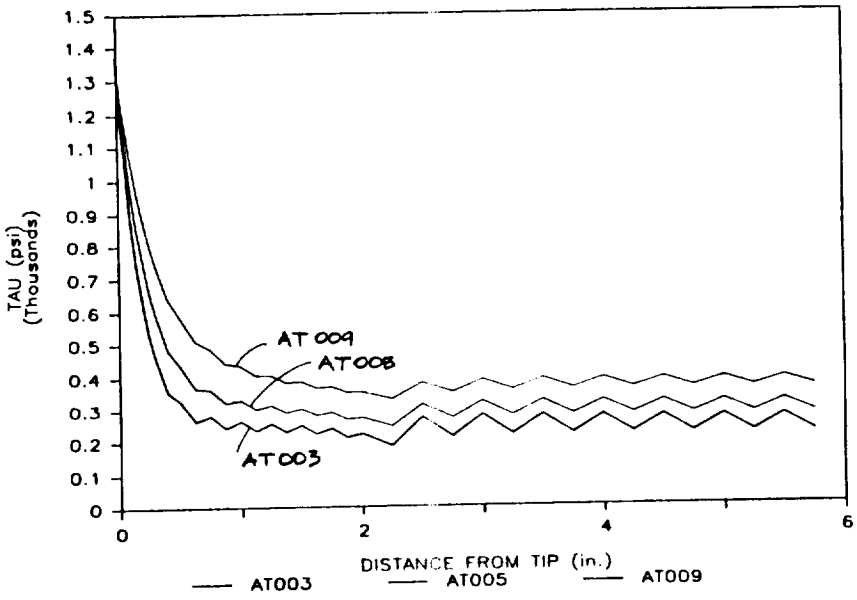

(a) Elastic solution.

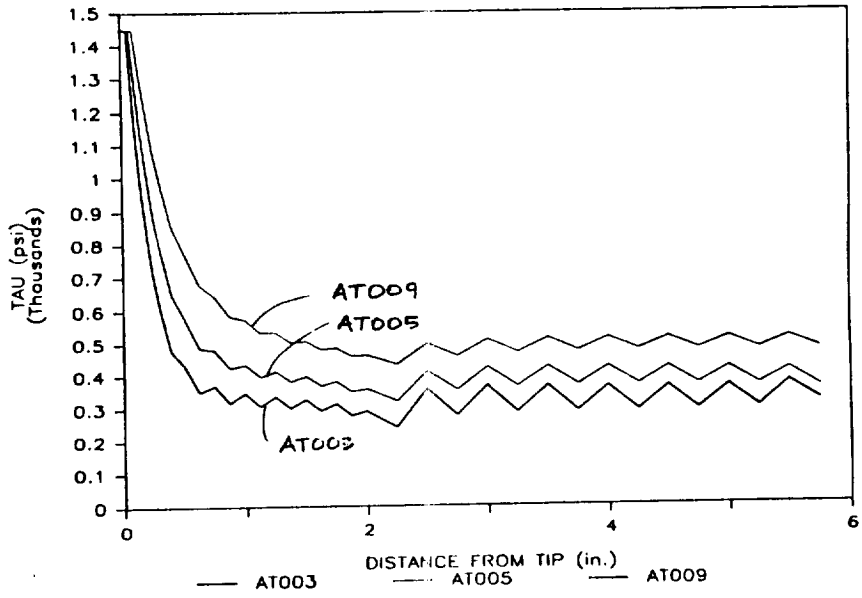

(b) Elastic-plastic solution.

Figure D-4. - Effect of adhesive thickness on shear stress distribution.

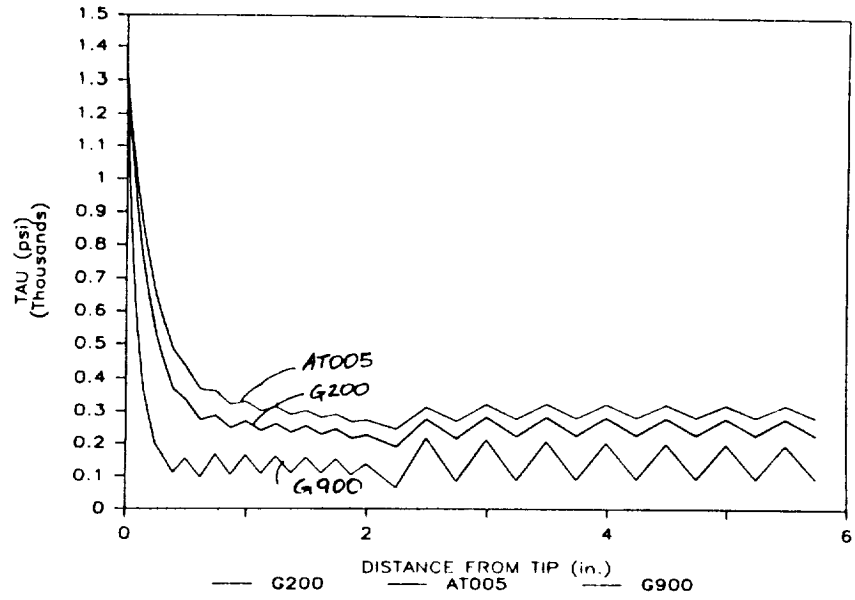

(a) Elastic solution.

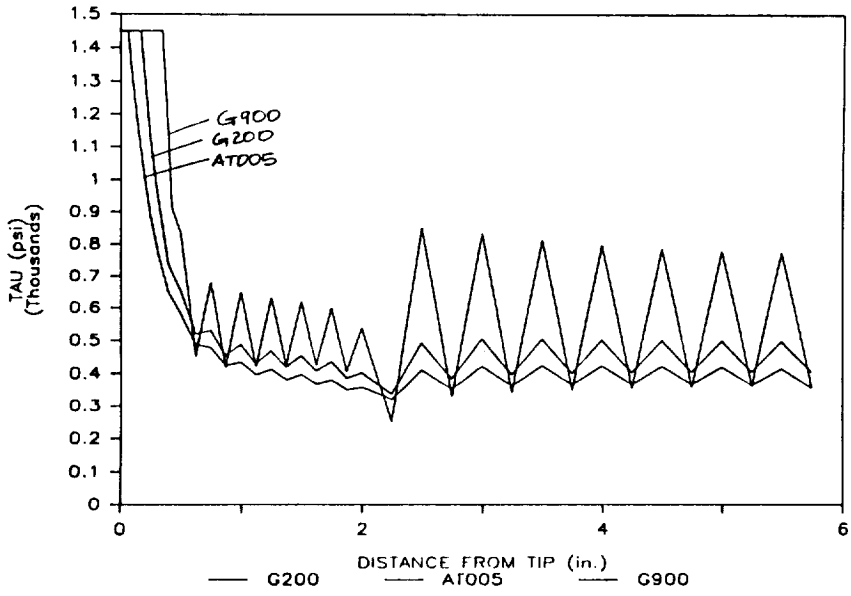

(b) Elastic-plastic solution.

Figure D-5. - Effect of adhesive shear modulus on shear stress distribution.

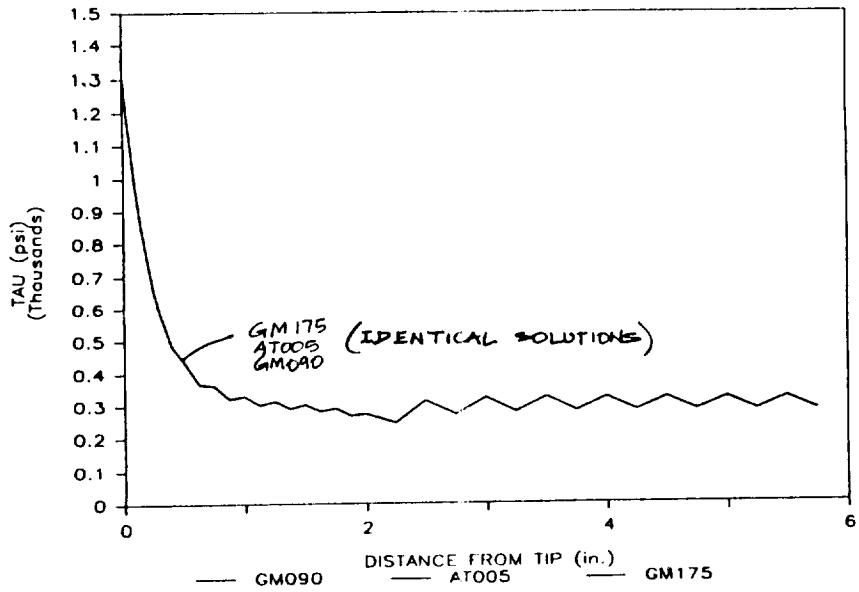

(a) Elastic solution.

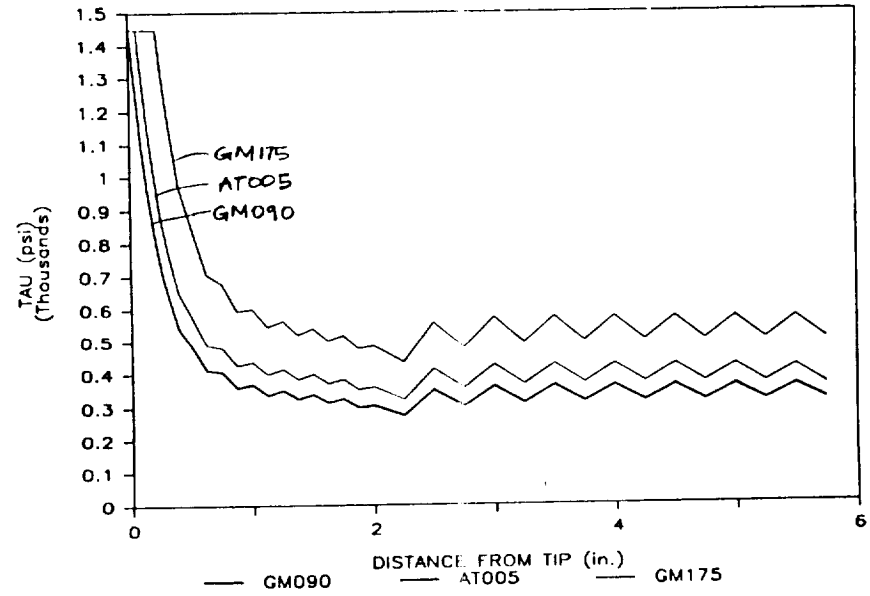

(b) Elastic-plastic solution.

Figure D-6. - Effect of adhesive maximum shear strain on shear stress distribution.

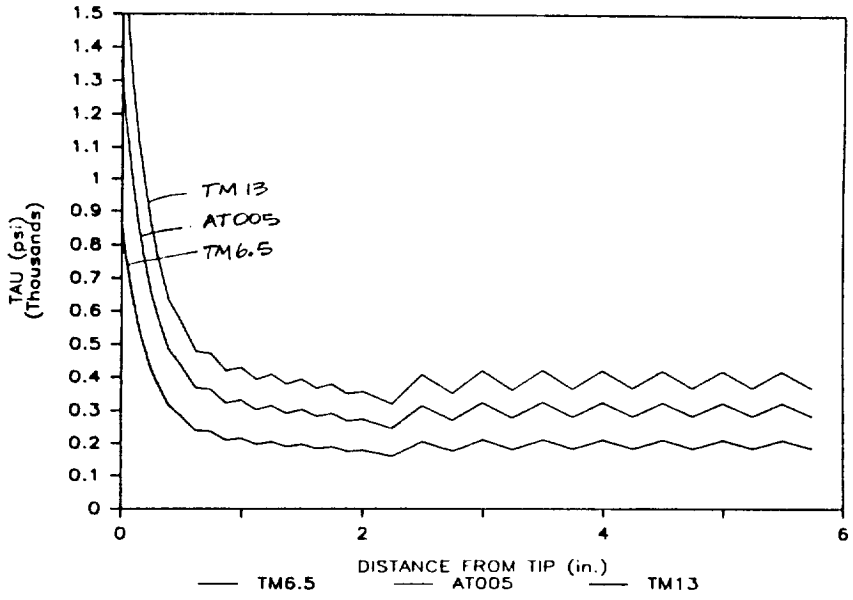

(a) Elastic solution.

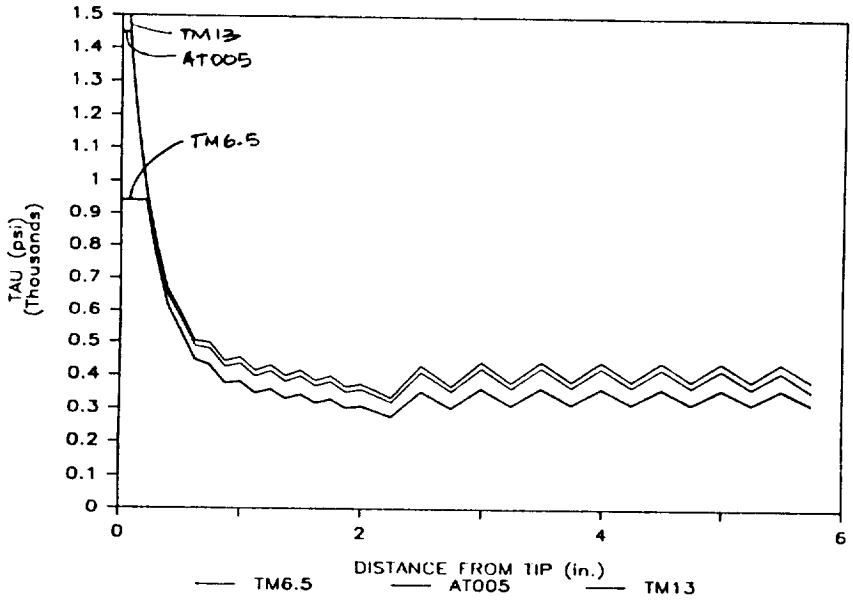

(b) Elastic-plastic solution.

Figure D-7. - Effect of maximum shear stress on shear stress distribution.

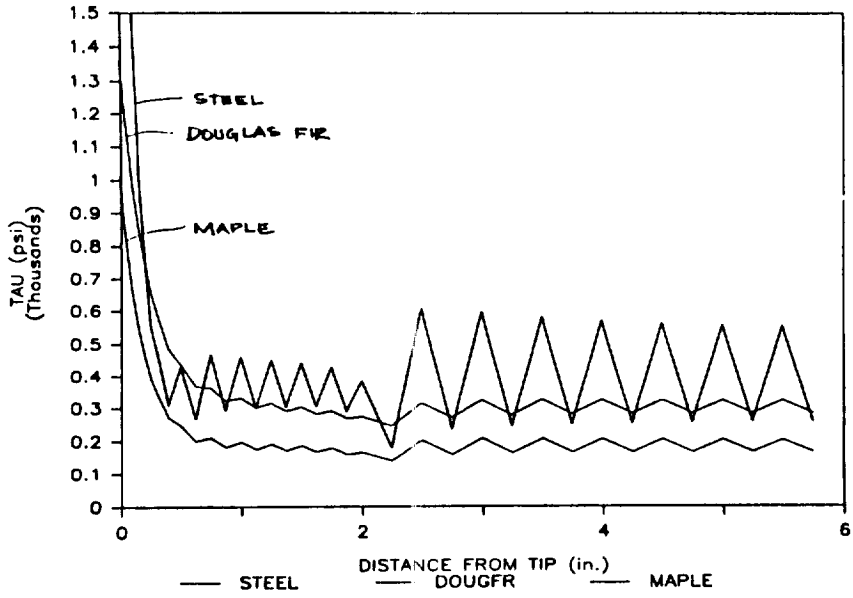

(a) Elastic solution.

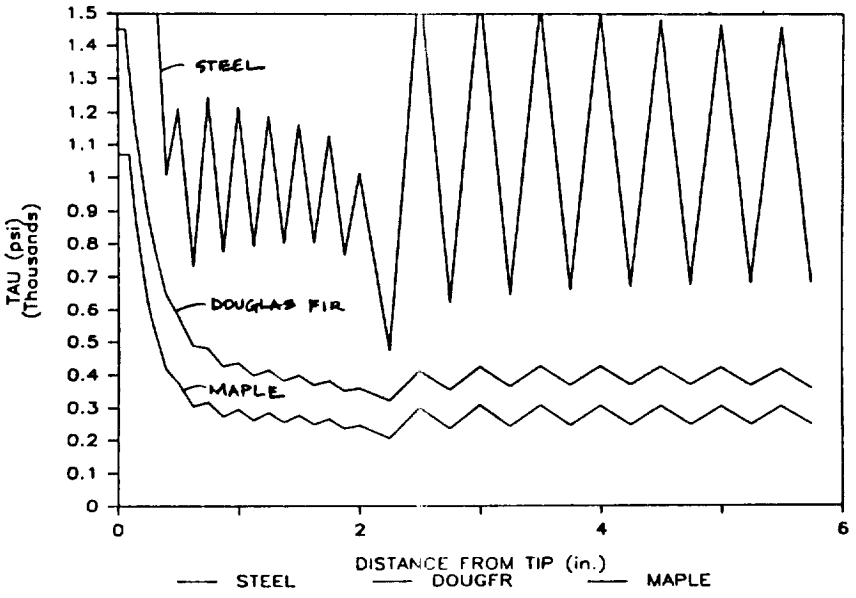

(b) Elastic-plastic solution.

Figure D-8. - Shear stress distributions calculated using average adhesive properties measured by short-lap shear tests with steel, Douglas-fir, and maple adherends.

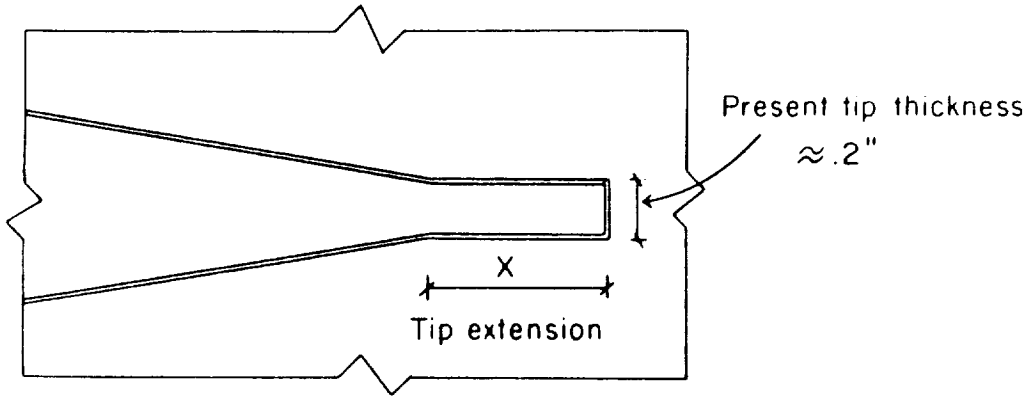

(a) Extended tip.

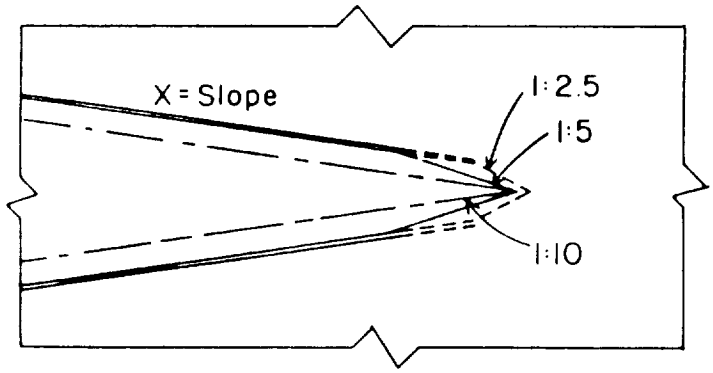

(b) Modified tip slopes.

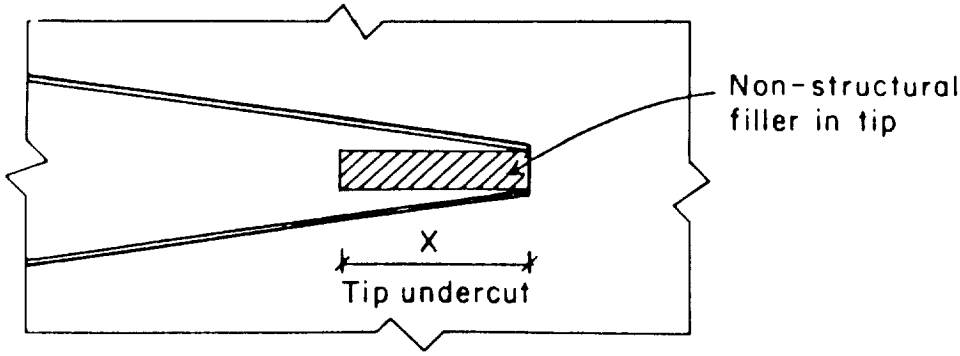

ML86 5373

(c) Reduced tip stiffness.

Figure D-9. - Modified joint geometries analyzed.

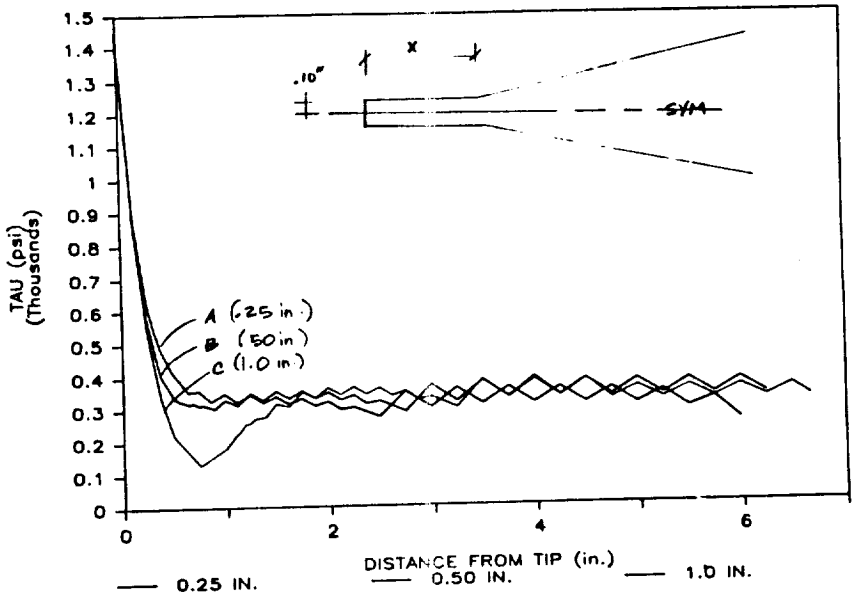

(a) Elastic solution.

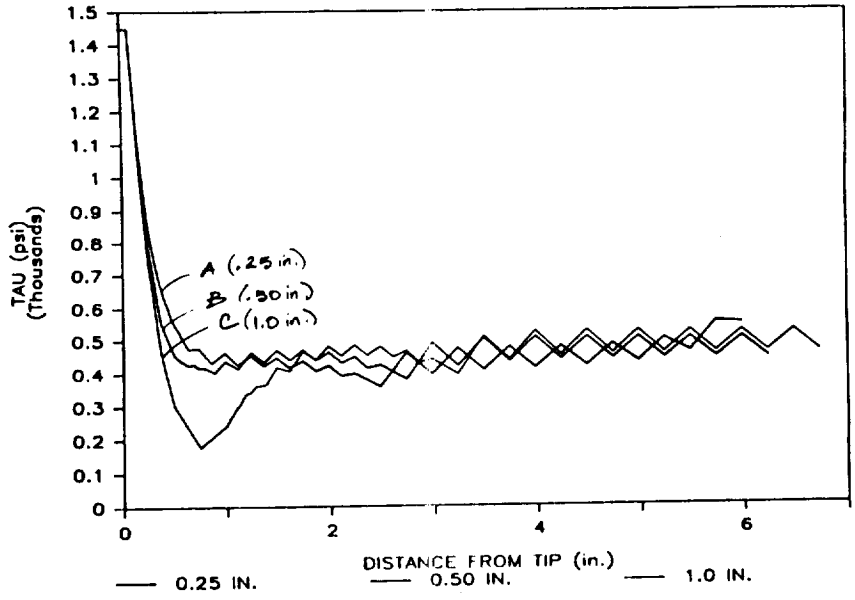

(b) Elastic-plastic solution.

Figure D-10.- Effect of tip extensions on shear stress distribution.

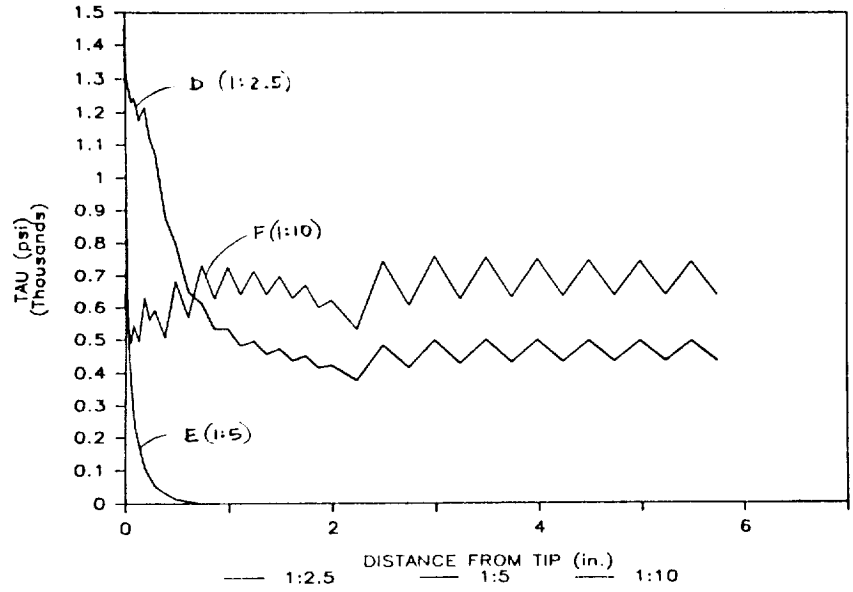

(a) Elastic solution.

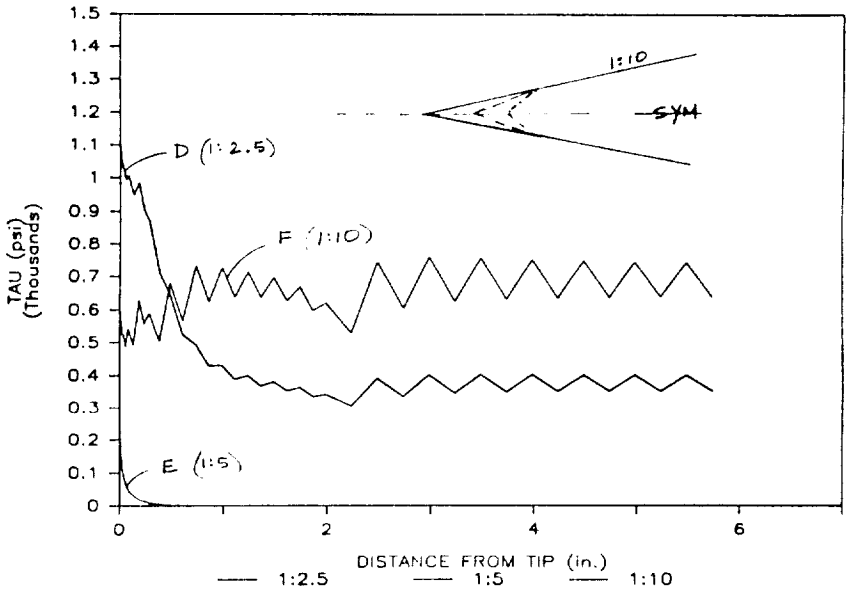

(b) Elastic-plastic solution.

Figure D-11.- Effect of varying the tip slope on shear stress distribution, while maintaining 11.5-inch joint length.

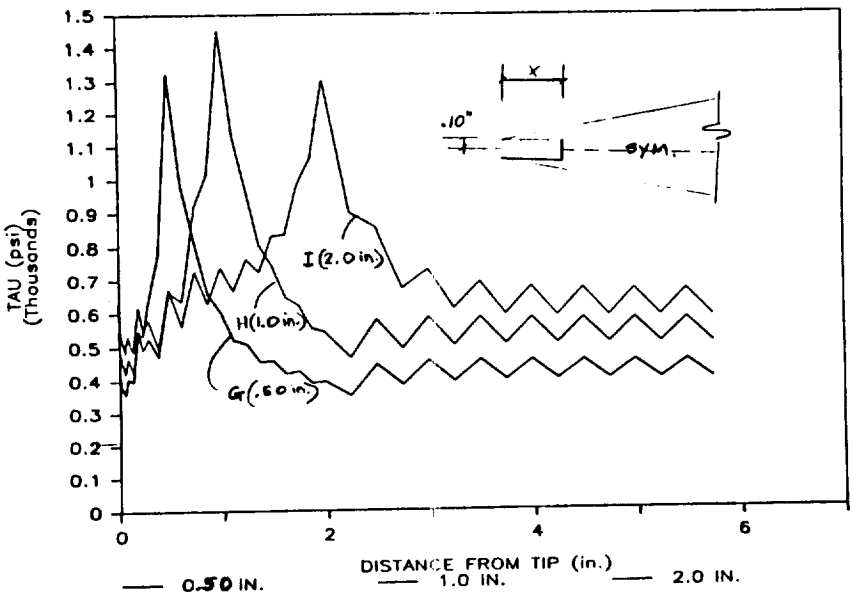

(a) Elastic solution.

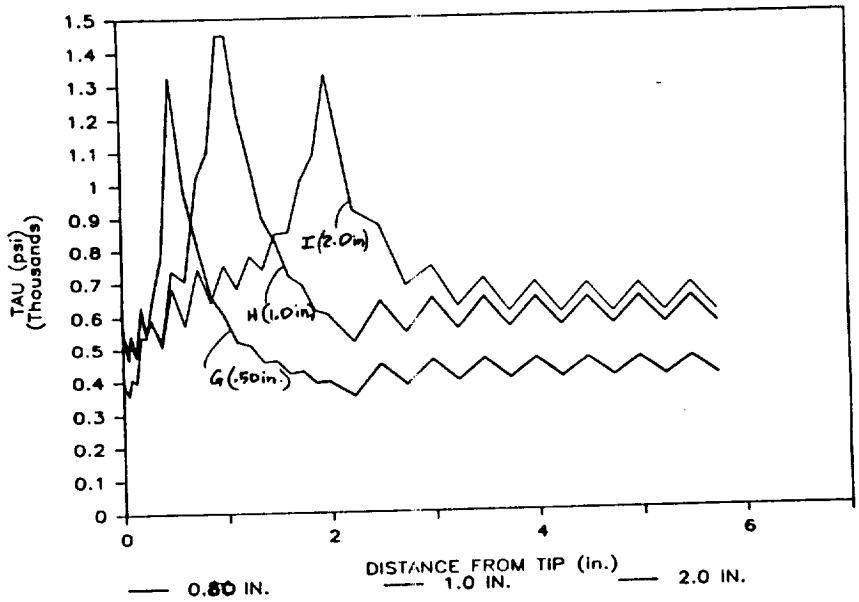

(b) Elastic-plastic solution.

Figure D-12.- Effect on shear stress distribution of undercutting finger tip to reduce tip stiffness.

NASA
National Aeronautics and Space Administration

Report Documentation Page

1. Report No.	2. Government Accession No.	3. Recipient's Catalog No.
NASA CR-182165 DOE/NASA/0015-1		

4. Title and Subtitle

Improving the Fatigue Resistance of Adhesive Joints in Laminated Wood Structures

5. Report Date

August 1988

6. Performing Organization Code

7. Author(s)

Theodore L. Laufenberg, Bryan H. River, Lidija L. Murmanis, and Alfred W. Christiansen

8. Performing Organization Report No.

10. Work Unit No.

9. Performing Organization Name and Address

Forest Products Laboratory
U.S. Department of Agriculture
Madison, Wisconsin 53705-2398

11. Contract or Grant No.

C-80015-F

13. Type of Report and Period Covered

Contractor Report
Final

12. Sponsoring Agency Name and Address

U.S. Department of Energy
Wind/Ocean Technology Division
Washington, D.C. 20546-0001

14. Sponsoring Agency Code

15. Supplementary Notes

Prepared under Interagency Agreement DE-AI01-76ET20320. Project Manager, David A. Spera, Structures Division, NASA Lewis Research Center, Cleveland, Ohio 44135.

16. Abstract

The premature fatigue failure of a laminated wood/epoxy test beam containing a cross-section finger joint was the subject of a multidisciplinary investigation to assess and advance the technology of adhesive joints in composite wood structures. This investigation, which has wide-spread applicability to all adhesively bonded joints, included (1) analysis of the data collected during fatigue testing, (2) microscopic examination of failed and unfailed surfaces and materials, (3) chemical characterization of the adhesive resin and its cure in the presence of wood and asbestos fibers, (4) testing of the filled adhesive on various adherent systems for its mechanical properties and its performance in prototype finger joints, and (5) analysis of the finger joint's load-carrying capabilities, including the effects of specific design modifications. Four major problem areas were identified which appeared to contribute to the premature fatigue failure. Recommended solutions of these problems would reduce the void content in the veneer-veneer and finger joint bondlines, provide a well-configured finger tip for the joint, improve the adhesive's penetration and bonding to the wood substrate, and provide a cleanly-machined surface.

17. Key Words (Suggested by Author(s))	18. Distribution Statement
Wood; Laminated wood; Adhesive joints; Finger joints; Scarf joints; Fatigue; Stress analysis; Chemical analysis; Douglas fir; Epoxy; WEST System	Unclassified – Unlimited Subject Category 24 DOE Category UC-25

19. Security Classif. (of this report)	20. Security Classif. (of this page)	21. No of pages	22. Price*
Unclassified	Unclassified	94	A05

NASA FORM 1626 OCT 86

*For sale by the National Technical Information Service, Springfield, Virginia 22161